UNIVERSIDAD AUTÓNOMA DE MADRID

FACULTAD DE CIENCIAS

DEPARTAMENTO DE BIOLOGÍA MOLECULAR

Doctoral Thesis

Nanobiotechnology and Nanomaterials for Gene Expression and Bacterial Growth Control

Siamak Javani

Madrid,
November 2015

TO MY FAMILY

PARENTS

BROTHER and SISTER

The research described in this thesis was carried out at the Department of Molecular Biology, the Institute for Advanced Studies in Nanoscience (IMDEA Nanociencia) and the National Centre for Biotechnology (CNB-CSIC), Madrid, Spain.

Director: Prof. Jose Pascual Abad

Dr. Alvaro Somoza

Co-director: Dr. Aitziber Lpez Cortajarena

TABLE OF CONTENTS

ABBREVIATIONS

AgNCs	Sliver nanoclusters
AgNps	Silver nanoparticles
AMD	Age-related Macular Degeneration
AS-ODNs	Antisense oligonucleotides
AuNCs	Gold nanoclusters
AuNPs	Gold Nanoparticles
BC	Before Christ
CARMA1	CARD and MAGUK domain-containing protein-1
CD	Circular Dichroism
CHD	1,3-Cyclohexanedione
CMV	Cytomegalovirus
ConA	ConcanavalinA
CPG	Controlled Pore Glass
DC	Direct Current
DCF	Dichlorofluorescine
DCFH	Dichlorodihydrofluorescin
DEPC	Diethylpyrocarbonate
DHAP	Dihydroxyacetophenone
DIPEA	Diisopropylethylamine

DLS	Dynamic Light Scattering
DMA	Dimethylanthracene
DMAP	Dimethylaminopyridine
DMF	Dimethylformamide
DNA	Deoxyribonucleic acid
DNA-AgNCs	DNA-templated Silver nanoclusters
EDTA	Ethylene diaminetetra acetic acid
ERK	Extracellular signal-regulated kinase
FACS	Fluorescence-activated cell sorting
FAM	Fluorescein Amidite
FCS	Fetal calf serum
FDA	Food and Drug Administration
HE	Hydroethidine
HEA	Hydroxyethyl acrylate
HEPES	Hydroxyethyl piperazineethanesulfonic acid
HEX	Hexachlorofluorecein
HoFH	Homozygous familial hypercholesterolemia
IC_{50}	Half maximal inhibitory concentration (50% of growth inhibition)
IL2	Interleukin-2

LB	Luria-Bertani
MALDI-TOF	Matrix-assisted laser desorption ionization-time of flight
MBC	Minimal bactericidal concentration
MDR	Multi Drug-Resistant
miRISC	miRNA induced silencing complex
miRNA	microRNA
mRNA	messenger RNA
MS	Mass Spectrometry
NCs	Nanoclusters
NMR	Nuclear Magnetic Resonance
NP40	Nonyl phenoxypolyethoxylethanol
NPs	Nanoparticles
NS	Nonsense sequence
Nt	Nucleotide
OD	Optical Density
OMePs	O-methylphosphorothioate
ONs	Oligonucleotides
PACT	Photodynamic antimicrobial chemotherapy
PAGE	Poly acrylamide gel electrophoresis
PAMAM	Polyamidoamine

PBPs	Penicillin-Binding Proteins
PCR	Polymerase Chain Reaction
PD	Pancreatogenic Diabetes
PDI	Polydispersity indexes
PDT	Photodynamic therapy
PKCθ	Protein kinase C-theta
PMMA	Poly methyl methacrylate
PS	Photosensitizer
PTGs	Post Transcriptional Gene silencing
RISC	RNA*i*-induced silencing complex
RNA	Ribonucleic acid
RNA*i*	RNA interference
ROS	Reactive Oxygen Species
siRNA	Small interfering RNA
SPR	Surface Plasmon Resonance
TBS	Tert-Butyldimethylsilyl ether
TCR	T-cell receptor
TEAA	Triethyl ammonium acetate
TEM	Transmission Electron Microscopy
Ti/Ni	Titanium/Nickel
TXRF	Total Reflection X-ray Fluorescence

UTR	Untranslated region
UV-vis	UV-visible spectroscopy
XRD	X-Ray Diffraction
zVAD	Benzyloxycarbonyl-Val-Ala-Asp (Ome) fluoromethyketone; apoptosis inhibitor

PRESENTACION

El desarrollo de antibióticos ha permitido combatir distintas enfermedades infecciosas durante el siglo XX, como la tuberculosis, neumonía, fiebre tifoidea o meningitis. Desafortunadamente, el uso inadecuado de los antibióticos ha conducido a la aparición de cepas resistentes a distintitos fármacos, y actualmente se considera uno de los principales problemas de salud pública a nivel global del siglo XXI.

Los avances recientes en nanotecnología han permitido la preparación de distintos nanomateriales, como nanopartículas, con un amplio espectro de propiedades. Diversos sistemas basados en nanotecnología se han propuesto como herramientas eficaces para el control de microorganismos resistentes a antibióticos. En esta línea, nosotros hemos propuesto el uso de bacterias psicrófilas para la preparación de nanopartículas de plata (AgNPs) a baja temperatura, que permitan controlar el crecimiento de bacterias patógenas. En concreto hemos evaluado cuatro bacterias psicrófilas en la obtención de AgNPs bajo diferentes condiciones, como la presencia de NaCl o la temperatura. La actividad antimicrobiana de las nanopartículas obtenidas ha sido evaluada tanto en bacterias Gram-positivas como en Gram-negativas.

Otro tipo de nanomaterial empleado en este trabajo, son los nanoclústeres de plata estabilizados por oligonucleótidos (DNA-AgNCs), los cuales presentan propiedades fluorescentes que pueden ser moduladas por la selección del oligonucleótido empleado. Estos derivados se han utilizado ampliamente en el desarrollo de sensores, pero su uso como agentes antimicrobianos no ha sido descrito.

Por otra parte, oligonucleótidos modificados con una molécula fluorescente han sido evaluados en terapia fotodinámica contra bacterias patógenas.

Finalmente, en un proyecto en colaboración con el Centro Nacional de Biotecnología (CNB) se ha explorado el uso de nanopartículas de oro modificadas con oligonucleótidos para controlar la expresión del gen p21 en células T.

Por tanto, los tres objetivos principales de esta tesis doctoral son:

1. Preparación de AgNPs utilizando extractos de bacterias obtenidas en la Antárctica y su evaluación biológica.
2. Evaluación de DNA-AgNCs como nuevos agentes antimicrobianos.
3. Desarrollo y evaluación de conjugados de oligonucleótidos en terapia fotodinámica.

Por otra parte, se han iniciado un proyecto donde se explora otro uso de nanomateriales en biomedicina como es:

4. La regulación de p21 mediante nanopartículas de oro modificadas con oligonucleótidos.

En esta tesis doctoral se han utilizado cuatro cepas de bacterias psicrófilas obtenidas de la Antártica (*Psychrobacter sp*., *Aeromonas salmonicida*, *Pseudomonas veronii*, and *Yersinia kristensenii)*, las cuales no han sido empleadas anteriormente en la preparación de AgNPs. Las nanoestructuras obtenidas han mostrado una buena actividad antimicrobiana contra bacterias Gram-positivas (*Staphylococcus epidermidis*) y Gram-negativas (*Escheriachia coli* and *Klebsiella pneumonia*).

La actividad antimicrobiana de DNA-AgNCs ha sido evaluada contra *E. coli* y *S. epidermidis* y sorprendentemente, la actividad depende de la secuencia empleada en la estabilización de los nanoclústeres de plata. La secuencia más activa ha sido utilizada en la preparación de un trímero que ha mostrado una actividad superior al monómero.

Para la última estrategia evaluada para controlar el crecimiento bacteriano se han preparado conjugados de oligonucleótidos con moléculas fluorescentes, que al ser excitadas por una luz inducen la muerte de las bacterias a baja concentración (0.750 and 1.5µM). En este caso el estudio se llevó a cabo en *E. coli*, *P. aeruginosa* y *S. aureus* y también se ha observado que la actividad depende en gran parte de la secuencia empleada.

ABSTRACT

In this thesis, we have initiated four research projects. Three of them related to the development and evaluation of nanomaterials as antimicrobials. The fourth one is devoted to the assessment of gold nanoparticles modified with oligonucleotides as regulators of p21 expression.

The first project has been carried out at the Universidad Autónoma de Madrid and deals with the preparation of silver nanoparticles (AgNPs) using broths from bacteria and their evaluation as antimicrobials. Particularly, four psychrophilic bacteria isolated from Antarctica have been evaluated. Different conditions were assessed, including the addition of NaCl and incubation temperatures. The AgNPs obtained were characterized and their antimicrobial properties evaluated against Gram-negative and Gram-positive bacteria.

We also have evaluated the antimicrobial properties of silver nanoclusters stabilized by DNA (DNA-AgNCs), which are novel fluorescent materials. After testing 9 oligonucleotides with different sequence and length we found that the antibacterial activity depends on the sequence of the oligonucleotides employed. The sequences tested yielded fluorescent AgNCs, which can be grouped in blue, yellow and red emitters. Interestingly, blue emitters yielded poor antibacterial activity whereas yellow and red emitters afforded an activity similar to $AgNO_3$. Finally, we prepared a trimeric structure containing the sequence that afforded the best antimicrobial activity, which inhibited the growth of Gram positive and negative bacteria in the sub-micromolar range.

In the third project, we demonstrated that oligonucleotides modified with a fluorescent dye (HEX) can be used in photodynamic therapy to kill bacteria. Interestingly, the sequence of the oligonucleotide employed modulates the antimicrobial activity of the system.

The last project has been done in collaboration with the Centro Nacional de Biotecnología (CNB) and the preliminary results of the regulation of p21 with modified gold nanoparticles are presented. P21 is involved in cell senescence and replication, and its regulation can be done using different oligonucleotides, such as antisense and siRNAs. However, the translocation into the cells of nucleic acids is not easy and transfection systems are required. In this case, oligonucleotides were conjugated to gold nanoparticles (AuNPs) and used in T-cells. The results suggest that the approach employed is valid although further optimization is required.

1. INTRODUCTION

1. INTRODUCTION

1.1. Nanomedicine

Nanotechnology is the engineering and control of organic and inorganic materials generally in the 1-100 nm dimension range, where the materials can present new or enhanced properties[1,2]. A subarea of nanotechnology is nanomedicine, which exploits the properties of nanomaterials in biomedicine and includes, but is not limited to, the development of nanoparticles (NPs), nanofibers, and nanopatterned surfaces for different applications such as, drug delivery[3], regenerative medicine[4] , imaging[5] and sensing[6]. Nowadays, nanomedicine is a promising research area that can provide alternative solutions to the detection and treatment of a variety of maladies, including autoimmune diseases[7], vascular diseases[8] and cancer[9-11].

Among the different materials employed in nanomedicine, NPs are the most widely used due to the ease of preparation and modification, even at large scale. This kind of nanostructures can be obtained from a variety of compounds such as phospholipids[12] , lactic acid[13] , chitosan[14], dextran[15] , silica[16] and a diversity of metals, such as: gold[17] , nickel[18] , silver[19] , iron oxide[20] , zinc oxide[21] , gadolinium[22] and titanium dioxide[23]. Each NP has unique properties that make it ideal for a given application. In our case we have focused our work mainly in silver derivatives due to their antimicrobial properties discussed below.

1.2. Silver and Silver Nanoparticles

Silver is one of the first metals employed in medicine due to its antimicrobial properties. In this sense, ancient Macedonians were probably the first to use silver derivatives to improve wound healing. Similar applications where implemented in Greece, Rome, and Phoenicia where silver was used extensively to control infections and prevent spoilage of water and food[24].

A common application of silver uses silver nitrate to prevent infections and promote healing in topical burns or the eye infection of newborns. However, it has to be employed at low concentrations (0.5-1%) due to its toxic effects[25,26].

On the other hand, metallic NPs have been around us also since ancient times, particularly in the elaboration of stained glass. One of the most famous examples is the “Lycurgus Cup”,

dating back to the 4th century A.D. The Lycurgus Cup, as well as the medieval cathedral windows, contain metallic NPs that bring their unique optical properties to produce aesthetically pleasing colours. Particularly, gold and silver nanoparticles (AgNPs) within the glass are responsible of the brilliant red and green colors that contribute to the light scattering phenomena observed (Fig 1.1). In addition, the colour of the glass changes depending whether the light is reflected on or transmitted through the glass. This colour change must have fascinated the ancient people during that time.

Figure1.1. The "Lycurgus Cup" and " Cathedral Window" (Saint Chapelle in Paris) older applications of nanotechnology.

Although the applications of silver for biomedical purposes and AgNPs as glass stain have been around us for centuries, the use of AgNPs to treat diseases is more recent. In 1889, M.C. Lea, reported the synthesis of a citrate stabilized AgNPs (known as colloids in the past), which diameter was between 7 and 9 nm. Later on, in 1897, different formulations of AgNPs were manufactured and used for medical applications, such as Collargol, Argyrol and Protargol[27]. Since then, multiple medical applications of AgNPs have been reported, due to their unique optical, electrical and thermal properties.

These properties are mainly due to the collective excitation of the conductive electrons (plasmons), which in the particles are localized in the surface[28]. When the light interacts with the particles it excites the surface plasmons, causing a coherent oscillation of the conduction band of electrons, known as surface Plasmon resonance (SPR). This effect can be observed in the visible region of the spectrum and dependents on the particle composition, size, shape, and surrounding dielectric environment[29]. It is worth mentioning that AgNPs are able to absorb

and scatter light better than other metallic NPs (e.g. Au)[30,31] making them one of the most interesting nanomaterials for optical applications.

Due to the properties mentioned above the applications of AgNCs are mainly focused in sensing of different materials (nucleic acids[32], metal ions[33,34], organic molecules[35] and proteins[36]) and to control the growth of unhealthy bacteria. In this regard, AgNPs have some advantages compared to other silver derivatives such a low toxicity to human cells[37], probably due to the slow release of Ag^{+}[38]and the improved interaction with bacterial cells[39-42]. For these reasons, AgNPs are currently been used as an additive to prevent bacteria growth in multiple elements, such as in apparel, footwear, paints, wound dressing, appliances, cosmetics and plastics[43].

1.2.1. Synthesis of AgNPs

AgNPs can be obtained by different strategies than can be grouped in three different and complementary approaches, known as **1**).Chemical methods, **2**). Physical methods and **3**). Biological methods.

1). Chemical methods: In this case a silver salt is reduced to yield the final AgNP, which can be carried out in different ways involving chemical[44,45], electrochemical[46], and pyrolytic reductions[47].

2). Physical methods: By contrast, physical methods do not involve chemicals and usually have fast processing time. Such methods include physical vapor condensation[48], arc-discharge[49], energy ball milling method[50], and direct current (DC) magnetron sputtering[51].

3). Biological methods: In the biological synthesis of AgNPs, the toxic reducing agents and stabilizers are replaced by non-toxic molecules (proteins, carbohydrates, antioxidants) produced by living organisms, including bacteria[52], fungi[53], yeasts[54], and plants[55]. In these cases the reduction might involve enzymatic (e.g., NADPH reductase) processes[56] as well as a variety of biomolecules (e.g. aminoacids, polysaccharides and vitamins)[57].

The use of organisms to generate AgNPs presents some advantages versus the chemical and physical methods. Particularly, the lack of toxic chemicals, which are replaced by extracts from plants or large variety of microorganism[58], the easy set-up required, which can be scaled-up, make the whole process very cost-effective[59,60].

1.2.2. Biosynthesis of AgNPs

The first intercellular synthesis of AgNPs by bacteria was reported in 1999 where *Pseudomonas stutzeri* AG259 was employed[61]. In this case particles with a diameter below 200 nm were obtained. Since then, different bacteria have been employed to obtain this type of nanostructures[62,63] .

The generation of AgNPs by microorganisms implies that they can tolerate metal ions at high concentrations. Then, through different mechanisms the bacteria are able to transform the salts into the metallic NPs[64].

Extremophiles seem to be good candidates as NPs producers, since these microorganisms have been adapted to grow in harsh conditions such as extreme pH, temperature, salinity and absence of oxygen[65,66].

Among this group, psychrophiles are extremophilic bacteria that live in very cold environments (-20 °C to +10 °C) and usually at high salt concentration[67]. A couple of reports have shown the capabilities of this family of bacteria in the production of AgNPs[68,69]. Interestingly, Ramanathan and co-workers were able to control the shape of the AgNPs using *Morganella psychrotolerans*[70]. S. Shivaji and co-workers employed cell-free culture supernatants of five psychrophilicbacteria (*Pseudomonas antarctica*, *Pseudomonas proteolytica*, *Pseudomonas meridiana*, *Arthrobacter kerguelensis* and Arthrobacter *gangotriensis*) and two mesophilic bacteria (*Bacillus indicus* and *Bacillus cecembensis*) to synthesize AgNPs. In this case the size of the AgNPs ranged from 6 to 13 nm and were stable for 8 months when stored in the dark[69].

1.2.3. Why AgNPs?

The introduction of antibiotics is one of the most important medical interventions with regard to reducing human morbidity and mortality[71]. The penicillin was discovered by Sir Alexander Fleming in 1928, and since then, a variety of antibiotics have been developed to treat a myriad of bacterial infections. Unfortunately, in the past decade the number of antibiotics to which bacteria have developed resistance has increased considerably. As a consequence, some agents are no longer useful for the treatment of infections and even

several strains are becoming resistant to more than one antibiotic[72]. For these reasons there is a great urgency to develop novel antibiotics[73].

The specific target for most antibiotics are the cell wall synthesis (e.g. Penicillin[74], Cephalosporins[75] and Carbapenems[76]), the protein or RNA synthesis (Tetracyclines [77]and Rifamycins[78]), the DNA replication (Quinolones[79] and Metronidazole[80]) or the energy metabolism. The activity of antibiotics depend on the strain tested, but two big groups are stablished related to the cell wall structure, Gram-positive and Gram-negative.

Most prokaryotes have a rigid cell wall, which is an essential structure that protects the cell protoplast from mechanical damage and from osmotic rupture or lysis. In the Gram-positive bacteria (those that retain the purple crystal violet dye when subjected to the Gram-staining procedure), the cell wall consists of cytoplasmic lipid membrane, with a thick peptidoglycan layer, lipoteichoic acids, peptidoglycans and a small periplasmic space. In the Gram-negative bacteria, which do not retain the crystal violet, the cell wall is composed of a cytoplasmic membrane with a thin peptidoglycan layer and larger periplasmic space. In addition they have an outer membrane containing lipopolysaccharides and porins[81,82](Fig 1.2).

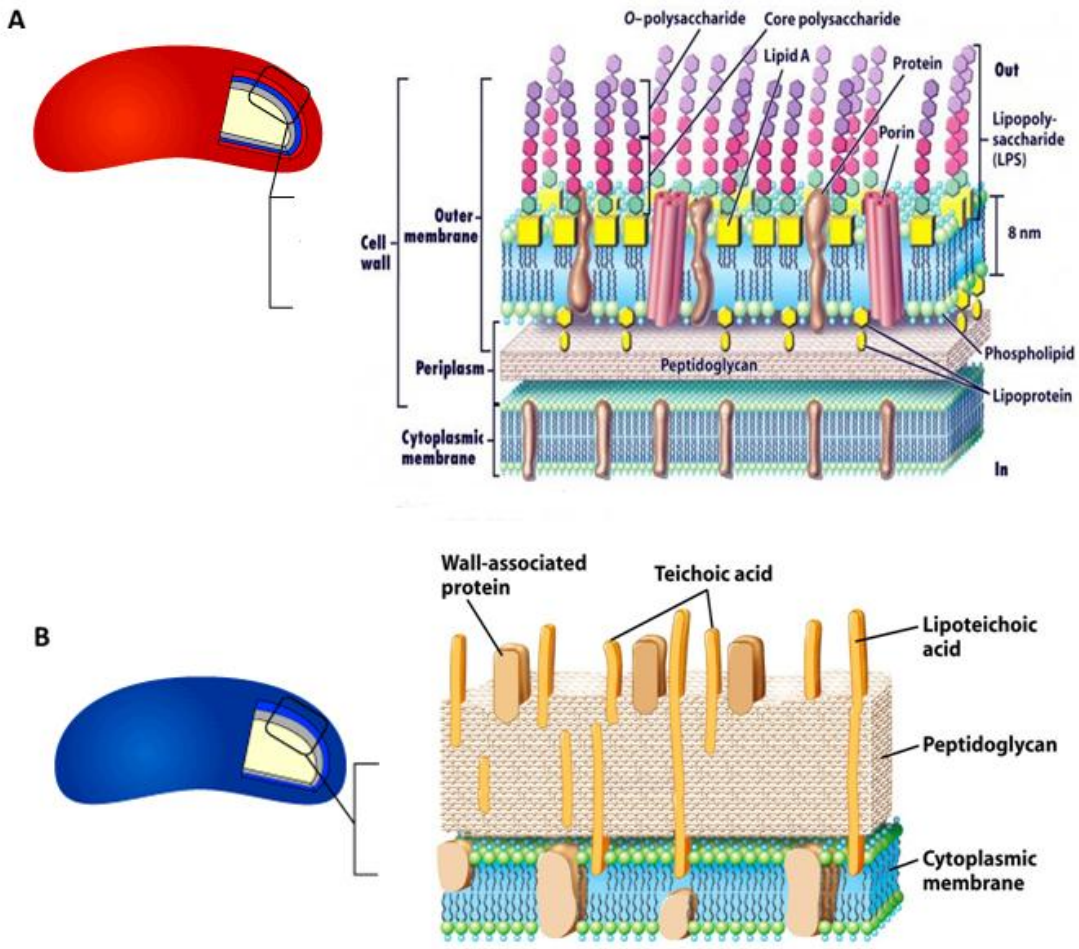

Figure1.2. The structure of the cell wall in **A**). Gram-negative and, **B**). Gram-positive bacteria (adapted from 83-85).

Bacterial cell walls are unique structures that are not present in mammalian cells, and therefore serve as ideal targets for antimicrobial drugs. Understanding the molecular basis of interaction and effect of antibiotics in bacterial membranes is key to design new drugs to overcome the current resistance[86,87].

There are different mechanisms that bacteria can use to develop resistance to antibiotics. For example, plasmid-mediated enzyme production of proteins that inhibit the activity of antibiotics (e.g. aminoglycosides or penicillins), alteration of the target site of antibiotics, such as mutations in the Penicillin-Binding Proteins (PBPs), or the alteration in metabolic pathways to circumvent the drug activity [88,89](Fig 1.3).

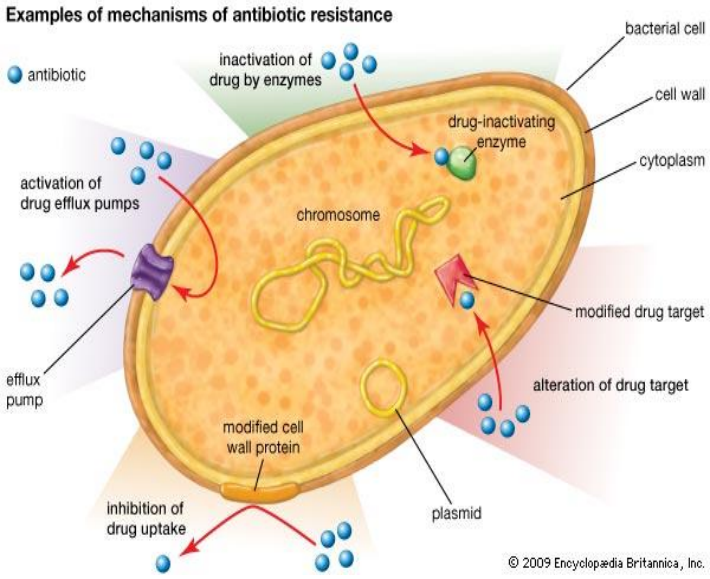

Figure1.3. Various mechanisms that bacteria use to resistance to antibiotics[90].

However, the use of silver derivatives and particularly AgNPs seems to reduce the development of bacteria resistance compared to traditional antibiotics, due to the low number to reported cases despite its widespread use, making them ideal candidates for the development of novel nanoantibiotics [91-94].

1.2.4. Silver nanomaterials-based antimicrobial: mechanism of action

AgNPs, compared to silver ions and standard metallic silver, are effective in the broader spectrum of microorganisms (bacteria, antibiotic resistant strains, fungi and virus)[95-98]. However, the mechanism of action is not completely clear and different processes seem to be involved. Particularly, AgNPs interact with the cell wall increasing its permeability leading to osmotic unbalances and uncontrolled transport through the cytoplasmic membrane, which cause the death of the bacteria[99-101]. In addition, after penetrating the bacteria, AgNPs can react with proteins and DNA[99-103]. AgNPs modulate the phosphotyrosine profile of putative bacterial peptides that can affect cellular signaling, with leads to growth inhibition in bacteria[104].

One of the most established antimicrobial mechanism of silver derivatives is related with the generation of reactive oxygen species (ROS), which are generated on different oxidized molecules, such as O_2, H_2O_2, OH^-, and NO[105,106] due to the susceptibility of oxygen to get reduced. This kind of species are very reactive and can attack different molecules including lipids[107] proteins[108], and nucleic acids[109] . ROS are produced as a by-product in every organism during oxidative processes such a respiration and under regular conditions the organisms have efficient ways to neutralize them. Indeed, in *Escherichia coli* up to 87% of the H_2O_2 is generated along the respiratory chain[110]. However, when there is an increase of these reactive molecules significant damage can be produced leading to cell death. This is the case when some antibiotics[111] or silver derivatives, such as, AgNPs[112] and silver nanoclusters (AgNCs)[113] are employed.

The detection of ROS, including, super oxide radical, hydrogen peroxide, singlet oxygen, hydroxyl radical and peroxyl radical, can be done easily with their specific fluorescent probes, hydroethidine (HE), 2´,7´-dichlorodihydrofluorescin (DCFH), 9,10-dimethylanthracene (DMA), 1,3-cyclohexanedione (CHD) and, dipyridamole[114] respectively. One of the most commonly used probe is 2´,7´-dichlorodihydrofluorescin diacetate (DCFH-DA), which acetyl groups can be removed by esterases inside the cells to yield 2´,7´-dichlorodihydrofluorescin (DCFH). Then, in the presence of hydrogen peroxide it is oxidized to the highly fluorescent 2´,7´-dichlorofluorescin (DCF) (Fig 1.4).

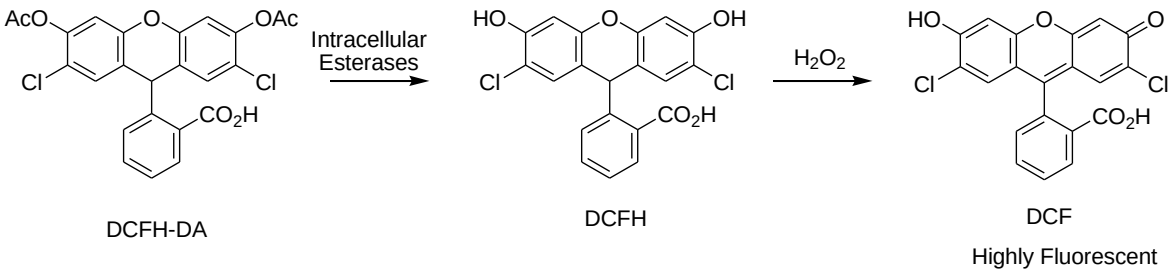

Figure1.4. Fluorescent probe employed to detect ROS.

On the other hand, several studies have shown that AgNPs can be toxic in mammalian cells, thus, in the last years several groups are working on strategies to reduce the toxicity of AgNPs[115-117]. Some of the methods developed involve the use of drug delivery systems, which when used in combination with antibiotics can reduce the toxicity of both compounds and

enhance their antibacterial activity[118,119]. It is important to mention that some factors that control the activity of AgNPs are their size[120,121]and shape[122]. In this sense, AgNPs of 25 nm have shown higher antibacterial activity than smaller ones[123]. Regarding their shape, triangular[124], spherical, rod and flower shaped nanostructures have been evaluated where the spherical structures turned to be the less active[125].

1.3. Metal Clusters

As mentioned before metallic NPs have different properties compare to the bulk material. Interestingly, even within the nanoscale new properties can appear when metallic nanostructures have sizes below 2 nm, such as fluorescence. In this case, they are known as nanoclusters (NCs) and are composed of just few atoms of the corresponding metal[125-129].

Fluorescent structures are very interesting materials with applications in different disciplines such as, nanotechnology, biotechnology and medical research. The fluorescent systems currently employed can be divided in three major groups: organic molecules[130], fluorescent proteins[131] and nanocrystals[132]. Despite their good fluorescent properties all of them have some drawbacks (e.g. photobleaching, large size, toxicity) and for this reason novel fluorescent materials are welcome. In this regard, metal NCs are promising new fluorescent materials, due to their small size, excellent photostability and low toxicity.

NCs can be obtained from their corresponding salts through radiolytic[133], chemical[134], or photochemical reduction[135]. However, in order to prevent their degradation and control their size, capping agents are required such as zeolites[136], PAMAM[137], PMMA[138], polyacrylate[139], poly (NIPAM-AA-HEA) microgels[140], sugar molecules[141], peptides[142]mercaptosuccinic acid[143], lipoic acid[144] and other thiolated derivatives[145], and DNA[146].

Due to the fluorescent properties of NCs multiple applications have been developed for the detection of different molecules[147] such as, ions[148], small molecules[149], nucleic-acid[150], proteins, even in cell models[151].

1.3.1. DNA-Stabilized Silver Nanoclusters

Among the different stabilizing agents employed in the preparation of AgNCs, oligonucleotides can provided additional features to the nanostructures, which have motivated lot of research in this area. Particularly, the fluorescent properties of DNA-templated silver nanoclusters (DNA-AgNCs) can be tuned by the selection of the oligonucleotide employed. In this sense, it is possible to prepare emitters from the blue to the near-infrared region just by the selection of the proper oligonucleotide. Additionally, the fluorescence properties of DNA-AgNCs are very sensitive to the environment and for this reason they have been employed in the preparation of multiple sensing systems for small molecules[152], ions[153] , enzymes[154] and nucleic acids[155] .

1.4. Gold Nanoparticles

Another interesting metallic nanostructures are those derived from gold. Gold possesses interesting physical and chemical properties in both the macroscopic and microscopic states. At the macroscopic scale gold is known for its unique yellowish color, its chemical stability, metallic behavior and high redox potential. On the other hand, at the nanoscale metallic gold is less stable, semiconductor and has a reddish colour due to 1) the high ratio of surface atoms vs bulk atoms[156], 2) the quantum effects that explain the change from metallic to semiconducting character of very small particles[157] , and 3) the electromagnetic confinement of electrons[158].

Gold nanoparticles (AuNPs) can be obtained easily using different approaches such as the Turkevich and Frens method[159], the Brust method[160], the microemulsion method[161,162], the seeding method[163], the Zhong method[164],the Xia method[165] as well as biological methods where microorganisms[166], enzymes[167], and plants or plant extracts are employed[168].

AuNPs have been used in biomedicine in a variety of applications[169] such as: diagnostics and sensing[170-172], imaging[173-175], photothermal therapy[176] and drug delivery[177-179]. In this thesis we have employed them as carriers of different nucleic acids to control the expression of the p21 gene.

1.5. Photodynamic Therapy for the treatment of Infectious Diseases

Historically, phototherapy began in Ancient Egypt, Greece, and India[180] , where light was employed to treat skin diseases, such as psoriasis[181], but disappeared for many centuries and was rediscovered at the beginning of the twentieth century. Photodynamic therapy (PDT) is a form of phototherapy that requires three key components: a photosensitizer (PS), a light source, and oxygen. PS are light-sensitive molecules that can be excited with light to produce ROS in the presence of oxygen. These ROS are generated during PDT through two types of reactions[182]. Type I involves electron/hydrogen transfer directly from the PS, producing ions, or electron/hydrogen abstraction from a substrate molecule to form free radicals. Type II produces the electronically excited and highly reactive state of oxygen known as singlet oxygen[183] (Fig 1.5).

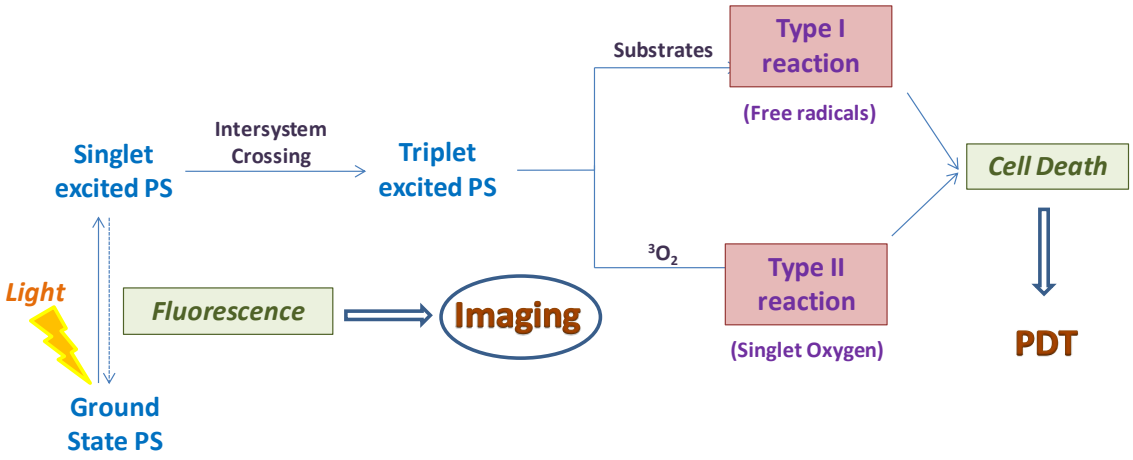

Figure1.5. Schematic illustration of a typical photodynamic reaction.

PDT is used clinically to treat a wide range of diseases, such as infectious diseases, cancer, and even psychosis with very low toxicity.

Recently, PS for antimicrobial PDT or PACT on antibiotic resistance bacteria have been reported [184-186]. One of the advantages of PACT is that antibiotic resistant and susceptible bacteria can be killed effectively. Moreover, it is possible to selective target the pathogenic

bacteria using a targeting moiety such as an aptamer[187,188] improving its efficacy and reducing the side effects.

Multiple PS have been employed against Gram-positive and Gram-negative bacteria such as methylene blue[189], porphyrins[190], cyanine[191] as well as fluorescein derivatives, such as erythrosine and Rose Bengal[192]. For instance, Rose Bengal at 50 µmol/l excited with blue light was employed to inhibit the growth of Enterobacteriaceae strains .

In this thesis we plan to evaluate oligonucleotides modified with PS as antimicrobials.

1.6. Nucleic Acids For Gene Regulation

The central dogma of molecular biology, "DNA makes RNA and RNA makes protein" was first stated by Francis Crick in 1956[193]. Since then, great efforts have been focused on sequencing the information encoded in the DNA that leads to the generation of proteins. However, nowadays it is known that the central dogma of molecular biology is involved only in a small section of the information encoded in the DNA and most of the information encoded deals with regulation[194,195].

It is known that many diseases are related with the genes, from a mutation in a gene that can lead to an inactivated or aberrantly expressed protein, to a dysregulation in their expression, which can increase or reduce the amount of the proteins present in the cell. In this regard, regulatory RNAs, which control the expression of the genes, are been evaluated as biomarkers for the detection of diseases and even as drug targets for their treatment[196]. In order to control their activity different strategies involving oligonucleotides have been developed as detailed below.

1.6.1. Antisense therapeutics

Antisense oligonucleotides (AS-ODNs) are short oligonucleotides (18-25 bases) designed to bind specific RNA sequences inside cell. The ODN-RNA duplex generated then prevents protein translation by RNase H, which decompose the RNA, or by preventing the ribosomal access and/or assembly[197]. The use of As-ODNs to treat diseases, has multiple hurdles, such as the delivery[198], stability[199] and off-target effects[200,201]. Additionally, the uptake and sequestration of

AS-ODNs in the reticuloendothelial system and intracellular sequestration by oligo-protein complexes and phagolysosomes[202] can reduce its activity. Most of these problems have been addressed using different chemical modifications in the phosphodiester back bone, the nucleobase and/or the sugar moiety, which can increase the affinity and specificity of AS-ODNS for RNA target sequences [203] (Fig 1.6).

The most widely used modifications are the 2´O-methyl and phosphorothioates (2´OMePS), which exhibit improved stability and increased cellular uptake[204,205].

These improvements have led to the development of novel therapeutic compounds based on oligonucleotides such as Fomivirsen[206](marketed as Vitravene), which was approved by the FDA in 1998 for treatment cytomegalovirus retinitis (CMV) and Mipomersen[207] (marketed as Kynamro) for the treatment of homozygous familial hypercholesterolemia (HoFH) and also pegaptanib sodium injection[208] (marketed as Macugen), an anti-angiogenic for the treatment of neovascular age-related macular degeneration (AMD).

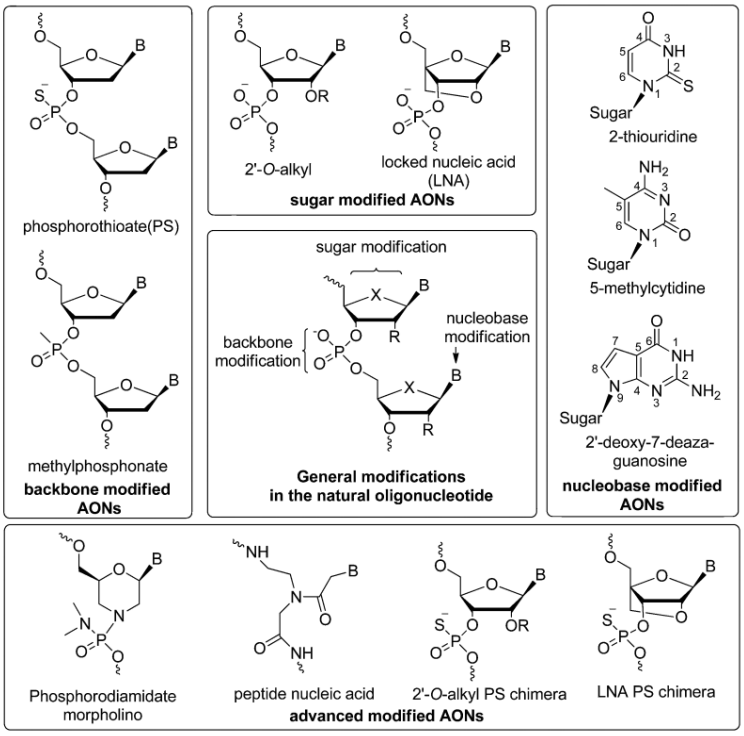

Figure1.6. An overview of different chemical modifications of antisense oligonucleotids (AONs); B=nucleobase[205].

1.6.2. RNA interference (RNAi)

RNAi is an intracellular defense system which historically was called "co-suppression, post transcriptional gene silencing" (PTGS) and quelling[209]. In the RNAi process, long double-stranded RNAs can trigger the cleavage activity of the intracellular enzyme, Dicer, leading to small RNA duplexes of 19-21 nucleotides, known as small interfering RNAs (siRNA). Then, a protein complex (RISC), binds the siRNA duplex and removes one of the strands of the duplex, known as passenger. At this point the RISC complex is activated and will use the guide strand to find the complementary sequence in the mRNA present in the cytoplasm, which is cut in two pieces by the endonuclease activity of the RISC complex[210] (Fig 1.7). The process can be repeated by the RISC complex multiple times leading to an effective reduction of the protein expressed in the target mRNA. Due to the high selectivity and activity of the RNAi process it is currently being assessed as a novel therapeutic by targeting the expression of proteins involved in different diseases such as cancer, Crohn's disease, macular degeneration or hypercholesterolemia. However, one of the main limitations of this technology in humans is the delivery, which can be improved using different carriers.

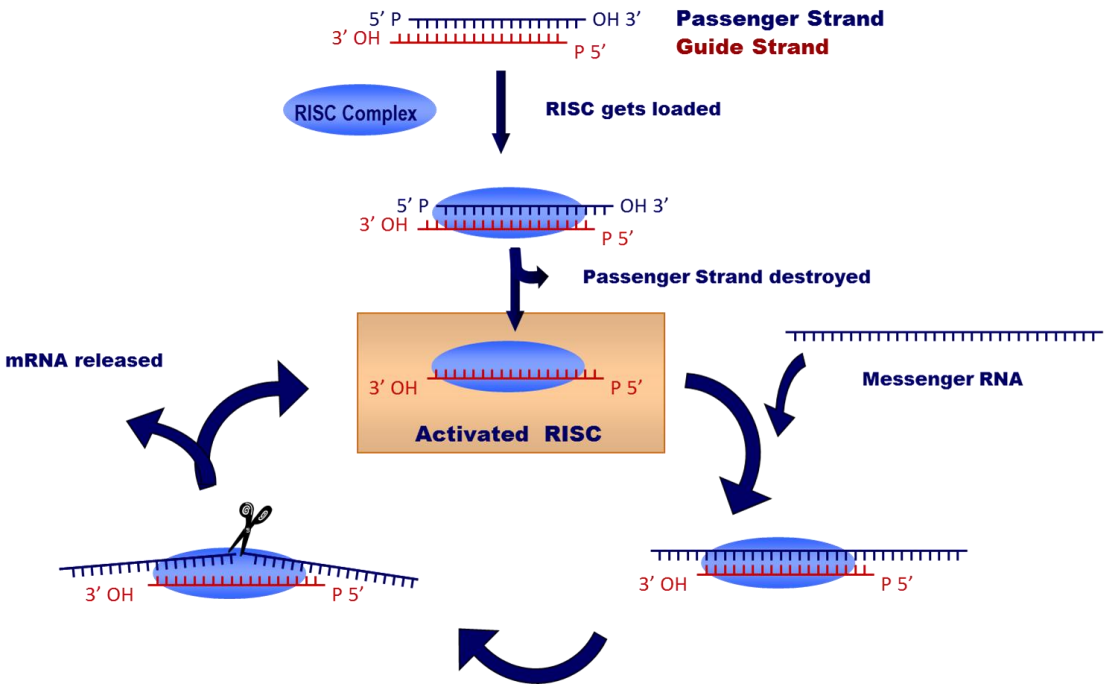

Figure 1.7. Schematic representation of the mechanism of RNA interference.

-MiRNAs

MiRNAs are 20-24 nucleotide long RNA structures that bind to the 3´ UTR (untranslated region) of target mRNAs, leading to translational repression or mRNA degradation. MiRNA have a key role in proliferation, development, differentiation, apoptosis, angiogenesis, and immune response and other normal physiological functions. It is proved that miRNAs are important regulators of gene expression in eukaryotes[211-213]. To date it have been reported, around 15,000 miRNAs in eukaryotic organisms and the number is increasing every day. In humans around 30% of protein coding genes are controlled by miRNAs[214]. MiRNAs are involved in the pathogenesis of several human diseases including cancer[215], immune[216], cardiovascular[217] and neurological disorders[218] and can be found almost in every fluid. For these reasons, miRNAs are very attractive biomarkers for different human diseases.

MiRNAs are generated by RNA polymerase II or III from the stem loop that transcribed pri-mRNA pathway or an alternative miRtron pathway. Recently, miRtron pathway has been found in mammals, drosophila and nematodes. The miRtron pathway involves the Drosha-DGCR8 complex, which leads the formation of pre-miRs of 70nt length, from their corresponding pri-miRs. Then pre-miRNAs are exported to the cytoplasm through Exportin-5-Ran complex, and then cleaved by Dicer yielding 20bp mi-RNA:mi-RNA duplexes. The miRNA induced silencing complex (miRISC) is formed by one of the strands of the duplex and a protein complex know as RISC, which is able to control the expression of the genes through translational repression or mRNA cleavage, similar as in the case of RNAi.

1.6.3. p21 Gene

In this thesis we plan to use different oligonucleotides conjugated to AuNPs to control the expression of the p21 gene. The corresponding protein plays multiple biological roles such as a cell-cycle regulator in response to DNA damage, regulator of transcription, senescence, apoptosis, and DNA repair[219,220].The p21 (CIP1/WAF1) protein can inhibit the activity of cyclin-CDK2, CDK1, and CDK4/6 complexes. In humans this protein is encoded by the CDKN1A gene located on chromosome 6 (6p21.2) and produces a polypeptide with 164 amino acids[221]. P21 activity is involved in a number of human diseases such as Alzheimer[222], and various types of cancers[223], and can be regulated by different miRNAs including miR-17-92, miR-106a-363, and miR-106b-25 clusters[224].

2. OBJECTIVES

OBJECTIVES

Antibiotic-resistant bacteria that are difficult or impossible to treat are becoming increasingly common and are causing a global health crisis[104], thus, the discovery, of new and effective antibiotics is urgent.

In this sense, nanotechnology can provide alternative approaches to tackle this problem. For instance, silver based nanomaterials have shown interesting antimicrobial properties. Among them, AgNPs are the most employed, which preparation can involve chemical, physical or biological transformations[96]. Among the latter approach, the use of bacteria to obtain AgNPs have several advantages compared with the other methods and yields AgNPs with high antibacterial properties[96]. Other silver derivatives with antimicrobial activity are silver nanoclusters (AgNCs), which have been obtained using different methods and stabilizing agents[188,189]. In the last years the use of oligonucleotides to stabilize AgNCs has attracted the interest of scientific community. In this case, the nanostructures obtained are fluorescent, which properties can be modulated by the selection of the sequence of the oligonucleotide. There are multiple applications of DNA-AgNCs, most of them focused in the preparation of sensors. However, the bactericidal properties of AgNCs stabilized by oligonucleotides (DNA-AgNCs) have not been evaluated so far. Other methods that have shown good results in the treatment of resistance bacteria are those based on photodynamic therapy (PDT). In this case a molecule is exited by a light leading to the generation of reactive oxygen species (ROS), which destroy the bacteria. To the best of our knowledge the combination of this strategy with AgNCs has not been assessed.

Thus the three main objectives of the present work are:

1. Preparation of AgNPs using bacteria obtained in Antarctica and its evaluation as antimicrobial.

2. Evaluation of DNA-AgNCs as novel antimicrobials.

3. Evaluation of PDT combined with DNA-AgNCs.

In addition, and related to the use of oligonucleotides for biomedical applications we plan to address the following objective.

4. p21 regulation with oligonucleotides conjugated to gold nanoparticles.

3. MATERIALS & METHODS

MATERIALS & METHODS

3.1. Synthesis and antimicrobial activity of silver nanoparticles generated with Antarctic bacteria broths

3.1.1. Bacterial isolates

Four bacteria were chosen from a collection of bacterial isolates obtained from ice-melting waters collected at the St. George Island in Antarctica. The bacteria were isolated at 4 °C using nutritive medium (meat extract (Merck) 3 g/l, bacto-peptone (Difco) 10 g/l, NaCl (Merck) 5 g/l). Bacteria were identified based on their 16S rDNA sequences. For this, a colony of each isolate was suspended in lysis Buffer (SDS (Merck) 0.005%, Proteinase K (Roche) 400 ng/µl) and treated as previously described[225]. This DNA containing solution was used as the template for the amplification by the polymerase chain reaction (PCR) of most of the 16S rDNA sequence using the 27F and 1492R bacteria universal primers[226]. The amplicons were purified by the polyethylenglycol-NaCl method and sequenced by Macrogen (http://www.macrogen.com). Sequences obtained were edited using Finch TV (http://www. geospiza.com/Products/finchtv.shtml), and used for the phylogenetic adscription of the isolates by comparison with sequences in GenBank using the BLAST tool at the NCBI (http://blast.ncbi.nlm. nih.gov/Blast.cgi).

3.1.2. Synthesis of AgNPs

Psychrophilic bacteria were grown in whole or NaCl-deprived nutritive medium at 4 °C or 30 °C until the cultures achieved stationary phase. For testing the capability of broths to synthesize AgNPs, cells were eliminated by centrifugation at 17.530 × g at 4 °C and supernatants filtered through 0.22 µm pore size filters (Millipore). Supernatants were kept at 4 °C until used in the next few days. For AgNPs synthesis, equal volumes of supernatant and 2 mM $AgNO_3$ (Merck) solution were mixed and kept at the required temperature under fluorescent household lamps or in the dark. For kinetics studies, aliquots were taken at different times and the UV–vis spectrum recorded. Controls experiments containing

$AgNO_3$ (1mM), and medium supplemented with $AgNO_3$ were set and treated in the same light and temperature conditions.

3.2. Characterization of AgNPs

3.2.1. UV–vis spectroscopy

A spectrophotometer (WPA Biowave II+) was used for spectra recording between 300 and 700 nm, using the software provided by the company (PVC Biochrom). Measurements were done in conditions in which absorbance at λ_{max} was <1.5 by using dilutions of the samples in distilled water when needed.

3.2.2. Total Reflection X-ray Fluorescence (TXRF)

TXRF was used to determine AgNPs composition and concentration. AgNPs preparations were centrifuged to recover NPs (17.530 × g, 30 min), which were then washed twice with Milli-Q water before sent to the X-Ray facility of the Servicio Interdepartamental de Investigación (SIdI) at the Universidad Autónoma de Madrid. TXRF analysis were performed with a benchtop S2 PicoFox TXRF spectrometer from Bruker Nano (Germany), equipped with a molybdenum X-ray source working at 50 kV, 600 µA and 500 s with a XFlash SDD detector, effective area of 30 mm^2 and an energy resolution better than 150 eV for Mn K α.

3.2.3. Transmission Electron Microscopy (TEM)

AgNPs, samples were deposited on carbon covered copper grids and dried before visualizing them at the Electron Microscopy Service of the Centro de Biología Molecular Severo Ochoa under a JEM1010 Jeol (Japan) microscope working at 80 Kv. Photographs were taken using a TemCam F416 from TVIPS (Gauting, Germany), with a 4K × 4K sensor. For size determination, the Image J software (http://imageJ.nih.gov/ij) was used.

3.2.4. X-Ray Diffraction (XRD)

A diffractometer X'Pert PRO theta/2theta from Panalytical, with a Ge primary monochromator (Johansson monochromator) and an X'Celerator detector was used for analysis of the crystal structure of the AgNPs deposited on glass 2 × 2 cm microscope coverslips.

3.2.5. Dynamic Light Scattering (DLS)

The zeta potentials of AgNPs were measured at the Instituto Madrileno de Estudios Avanzados en Nanociencia (IMDEA) using a Zetasizer Nano series apparatus and Malvern 7.01 software.

3.3. Antimicrobial activity of AgNPs

To test antimicrobial activity, three types of bacteria were used: two Gram-negative: *Escherichia coli* (ATCC: 10536) and *Klebsiella pneumoniae* (ATCC: 29665), and a Gram-positive: *Staphylococcus epidermidis* (ATCC: 12128). Bacteria were grown in nutritive medium at 37 °C in a shaker at 230 rpm, then a dilution in fresh medium was performed and growth checked at 550 nm until the optical density (OD) reached 0.5.

For testing the antimicrobial activity of AgNPs, these were pelleted 30 min at 17530 × g, the supernatant removed and NPs resuspended in sterile Milli-Q water. For each AgNPs preparation, the UV–vis spectrum was recorded. Serial half dilutions of the AgNPs were performed in sterile Milli-Q water down to 1/64 and used for the tests, which were done in microtiter 96 wells plates, with duplicates for each concentration. Turbidity at 550 nm was recorded every hour in a Benchmark microplate reader (Biorad). For comparisons and IC_{50} calculations a 7h time of incubation was chosen. Concentrations of AgNPs preparations were determined by quantitative TXRF analysis of silver and NPs concentration expressed as their silver content. The IC_{50} data were extracted by using the Prism 6 software (http://www.graphpad.com/scientific-software/prism/).

The antibacterial activity of citrate-stabilized AgNPs (SIGMA) with a 10 nm average diameter size was determined to compare to the activity of biological AgNPs. Those NPs were treated in

the same way than the previous AgNPs. They were recovered by centrifugation from the commercial suspension and resuspended in Milli-Q water to be added to the bacterial cultures. The concentration of NPs was expressed as the silver concentration measured by TXRF.

3.4. DNA Silver Nanoclusters as novel nanoantibiotics

3.4.1. Oligonucleotide Synthesis

The oligonucleotides were prepared using a MerMade4 DNA Synthesizer using commercial phosphoramidites (Link Technologies). After the automated synthesis, the solid supports were transferred to a screw-cap glass vial with 2 ml of ammonia solution (33 %) and incubated at room temperature for 16h. Then, the solutions were transferred to microcentrifuge tubes and evaporated to dryness using an evaporating centrifuge.

The samples were purified by polyacrylamide gel electrophoresis 20% and the oligonucleotides eluted from gel fractions using an elutrap system. The solutions were desalted using a NAP-10 column and concentrated in an evaporating centrifuge.

3.4.2. Quantification of oligonucleotides

The concentration was obtained measuring the absorbance at 260 nm in a plate reader (BioTek-Synergy H4). The Extinction Coefficients were obtained from Integrated DNA Technologies (IDT, http://eu.idtdna.com/calc/analyzer).

3.4.3. MALDI-TOF MS

Matrix-assisted laser desorption/ionization time-of-flight mass spectrometry (MALDI-TOF MS) were used to determine the mass of oligonucleotides using 2,5-dihydroxyacetophenone (2,5-DHAP) as matrix at the 'Centro Nacional de Biotecnología', member of ProteoRed network (Table 3.1).

Table 3.1. Sequences employed for the preparation of AgNCs.

Name	Sequence	λ_{ex}-λ_{em} (nm)	Emitting Color	Calculated mass	Found
Seq-1	5´-TTTTCCCCTTTT-3´	370/475	Blue	3528.3	3518.01
Seq-2	5´-CCCTTAATCCCC-3´	480/572	Yellow	3501.3	3493.05
Seq-3	5´-CCCCCCCCCCCC-3´	540/580	Red	3408.2	3407.4
Seq-4	5´-CCCTTTAACCCC-3´	340/485	Blue	3501.3	3499.7
Seq-5	5´-CCCCTTTTCCCC-3´	340/495	Blue	3468.3	3466.7
Seq-6	5´-GGGTTAGGGTCCCCCCACCCTTACCC -3´	494/570	Yellow	7844.1	6218
Seq-7	5´-GGGTGGGTCCCCCCACCCACCC -3´	512/582	Yellow	6618.3	6626
Seq-8	5´-CCTCCTTCCTCC -3´	525/620	Red	3468.3	3466.7
Seq-9	5´-AGGTCGCCGCCC -3´	540/629	Red	3607.4	3605.9
Trimer (Seq-3)	$(5´\text{-}CCCCCCCCCCCC\text{-}3´)_3$-Benzene	540/580	Red	11206.1	11200.3

3.5. Synthesis of AgNCs

To an aqueous solution of the corresponding oligonucleotide (25 µmol), six equivalents of $AgNO_3$ per oligonucleotide strand were added. The final volumes were adjusted to 100 µl. The mixtures were incubated at room temperature for 10 min. Then, six equivalents, per strand, of a fresh solution of $NaBH_4$ were added to each sample and vortexed for 1 min. The resulting solutions were stored in darkness at room temperature for 6h and the excess of reagents removed using Amicon centrifuge filters (3K). The course of the reactions was monitored by fluorescence (BioTek-Synergy H4).

3.5.1. TXRF

TXRF was used to measure silver composition and concentration in the aqueous solution of DNA-AgNCs (Seq-1, Seq-2 and Seq-3). TXRF analysis of the DNA-AgNCs samples (200µl) was performed at the X-Ray facility of the Servicio Interdepartamental de Investigacion (SIDI) at the Universidad Autonoma de Madrid in a benchtop S2 PicoFox TXRF spectrometer from Bruker nano (Germany) equipped with a molybdenum X-ray source.

3.5.2. Circular Dichroism (CD)

Structural changes of the oligonucleotides were determined by CD using a JASCO (J-815 CD Spectrometer). 150µl of each sample (Seq-1, Seq-2, and Seq-3) before and after formation of AgNCs was employed.

CD spectra were determined using a Jasco J-815 CD spectrometer and 1 mm path length quartz cells at room temperature. The scanning speed was adjusted to 200 nm/min, and three accumulations were acquired.

3.6. Synthesis of AgNPs

AgNPs were synthesized by the chemical reduction of $AgNO_3$, using the same procedure employed for AgNCs but without the addition of the oligonucleotides (See 3.5). The UV-Vis spectra showed characteristic peak at 390 nm due to the formation of AgNPs.

3.7. Antibacterial activity test

3.7.1. Growth Curve Method

Escherichia coli DH5 alpha (ATCC:668369, Gram-negative) and *Staphylococcus epidermidis* (ATCC:6538p, Gram-positive) bacteria were chosen as a bacterial model to study the antibacterial properties of DNA-AgNCs.

The susceptibility of *E.coli* and *S.epidermidis* were first determined by growth curve method. Bacteria were cultured in Luria-Bertani (LB) medium to saturation. Bacteria culture was diluted

and grown for two hours until mid exponential phase (OD=0.5). Then, the bacteria culture was diluted to an OD (650nm = 0.1) in LB, as the starting point of the growth curve, and incubated at 37 °C for 14 h under shaking. DNA-AgNCs concentration was adjusted to 0.750 µM, 1.5 µM, 2.25 µM, 3 µM, 4 µM and 5 µM (based on the oligonucleotides absorbance) in a final volume of 200µl. The corresponding oligonucleotides were used at the same concentration as controls, as well as, $AgNO_3$ and AgNPs. Bacterial growth was determined by measuring the optical density (OD) at 650 nm every 1 h.

3.7.2. Agar Disk Diffusion Test

Kirby-Bauer disk diffusion susceptibility test was performed to determine the antibacterial activity of complexes formed with Seq-1, Seq-2 and Seq-3. For this purpose, *E.coli* bacteria were cultured in LB agar medium. DNA-AgNCs (5µmol) were placed on sterile paper discs, which were transferred to the agar plate and incubated at 37 °C for 24h. The presence or absence of inhibition zone is used as indicator of the sensitivity or resistance of the bacteria.

3.8. Synthesis of Trimers-DNA AgNCs

1,3,5-tris(azidomethyl) benzene

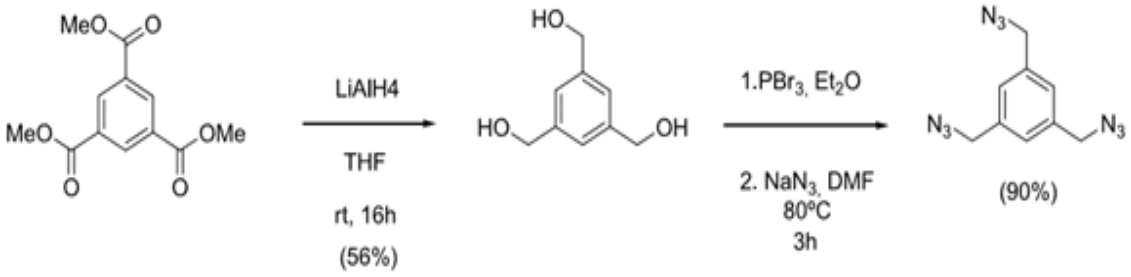

To a suspension of $LiAlH_4$ (247 mg, 6.5 mmol) in THF (5 ml) under N_2, was added slowly a solution of trimethyl benzene-1,3,5-tricarboxylate (500 mg, 1.97 mmol) in THF (5ml) and stirred for 16h at room temperature. The reaction mixture was hydrolyzed with MeOH at 0 °C and then with a saturated solution of sodium tartrate during 2 h. The mixture was washed with AcOEt and the aqueous phase acidified with HCl until neutral pH. Then, it was extracted with

AcOEt and after solvent evaporation the 1,3,5-tribenzyl alcohol was obtained and used without further purification as a colorless oil with 56% yield.

To a suspension of 1,3,5-tribenzyl alcohol (205 mg, 1.22 mmol) in (Et_2O 10 ml), PBr_3 (285 µl,3 mmol) was added and stirred for 16h. The mixture was hydrolyzed with a saturated solution of $NaHCO_3$ and extracted with AcOEt. After solvent evaporation, the white solid obtained was dissolved in DMF (5 ml) and NaN_3 (253 mg, 3.9 mmol) added and heated at 80 °C during 3 h. The mixture was washed with water, brine and extracted with AcOEt. After flash chromatography (eluent Hexane/AcOEt 8:1) 1,3,5-tris(azidomethyl) benzene was obtained as a colorless oil in 90% yield; ^1H NMR (300 MHz, $CDCl_3$) δ 7.26 (s, 3H), 4.40 (s, 6H).

3.9. Synthesis of modified solid support A (CPG-A)[146]

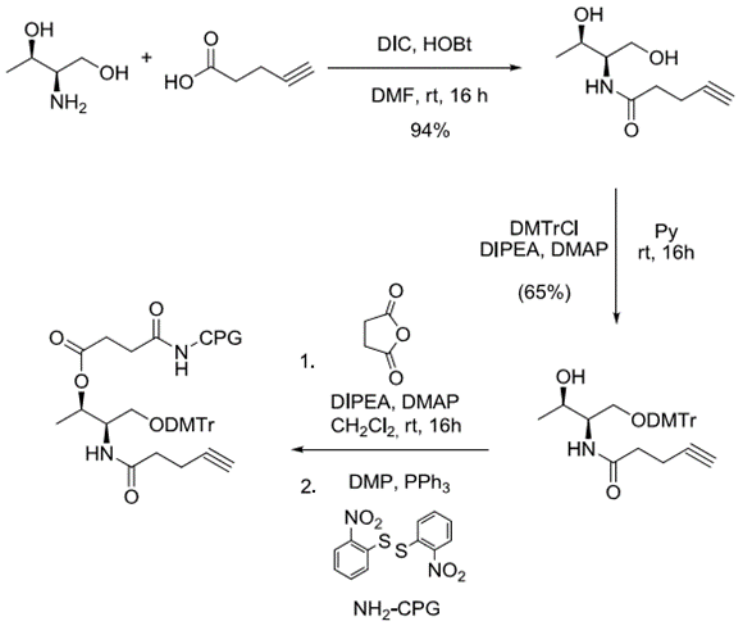

Figure3.2. Summary of CPG preparation.

***N*-((2R,3R)-1,3-dihydroxybutan-2-yl)pent-4-ynamide**

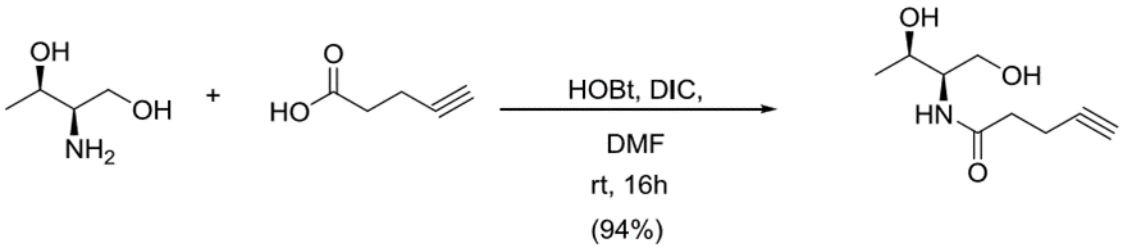

To a stirred mixture of 4-pentynoic acid (294 mg, 3.6 mmol), N-hydroxybenzotriazole (444 mg, 3.1 mmol) and N,N′-Diisopropylcarbodiimide (510 µL, 3.1 mmol) in DMF (7.2 ml) under N_2, L-threoninol (315 mg, 3mmol) was added at room temperature. After 16 h the reaction mixture was quenched with MeOH and the solvent evaporated in vacuum. After solvent evaporation and flash chromatography (eluent CH_2Cl_2/Hexane/MeOH 10:1:1) the desired compound was obtained as a colorless oil, in 94% yield; ^{1}H NMR (300 MHz, $CDCl_3$) δ 6.47 (s, 1H), 4.18 (d, J = 5.9 Hz, 1H), 3.82 (bs, 3H), 2.66 – 2.35 (m, 5H), 1.21 (d, J = 6.1 Hz, 3H); ^{13}C NMR (75 MHz, $CDCl_3$) δ 172.4, 82.8, 69.6, 67.7, 63.9, 55.1, 35.4, 20.2, 15.0; MS (ESI): m/z (%) 136 (27), 168 (M^+-OH, 39), 186 (M^++H, 25), 208 (M^++Na, 100); HRMS (ESI) calculated for $C_9H_{15}NO_3$ (M^++H) 186.1124, found 186.1141.

N-((2R,3R)-1-(bis(4-methoxyphenyl)(phenyl)methoxy)-3-hydroxybutan-2-yl)pent-4-ynamide

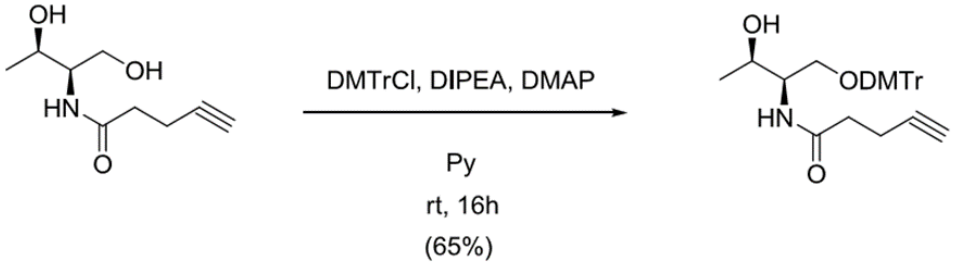

To a solution of the alkyne obtained previously (525 mg, 2.83 mmol) in pyridine (14 ml) at 0 °C, DIPEA (730 µl, 4.2 mmol), 4,4′-dimethoxytrithylchloride (1.15 g, 3.4 mmol) and DMAP (catalytic amount) were added. The mixture was stirred and allowed to reach room

temperature slowly. After 16 h, the solvent was evaporated and the residue purified by flash chromatography (eluent Hex/AcOEt 1:5 using silica gel deactivated with Et_3N) to obtain the desired DMT protected derivative in 65% yield as a yellow solid; ^{1}H NMR (300 MHz, $CDCl_3$) δ 7.42 (d, J = 7.2 Hz, 2H), 7.32 (d, J = 8.8 Hz, 4H), 7.38 – 7.22 (m, 3H), 6.88 (d, J = 8.8 Hz, 4H), 6.31 (d, J = 8.6 Hz, 1H), 4.22 – 4.09 (m, 1H), 3.99 (dd, J = 8.3, 2.4 Hz, 1H), 3.83 (s, 6H), 3.41 (ddd, J = 13.0, 9.6, 3.8 Hz, 2H), 2.63 – 2.44 (m, 4H), 2.02 (t, J = 2.4 Hz, 1H), 1.18 (d, J = 6.3 Hz, 3H); ^{13} C NMR (75 MHz, CDCl3) δ 171.3, 158.6, 144.3, 135.5, 135.3, 129.9, 129.9, 128.0, 127.9, 127.0, 113.3, 86.8, 82.9, 69.5, 68.6, 65.3, 55.2, 53.4, 35.5, 19.8, 15.0; MS (ESI): m/z (%) 303 (100), 510 (M^++Na, 23); HRMS (ESI) calculated for $C_{30}H_{33}NO_5$ (M^++Na) 510.2250, found 510.2249.

3.9.1. Solid Support A preparation

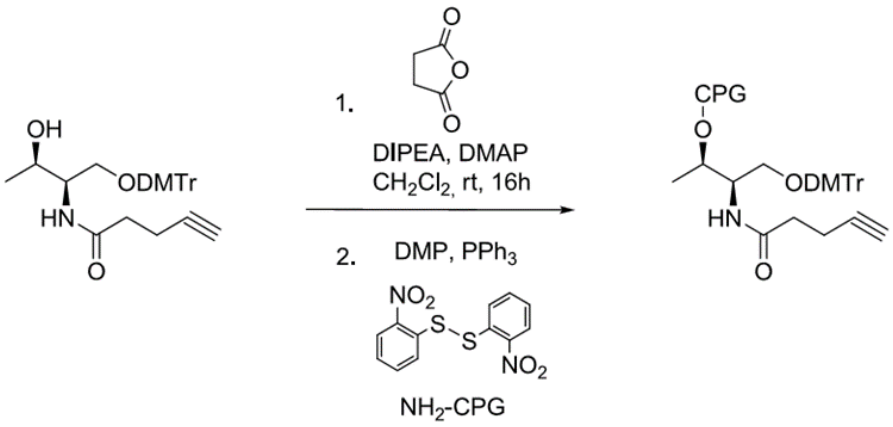

To a solution of DMT derivative obtained before (27 mg, 0.055mmol) in CH_2Cl_2 (0.4 ml), succinic anhydride (7.2 mg, 0.072 mmol), DIPEA (14 µl, 0.077 mmol) and DMAP (catalytic amount) were added under N_2 at room temperature. The mixture was stirred during 16 h, washed with water and dried with $MgSO_4$. After solvent evaporation, the residue obtained was dissolved in CH_3CN (1.2 ml) and DMAP was added. This solution was added to an eppendorf containing 2,2′-Dithiobis(5-nitropyridine) (25 mg, 0.08 mmol) and vortexed. This solution was added to a second eppendorf containing PPh_3 (21 mg, 0.08 mmol) and vortexed until complete dissolution. This mixture was added to 200 mg of Aminopropyl-CPG (500 Å) and stirred during 2h. The solvent was removed and the CPG washed with MeOH and CH_3CN. Once the CPG was

dry, 2 ml of a 1:1 mixture of capping reagents used on oligonucleotides synthesis [CAP MIX A: Acetic anhydride (400 µl)/ Py (600 µl)/ THF (500 µl); CAP MIX B: 1-Methylimidazol (400 µl)/ THF (1ml)] was added and stirred. After 25 min, the modified CPG was washed with MeOH, CH_3CN, and dried.

The CPG loading was calculated using the trityl quantification method. 10 mg of the modified CPG was treated with 5 ml of a detritylation solution (3 ml of perchloric acid and 2 ml of EtOH) and stirred during 30 min. Then, 100 µl of the mixture was diluted to 2.5 ml, and the absorbance was measured at 498 nm to quantify the trityl cation. Functionalization (F) was determined by Lambert-Beer law. The extinction coefficient (ε) at this wavelength is 70000 mol^{-1} dm^3 cm^{-1}. The loading obtained was 73.6 µM/gr.

3.9.2. Seq-3-alkyne modified click reaction

Seq-3 was synthesized with alkyne moiety at the 3'-end the modified CPG and then used in the preparation of Trimers through click reaction.

To an aqueous solution of the azide derivative (0.075 µmol), Seq-3-Alkyne (0.30 µmol, 4 equiv), NaCl (0.13M), CuI (1.78 mg, 9.35 µmol) and a solution of TBTA (tris[1-benzyl-1H-1,2,3-triazol 4yl)methyl] amine) (7.14 mg, 13.46 µmol) in DMF (357 µl) were added. The reaction was maintained at 55 °C for 16 hours. The product was purified by polyacrylamide gel electrophoresis 20% and eluted from gel fractions using an elutrap system. The solution was desalted using a NAP-10 column and concentrated in an evaporating centrifuge.

3.10. ROS Detection

To demonstrate the production of ROS in the presence of the different silver species used in this work, we used 2´,7´-dichlorodihydrofluorescin diacetate (DCFH-DA) as probe. In the presence of ROS, the acetyl residues are removed yielding the corresponding intermediate (DCFH), which is oxidized to the fluorescent 2',7'-dichlorofluorescin (DCF)[227].

Briefly, *E. coli* and *S. epidermidis* cells (OD 650= 0.1) were treated with 6 µl of a solution (0.750 µM) of the corresponding silver derivative, and incubated during 15h in a microplate reader, where the OD was recorded at intervals of 1h. At the end of the incubation time, cells were spun down at 9,300 x g, 4 °C for 5 min, washed thrice with water and resuspended in water. Then, 10 µl DCFH-DA (5 µM) was added and the final volumes adjusted to 200 µl. The cells were incubated during 2h at room temperature, with mild shaking (80 rpm) and in the dark. The fluorescence intensity was recorded ($\lambda_{ex/em}$= 488- 525 nm) after 2h. The ROS concentration can be directly related to the fluorescence intensity of the DCF dye. The ROS concentration was normalized by the cell density.

3.11. Modified oligonucleotides in photodynamic therapy for bacteria growth control

3.11.1. Synthesis of oligonucleotides bearing a photosensitizer

Different, oligonucleotides were prepared and purified containing hexachlorofluorecein (HEX) at the 5'end using the procedures described before for other oligonucleotides (Table 3.2).

Table 3.2. MALDI-TOF of the PS1, PS2, and PS3.

Name	Sequence	Calculated mass	Found
PS1	5´-HEX- CCCTTAATCCCC-3´	4245.43	4245.10
PS2	5´-HEX- CCCCCCCCCCCC-3´	4152.33	4152.08
PS3	5´-HEX- GGGTGGGTCCCCCCACCCACCC -3´	7362.43	7360.21

3.11.2. Synthesis of AgNCs

AgNCs were obtained as described before using the oligonucleotides modified with HEX.

3.11.3. Photodynamic therapy using oligonucleotides bearing HEX

The antibacterial activity test was carried out using two Gram-negative bacteria *E.coli* DH5 alpha (ATCC:668369) and *Pseudomonas aeruginosa* (ATCC:10145) and one Gram-positive bacteria *Staphylococcus aureus* (ATCC:25922). The susceptibility of *E. coli*, *P. aeruginosa* and *S.aureus* were determined by the growth curve method. Particularly, bacteria were cultured in LB medium to saturation, diluted and grown for two hours until mid exponential phase (OD=0.5). Then, the bacteria were diluted to an OD of 0.1 in LB, (the starting point of the growth curve), photoirradiated under the light system (intensity: 2.45 $mwcm^{-2}$ at 525 nm) for 2 hours and incubated at 37 °C for additional 24 h under mild shaking. HEX-DNA and HEX-DNA-AgNCs concentration was adjusted to 0.750 µM, 1.5 µM and 3 µM in a final volume of 200 µl. An oligonucleotide without HEX (Seq8), $AgNO_3$ and AgNPs were used as controls. The production of ROS was evaluated as described previously suing the DCFHDA probe (See 3.11).

3.12. p21 regulation with oligonucleotides conjugated to gold nanoparticles

3.12.1. Synthesis of citrate-capped AuNPs

To a boiling solution of $HAuCl_4$ (100 ml, 1 mM) in water, trisodium citrate (10 ml, 38.8 mM) was added and stirred for 15 min. The mixture was allowed to reach room temperature and filtered. Using its corresponding Extinction Coefficient ($2.7 \times 10^8 M^{-1}cm^{-1}$) and the Lambert-Beer's law the concentration was determined (13 nM).

Synthesis of modified solid support B for the release of oligonucleotides (CPG-B)

Synthesis of *N*-((2*R*,3*R*)-1,3-dihydroxybutan-2-yl)-3-mercaptopropanamide(A) .

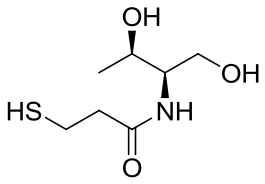

To a stirred mixture of 3-mercaptopropionic acid (100 mg, 0.94 mmol), *N*-hydroxybenzotriazole (135 mg, 1 mmol) and *N*,*N*´-Dicyclohexylcarbodiimide (206 mg, 1 mmol) in DMF (3 ml) under N_2, L-threoninol (100 mg, 0.94 mmol) was added at room temperature. After 16 h the reaction mixture was quenched with MeOH and the solvent evaporated in vacuum. To the residue 30 ml of CH_2Cl_2 was added, and the solid filtered off. After solvent evaporation and flash chromatography (eluent CH_2Cl_2/MeOH 15:1) compound A was obtained as a colorless oil, in 65% yield; ^{1}H NMR (300 MHz, $CDCl_3$) δ 6.55 (s, 1H), 4.17 (qd, *J* = 6.1, 2.0 Hz, 1H), 4.03 – 3.64 (m, 3H), 3.02 – 2.67 (m, 2H), 2.57 (t, *J* = 6.6 Hz, 2H), 1.63 (t, *J* = 8.3 Hz, 1H), 1.20 (d, *J* = 6.4 Hz, 3H); ^{13}C NMR (75MHz, $CDCl_3$) δ172.2, 67.7, 63.9, 55.1, 40.3, 29.6, 20.5; MS (ESI):*m/z* (%) 176 (M^+-OH, 11), 194 (M^++1, 10), 216 (M^++Na, 100); HRMS (ESI) calcd for $C_7H_{15}NO_3S$ (M^++1) 216.0660, found 216.0664.

Synthesis of 2-(Pyridyldithio)-ethylaminehydrochloride(PDA*HCl).

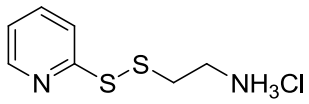

PDA*HCl was synthesized as reported (G.T. Zugates, D. G. Anderson, S. R. Little, I. E. B. Lawhorn, R Langer, *J. Am. Chem. Soc*. 2006, 128, 12726-12734)with some modifications. To a stirred solution of aldrithiol (213 mg, 0.96 mmol) in MeOH (1.1 ml), 2-mercaptoethylamine hydrochloride (109 mg, 0.96 mmol) was added. After stirring 1h, the solvent was evaporated and the residue washed with cold AcOEt three times. PDA*HCl was obtained as a white solid in 51% yield: ^{1}H NMR (300 MHz, d^6-CD_3OD)δ8.57 (d, *J* = 5.0 Hz, 1H), 7.83 (t, *J* = 7.7 Hz, 1H), 7.69 (d, *J* = 8.0 Hz, 1H), 7.35 (dd, *J* = 7.5, 5.0 Hz, 1H), 3.18 (t, *J* = 6.1 Hz, 2H), 3.07 (t, *J*= 6.8 Hz, 2H); MS (ESI):*m/z* (%) 107 (100), 153 (79), 187 (M^+-Cl, 12); HRMS (ESI) calcdfor $C_7H_{11}NS_2$(M^++1) 187.0366, found187.0391.

Synthesis of (*R*)-5-(1,2-dithiolan-3-yl)-N-(2-(pyridin-2-yldisulfanyl)ethyl)pentanamide (B).

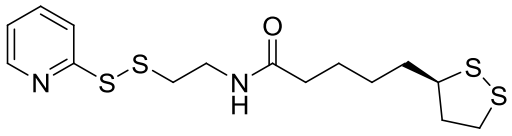

To a stirred mixture of (*R*)-(+)-α-Lipoic acid (134mg, 0.65 mmol), *N*-hydroxybenzotriazole (96 mg, 0.71 mmol) and *N*,*N´*-Dicyclohexylcarbodiimide (147, 0.71 mmol) in DMF (1.7 ml) under N_2, PDA*HCl (145 mg, 0.65 mmol) and DIPEA (147 µl, 0.71 mmol) were added at room temperature. After 16 h the reaction mixture was quenched with MeOH and the solvent evaporated in vacuum. To the residue 30 ml of CH_2Cl_2 was added, and the solid filtered off. After solvent evaporation and flash chromatography (eluent CH_2Cl_2/AcOEt 1:1) compound B was obtained as a colorless oil, in 14% yield;^{1}H NMR (300 MHz, $CDCl_3$) δ 8.48 (dd, *J* = 3.7, 1.1 Hz, 1H), 7.70 – 7.56 (m, 1H),7.51 (d, *J* = 8.0 Hz, 1H),7.23 – 7.08 (m, 2H),3.64 – 3.46 (m, 3H),3.22 – 3.02 (m, 2H),2.96 – 2.85 (m, 2H),2.43 (dq, *J* = 12.5, 6.4 Hz, 1H),2.21 (t, *J* = 7.4 Hz, 2H),1.97 – 1.80 (m, 1H),1.78 – 1.57 (m, 5H),1.54 – 1.38 (m, 2H);^{13}C NMR (75MHz, $CDCl_3$)δ172.9, 159.2, 149.7, 137.1, 121.4, 121.2, 95.7, 77.5, 77.1, 76.7, 56.4, 40.3, 39.0, 38.5, 37.3, 36.6, 34.7, 29.0, 25.4; MS (ESI):*m/z* (%) 225 (52), 264 (10), 375 (M^++1, 100); HRMS (ESI) calcdfor $C_{15}H_{23}N_2S_4$ (M^++1) 375.0675, found375.0687.

Synthesis of *N*-(2-((3-((2*R*,3*R*)-1,3-dihydroxybutan-2-ylamino)-3-oxopropyl)disulfanyl)ethyl)-5-((*R*)-1,2-dithiolan-3-yl)pentanamide (C)

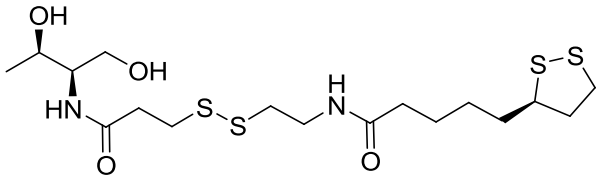

To a solution of disulfide B (45 mg, 0.12 mmol) in MeOH (1 ml) under N_2, a solution of compound A (23 mg, 0.12 mmol) in MeOH (1 ml) was added and stirred for 2 h. The solvent was evaporated and the residue purified by flash chromatography (CH_2Cl_2/MeOH 20:1) to obtain compound C as colorless oil in 88% yield; ^{1}H NMR (300 MHz, $CDCl_3$)δ6.88 (d, *J* = 8.3 Hz, 1H), 6.61 (t, *J* = 5.6 Hz, 1H), 4.23 – 4.03 (m, 1H), 3.91-3.74 (m, 5H), 3.62 – 3.47 (m, 3H), 3.02 (t, *J* = 6.8 Hz, 2H), 2.83 (t, *J* = 6.5 Hz, 2H), 2.68 (t, *J* = 6.7 Hz, 2H), 2.45 (dq, *J* = 12.4, 6.4 Hz, 1H), 2.22 (t, *J* = 7.4 Hz, 2H), 1.90 (dq, *J* = 13.7, 6.9 Hz, 1H), 1.78 – 1.55 (m, 5H), 1.45 (m, 3H), 1.19 (d, *J* = 6.4 Hz, 3H).^{13}C NMR (75 MHz, CDCl3) δ 173.9, 171.9, 68.6, 64.6, 56.4, 55.1, 40.2, 38.6, 38.5, 38.3, 36.5, 36.3, 34.9, 34.5, 28.8, 25.3, 20.4; MS (ESI):*m/z* (%) 301 (13), 457 (M^++1, 14),479 (M^++Na, 100); HRMS (ESI) calcd for $C_{17}H_{33}N_2O_4S_4$ (M^++1) 457.1334, found 457.1317; HRMS (ESI) calcd for $C_{17}H_{32}N_2O_4NaS_4$ (M^+) 479.1166, found 479.1137.

Synthesis of *N*-(2-((3-((2*R*,3*R*)-1-(bis(4-methoxyphenyl)(phenyl)methoxy)-3-hydroxybutan-2-ylamino)-3-oxopropyl)disulfanyl)ethyl)-5-((*R*)-1,2-dithiolan-3-yl)pentanamide (D).

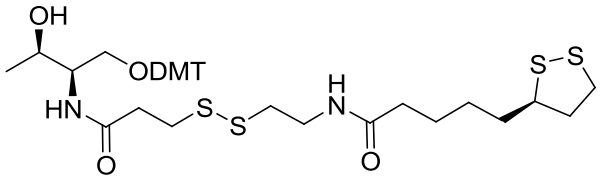

To a solution of compound C (74 mg, 0.16 mmol) in pyridine (0.8 ml) at 0 ºC, DIPEA (43 µl, 0.24 mmol) and 4,4'-dimethoxytrithylchloride (64 mg, 0.19 mmol) were added. The mixture was stirred and allowed to reach room temperature slowly. After 16 h, the solvent was evaporated and the residue purified by flash chromatography (eluent Hex/AcOEt 1:9 using silica gel deactivated

with Et_3N) to obtain compound D in 35% yield as a yellow solid; ^1H NMR (300 MHz, $CDCl_3$) δ7.39 – 7.27 (m, 2H), 7.27 – 7.11 (m, 7H), 6.76 (d, *J* = 8.8 Hz, 4H), 6.41 – 6.21 (m, 2H), 4.13 – 3.96 (m, 2H), 3.95 – 3.83 (m, 1H), 3.71 (s, 6H), 3.42-3.51 (m, 3H), 3.28 (ddd, *J* = 36.7, 9.6, 4.1 Hz, 2H), 3.13 – 2.97 (m, 2H), 2.92 (t, *J* = 6.8 Hz, 2H), 2.73 (t, *J* = 6.2 Hz, 2H), 2.57 (td, *J* = 6.9, 2.7 Hz, 2H), 2.45 – 2.26 (m, 1H), 2.10 (t, *J* = 7.4 Hz, 2H), 1.80 (dq, *J* = 13.5, 6.9 Hz, 1H), 1.57 (qd, *J* = 13.2, 11.1, 6.8 Hz, 4H), 1.46 – 1.26 (m, 2H), 1.07 (d, *J* = 6.4 Hz, 3H); MS (ESI): *m/z* (%) 303 (100), 781 (M^++Na, 15); HRMS (ESI) calcd for $C_{38}H_{50}N_2O_6S_4$ (M^++Na) 781.2455, found 781.2443.

Synthesis of Solid Support B (CPG-B)

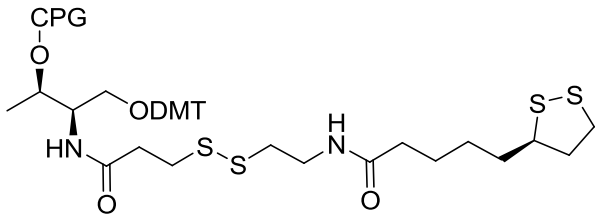

To a solution of compound D (40 mg, 0.052 mmol) in CH_2Cl_2(0.4 ml), succinic anhydride (6.8 mg, 0.068 mmol), DIPEA (13 µl, 0.072 mmol) and DMAP (catalytic amount) were added under N_2 at room temperature. The mixture was stirred during 16 h, washed with water and dried with $MgSO_4$. After solvent evaporation, the residue obtained was dissolved in DMF (1.2 ml), and HBOt (7 mg, 0.052 mmol) and DCC (10 mg, 0.052 mmol) were added. This mixture was added to 400 mg of CPG (500 Å) and stirred during 2h. The solvent was removed and the CPG washed with CH_2Cl_2 gently. Once the CPG was dry, 2 ml of a 1:1 mixture of capping reagents used on oligonucleotides synthesis [CAP MIX A: Acetic anhydride (400 µl)/ Py (600 µl)/ THF (500 µl); CAP MIX B: 1-Methylimidazol (400 µl)/ THF (1 ml)] was added and stirred. After 25 min, the modified CPG was washed with MeOH, CH_3CN, and dried.

3.12.2. Synthesis of p21 Antisense and Gampers

Two Antisense oligonucleotides (Antisense 1 and 2) with and without PolyT (T_5) as spacer were synthesized using 2´-O-Me (OMe) RNA Phosphoramidites (Link) using the solid support described above at the 3'-end. The antisense were designed to target the p21 gene at the regions 141-160 nt (antisense 1) and 521-540 nt (antisense 2) (Obtained from GenBank at the NCBI: Mus musculus cyclin-dependent kinase inhibitor 1A (P21) (Cdkn1a), transcript variant 1, mRNA). In the case of Gapmers a mixture of OMe-RNA (in bold) and DNA phosphoramidides were employed (Table 3.3).

Table 3.3. Sequences and MALDI-TOF of the Antisense and Gapmer. All sequences contain a dithiolane group at the 3'-end.

Name	Sequence	Calculated mass	Found
Antisense 1	5´- AGA CAA CGG CAC ACU UUG C-TTTTT-3´	7778.7	7653.8
Antisense 2	5´-AUAGAAAUCUGUCAGGCUG-TTTTT-3´	7820.7	8130.9
Gapmer	5´-**GAUAG**AAATCTGTCA**GGCUG**-3´	6671	6575.01

3.12.3. Synthesis of siRNA

In this case the siRNA against p21 was prepared using the sequence of the antisense 2. Commercial RNA phosphoramidites were employed, at uracil sites , 2'-OMe-Uracil derivatives were employed. The modified CPG bearing the dithiolane moiety was employed. After solid-phase synthesis, the solid support was transferred to a screw-cap glass vial with 2 ml of ammonia and 500 µl of Ethanol. The mixture was incubated at room temperature for 16 h and then evaporated to dryness using an evaporating centrifuge. Then, tetrabutyl ammonium fluoride (0.333 µl) was added and the mixture incubated at room temperature for 24 h. After that, 0.333 µl of triethylammonium acetate (TEAA, 1 M) in water and 0.333 µl of RNase-free water were added to quench the reaction. Then, the samples were desalted using NAP-10 columns and concentrated in an evaporating centrifuge. The oligonucleotides were purified by polyacrylamide gel electrophoresis 20% and eluted from gel fractions using an elutrap system. The solutions were desalted using a NAP-10 column, concentrated in an evaporating centrifuge

and quantified. The desired double stranded RNA structures, were obtained by an annealing process where the oligonucleotides at equimolar concentrations in an annealing buffer (10 µM Tris, 1 µM EDTA, 50 µM NaCl) were, heated at 90 °C for 3 min and cooled down slowly to room temperature. The siRNA duplexes were employed in the functionalization of AuNPs as described in section 3.12.2 (Table 3.4).

Table 3.4. MALDI-TOF of the Passenger and Guide strands. U are modified with 2'-OMe groups.

Name	Sequence	Calculated mass	Found
Passenger	5´- CAG CCU GAC AGA UUU CUA U-TTTTT-3´	7717.6	7742.2
Guide	5´- AUA GAA AUC UGU CAG GCU G-3´	6908.1	6655.9

3.12.4. Modified AuNPs

To 1 ml of the AuNPs solution the corresponding oligonucleotides was added (1 nM) and incubated at the room temperature by middle shake to overnight. After 2 h of the addition NaCl was added to reach a final concentration of 0.3 M to improve the functionalization of the AuNPs. At the end of the incubation time the oligonucleotides were spun down at 16,100 x g, 4 °C for 30 min, washed thrice and resuspended in RNase-free water and immediately were sent to CNB (Centro Nacional de Biotecnologia, Immunology & Oncology unit, Lab 412) for its evaluation (See 3.13).

3.13. p21 T-cell Transfection

3.13.1. Mice

Control C57BL/6 mice were obtained from Harlan Interfauna Ibérica (San Felíu de Codines, España). C57BL/6-p21-/-mice (p21-/-) were generated by crossing p21-/-129/Sv mice (laboratory of Dr. Gregory Hannon, Cold Spring Harbor Laboratory, NY, USA) with C57BL/6 mice over eight generations. Background analysis via microsatellite markers confirmed >99% identity with the B6 background 56. All mouse experiments were performed in accordance with European Union and national regulations, and were approved by the CNB Bioethics Committee.

3.13.2. Cell culture

Mouse $CD4^+$ spleen T-cells were purified by Negative Isolation Kit (Dynal Biotech), 85% pure $CD4^+$ T-cells were obtained. Purified naive T-cells (10^6/ml) were stimulated *in vitro* with concanavalin A (ConA; 3 mg/ml, Sigma) in medium containing 20 ng/ml human recombinant interleukin-2 (rIL-2, PeproTech). After 24h, cells were washed and cultured in medium with 20 ng/ml IL-2 (5 days).

3.13.3. Cell culture medium

Purified $CD4^+$ T-cells were cultured in RPMI-1640 medium supplemented with 10% FCS (fetal calf serum, Harlan Bioproducts, SeraLab), 2 mM L-glutamine, 100 U/ml penicillin, 100 mg/ml streptomycin, 1 mM sodium pyruvate, 10 mM HEPES pH 7.4, 0.1 mM nonessential amino acids and 50 mM β-mercaptoethanol (all from Gibco Life Technologies).

3.13.4. Treatment with Modified AuNPs

The incubation with AuNPs was carried out at the end of 5-days IL-2 expansion. T-cells were transfected also with siRNA against p21 using a conventional method (Amaxa-Lonza Mouse T-cell Nucleofector kit, VPA-1006) as a control. A nonsense sequence (poly T) was used as

control. Five million cells were transfected with 100 µl (different concentration from 100-200 nm) of siRNA conjugated to AuNPs in complete medium without serum and antibiotics. 4-24 hours after transfection, the cells were stimulated again with Con-A in presence of a caspase inhibitor zVAD (25 µM) in complete medium at different time points.

In the case of conventional method, the procedure was done according to the instruction manual. Briefly, the cells were centrifuged and resuspended in the 4D Nucleofector™ solution and siRNA added to cells. This mixture was added to the nucleocuvette™ Vessels and electroporated. Pre-warmed fully supplemented Mouse T-cell Nucleofector™ medium was added and incubated for 4 hours. Then restimulated again with ConA and zVAD at different times (Fig 3.3).

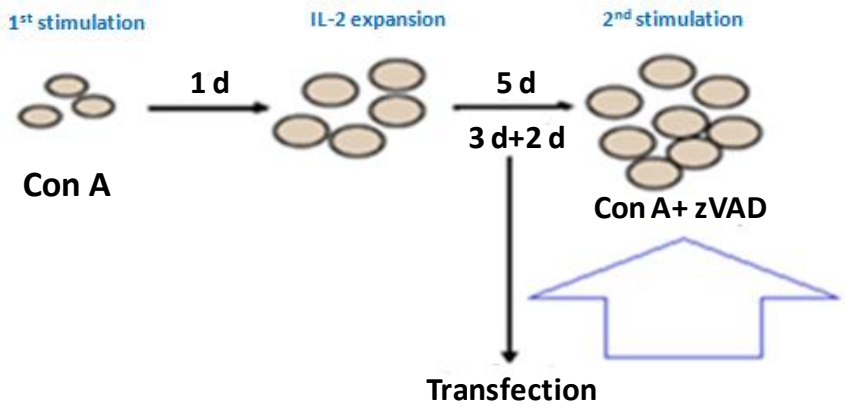

Figure3.3. T cell transfection by oligonucleotides (AuNPs and Electroporation methods).

3.13.5. Western blot

Protein lysates of cultured cells (5 x 10^6 cells/sample) were obtained by lysis of $CD4^+$ T-cells for 20 min on ice using a 0.2% NP-40 lysis buffer (10 mM Tris HCl pH 7.5, 150 mM NaCl, 0.2% NP40) supplemented with Phosphatase Inhibitor Cocktail (PhosStop) and Complete Protease Inhibitor Cocktail (both from Roche). After quantification of protein concentration by Bradford assay (Bio-Rad), equal protein amounts (5-15 µg) were separated on 12% acrylamide gels and transferred to a nitrocellulose membrane (Bio Rad). Membranes were blocked in 5% low fat milk (1x TBS + 0.05% Tween 20) and incubated with primary antibody dilutions as recommended by the manufacturer. Primary antibodies were purchased from Cell Signalling

(anti-pERK, -ERK, -AKT, -pPKCθ), Santa Cruz Biotechnology (anti-p21, -CARMA1) or Sigma (anti-β-actin). After incubation with appropriate peroxidase-conjugated secondary antibodies (all from Dako), proteins of interest were detected by chemiluminescence (ECL, Perkin Elmer) on X-ray film (Kodak Minolta).

3.13.6. Flow cytometry (Fluorescence-Activated Cell Sorting, FACS)

Transfection efficiency was evaluated by flow cytometry (CYTOMICS FC500, Beckman Coulter) at 24 h and 48 h after transfection 500 µl of each sample (modified AuNPs and siRNA using), poly T conjugated FAM ($\lambda_{ex/em}$= 494-525 nm) modified AuNPs, employed as fluorescein dye which directly applied to the cytometry and transfection was measured in FL1 (525 nm).

4. RESULTS

RESULTS

4.1. Synthesis and antimicrobial activity of silver nanoparticles generated with Antarctic bacteria broths

4.1.1. Synthesis of AgNPs

Silver nanomaterials have been produced using different bacteria, however, the reports where extremophiles[66] and particularly psychrophilic bacteria[68,69] are scarce.

In the present study, four psychrophilic bacteria isolated from Antarctic ice-melting waters have been identified by molecular analysis and their broths employed in the synthesis of AgNPs.

Their phylogenetic adscription was confirmed from a unique colony on nutritive solid medium through PCR amplification of the 16S rDNA genes, and sequencing using universal primers[226].

The isolated bacteria are strains belonging to the following species:

***Psychrobacter* sp**[228]. A Gram-negative, osmotolerant, oxidase-positive, and aerobic bacteria, considered rare opportunistic human pathogen.

Aeromonas salmonicida[229]. A Gram-negative, facultative anaerobic, non-motile bacterium, which is a fish pathogen.

Pseudomonas veronii[230]. A Gram-negative, rod-shaped, motile bacterium, which have industrial applications, such as bioremediation of contaminated soils from aromatic organic compounds.

Yersinia kristensenii[231]. A Gram-negative bacteria that is potentially infectious to mice.

To the best of our knowledge, the production of AgNPs mediated by these types of bacteria have not been evaluated. In this case, broths of cultures of the different bacteria were incubated with $AgNO_3$ to yield AgNPs. Since the bacteria employed are psychrophilic (grow in cold waters) we decided to evaluate the effect of the temperature during the production of the broths and also during the reaction with $AgNO_3$. Particularly, two different temperatures were evaluated, 4 °C and 30 °C.

The effect of the light was also assessed, since it has been shown that it is required in the biosynthesis of AgNPs[232,233] particularly the use of blue light[234], although in some cases AgNPs can be obtained without light[235].

In addition, the effect of NaCl in the reaction mixture was also studied. Different reports have shown that the presence of NaCl during the biosynthesis of AgNPs might induce their aggregation or decrease their yield[236,237], probably be due to the formation of the insoluble AgCl in the reaction mixture. However, N. Mokhtari *et al*, have reported that AgCl itself could be employed in the preparation of AgNPs using supernatants from *Klebsiella pneumonia* [238]. In addition, psychrophilic bacteria can stand salty water better than other bacteria. For these reason we decided to check the effect of NaCl in the production of AgNPs [238, 239].

Bacteria were grown in nutritive medium with and without NaCl at 4 °C or 30 °C. The corresponding supernatants were mixed with $AgNO_3$ (1 mM) and kept in the light or in the dark. The generation of AgNPs was followed by UV-vis spectroscopy, since they present a characteristic band around 400-450 nm due to the surface plasmon resonance (Fig 4.1). In our case, the production of AgNPs was only observed when the process was carried out under the light.

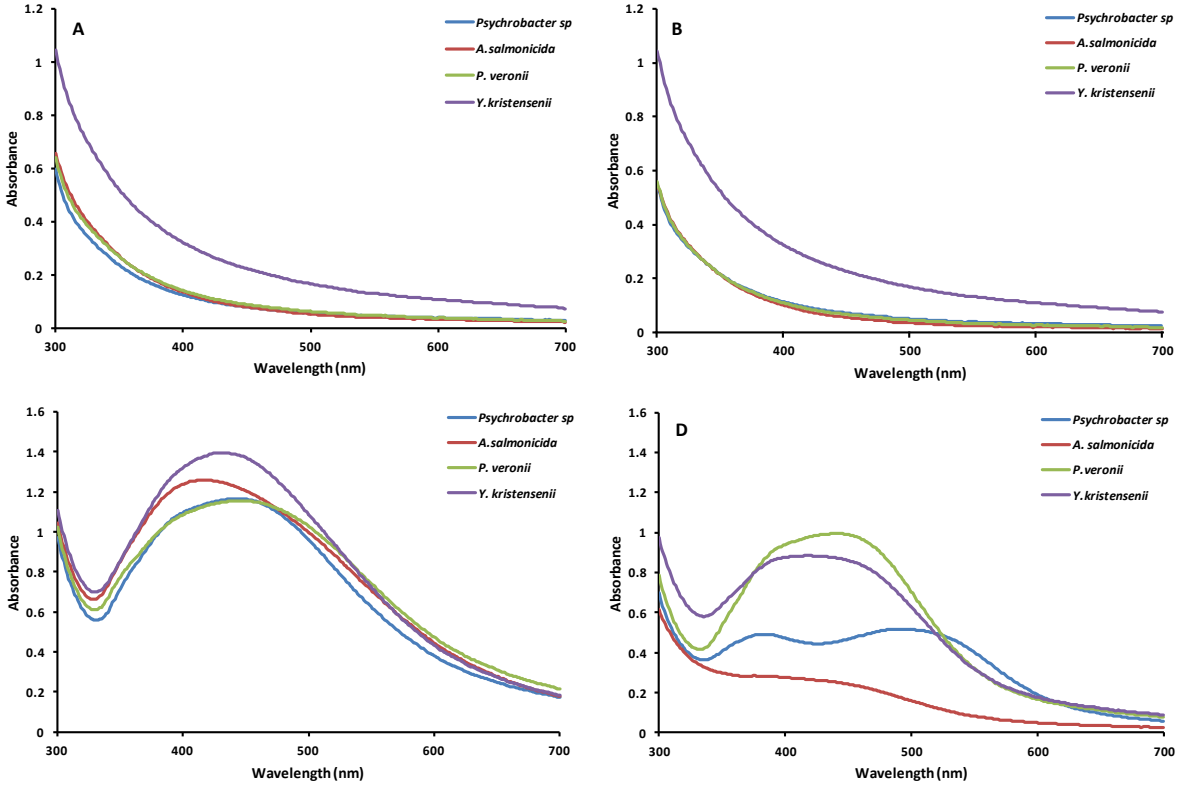

Figure 4.1. UV-spectra of reaction mixtures incubated in the dark during 5 days. **A**). at 30 °C and **B**). at 4 °C., and in the light during 5 days. **C**). at 30 °C and **D**). at 4 °C.

The UV-Vis spectra of the samples revealed that the production of AgNPs using broth from cultures containing NaCl (5 g/l, 85.5 mM) was lower than those carried out without NaCl at both temperatures (Fig 4.2). The low temperature (4 °C) also reduced the formation of AgNPs (Fig 4.2C and 4.2D), and when the addition of NaCl and low temperature where combined, the generation of AgNPs was completely suppressed (Fig. 4.2D).

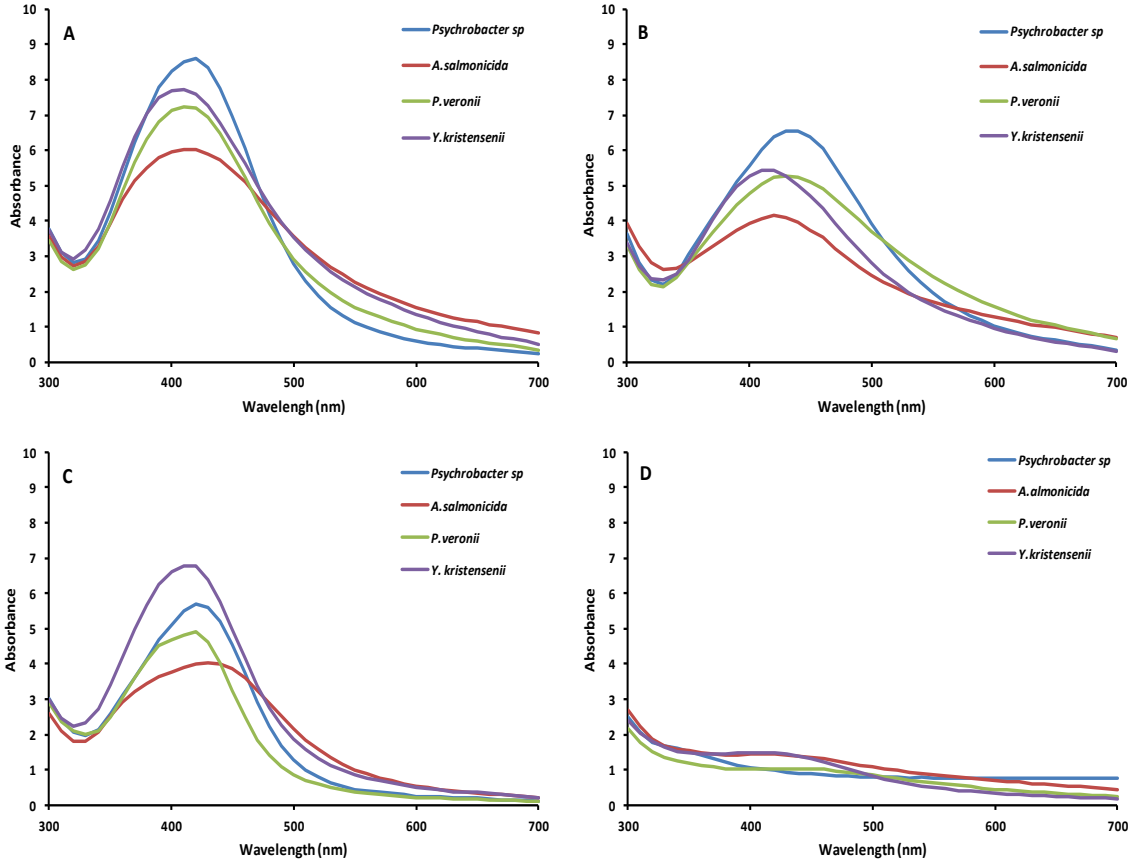

Figure 4.2. Comparison of UV-vis spectra of AgNPs produced with broths **A**). without NaCl ,**B**). with NaCl at 30°C and **C**). whitout NaCl, **D**).with NaCl at 4°C.

The evolution of the AgNPs was followed by UV-Vis spectrophotometry during many days. Broths from *Y. kristensenii* produced AgNPs more efficiently at both temperatures (Fig 4.3 and 4.4), reaching the maximum after 19 days at 30 °C and after 298 days at 4 °C. On the other hand, broths from *A. salmonicida* at 4 °C, were the less active. These results correlate well with the yields obtained at

day 9 from aliquots of each experiment (Table 4.1). Yields were obtained after 9 days by removing AgNPs from the suspension by centrifugation, and measuring silver concentration in the supernatants.

We observed that using broths of *Psychrobacter* sp. at 4 °C and *Y. kristensenii* at 30 °C the shape of the spectra showed a bimodal distribution with peaks at 394 and 403 in the first case and 461 and 464 nm in the later one. However only a single peak was detected after longer incubation times.

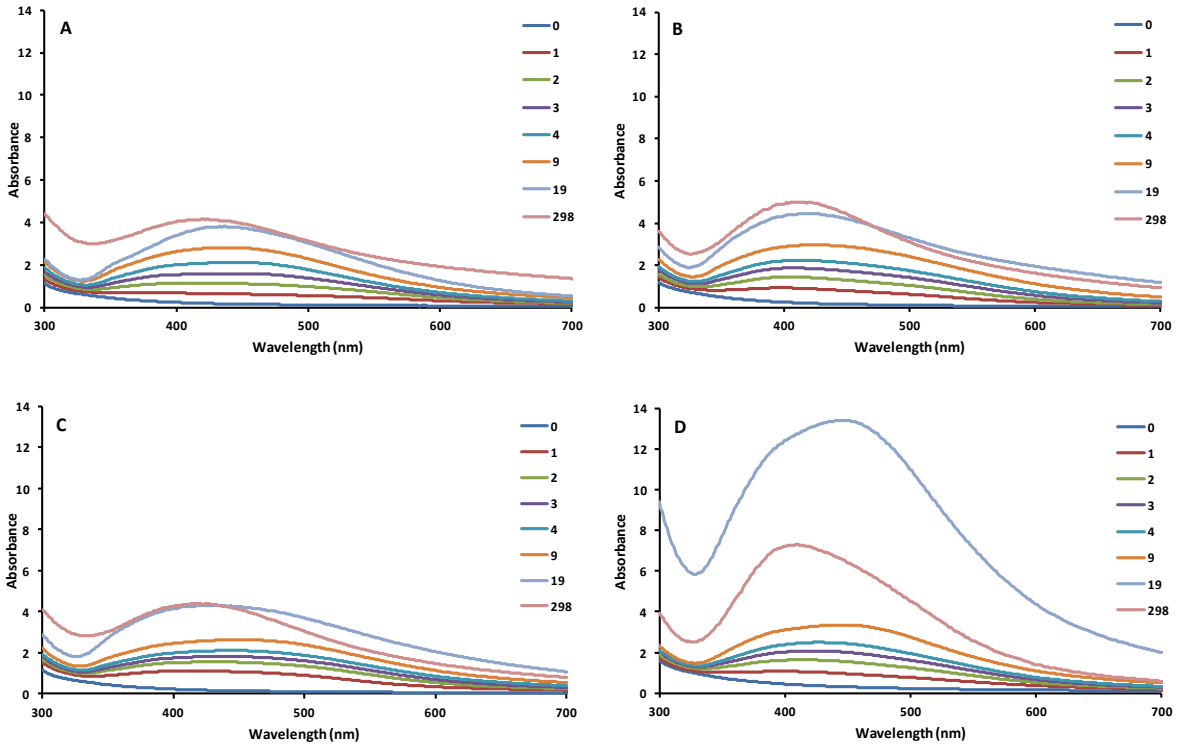

Figure 4.3 . UV-Vis spectra due to the generation of AgNPs along several days at 30 °C using broths from cultures of psychrophilic bacteria. **A**). *Psychrobacter* sp, **B**). *A. salmonicida*, **C**). *P.veronii*, **D**). *Y.kristensenii*.

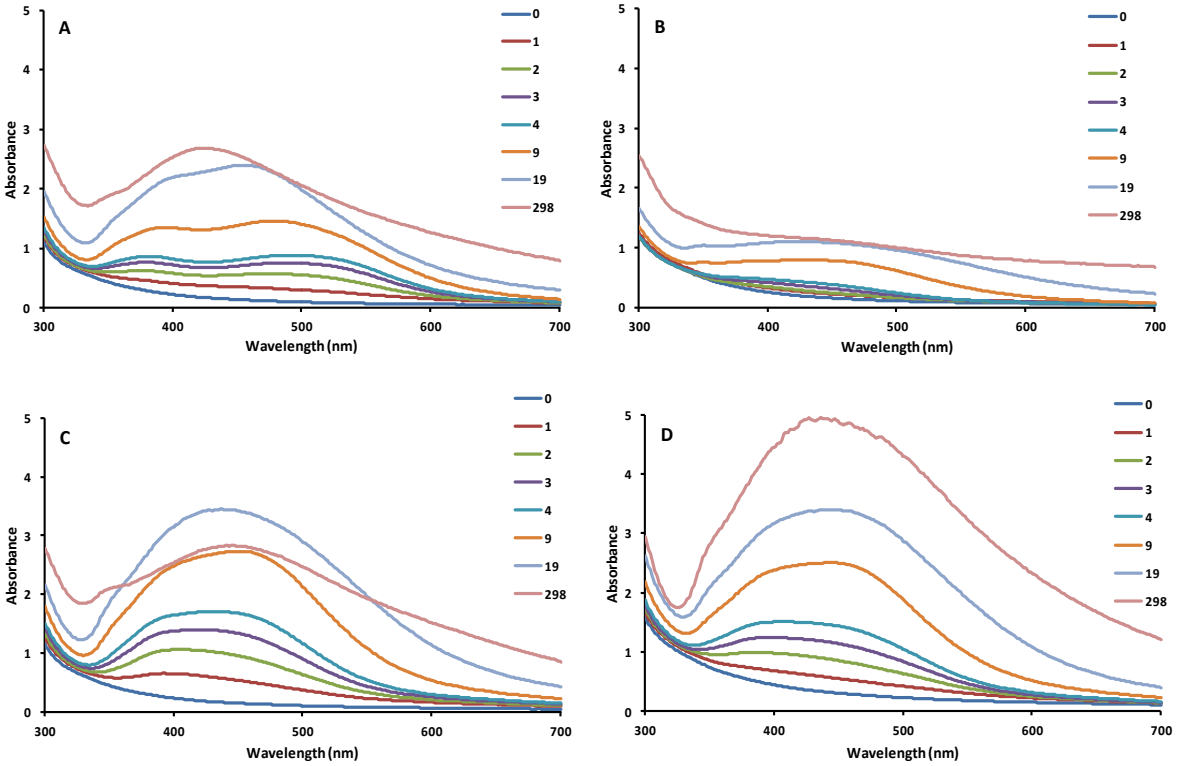

Figure 4.4 UV-Vis spectra due to the generation of AgNPs along several days at 4°C using broths from cultures of psychrophilic bacteria. **A**). *Psychrobacter* sp, **B**). *A. salmonicida*, **C**). *P.veronii*, **D**). *Y.kristensenii*.

4.1.2. Characterization of AgNPs

The shapes and sizes of AgNPs obtained at 30 °C (Fig. 4.5) and 4 °C (Fig 4.6) were studied by TEM. The shape of all the AgNPs was nearly spherical. The average size of AgNPs produced by the different bacteria was around 6 nm, with the exception of the AgNPs obtained with broths from *A. salmonicida* at 30 °C, which were noticeably larger (average size 11.1 nm) (Figure 4.6B).

Size distributions for the different AgNPs are shown as histograms in (Fig 4.7 and 4.8), where the averages sizes and PDIs obtained from the different broths and temperatures are summarized in Table 4.1. PDIs were calculated using the formula: PDI= (σ/γ)[241], were σ is the standard deviation of the measured diameter sizes of the NPs, and γ their mean[242].

Table 4.1. Yields, sizes and PDI obtained at different temperatures.

	T (°C)	*Psychrobacter sp*	*A.salmonicida*	*P.veronii*	*Y.kristensenii*
Yield(%)	4	24	12	38	36
	30	44	49	46	53
Average (nm)	4	7.6	6.2	5	6.1
	30	6.6	11.1	5.1	6.8
PDI	4	0.1	0.17	0.23	0.18
	30	0.25	0.21	0.21	0.21

PDI of 0.0 corresponds to monodisperse AgNPs, up to 0.1 AgNPs are considered very close monodisperse, from 0.1 to 0.4 AgNPs are moderate polydisperse, and values >0.4 indicate broad polydisperse[243, 244]. Following this classification most of our AgNPs can be considered as moderate polydisperse preparations, and those prepared at 4 °C using *Psychrobacter* sp. broth, as near-monodisperse. Except for AgNPs obtained with broths from *P. veronii*, the dispersity seems to be lower for preparations made at 4 °C than for those at 30 °C.

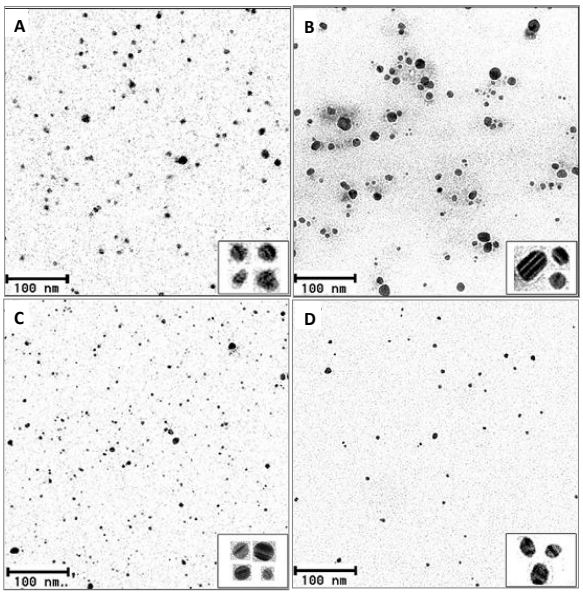

Figure 4.5. TEM representative images of AgNPs produced at 30 °C by the culture broths of **A**). *Psychrobacter* sp, **B**). *A. salmonicida*, **C**). *P. veronii*, **D**). *Y. kristensenii*. Inserts display a higher magnification of some NPs showing crystalline patterns.

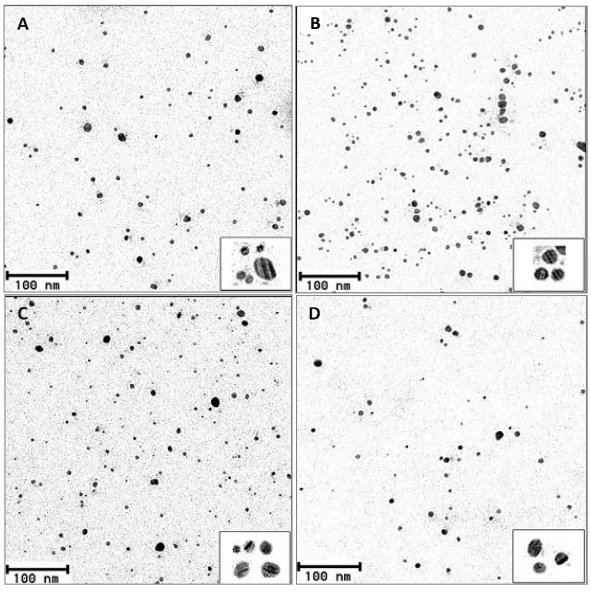

Figure 4.6. TEM representative images of AgPs produced at 4 °C by the culture broths of **A**). *Psychrobacter* sp, **B**). *A. salmonicida*, **C**). *P. veronii*, **D**). *Y. kristensenii*. Inserts display a higher magnification of some NPs showing crystalline patterns.

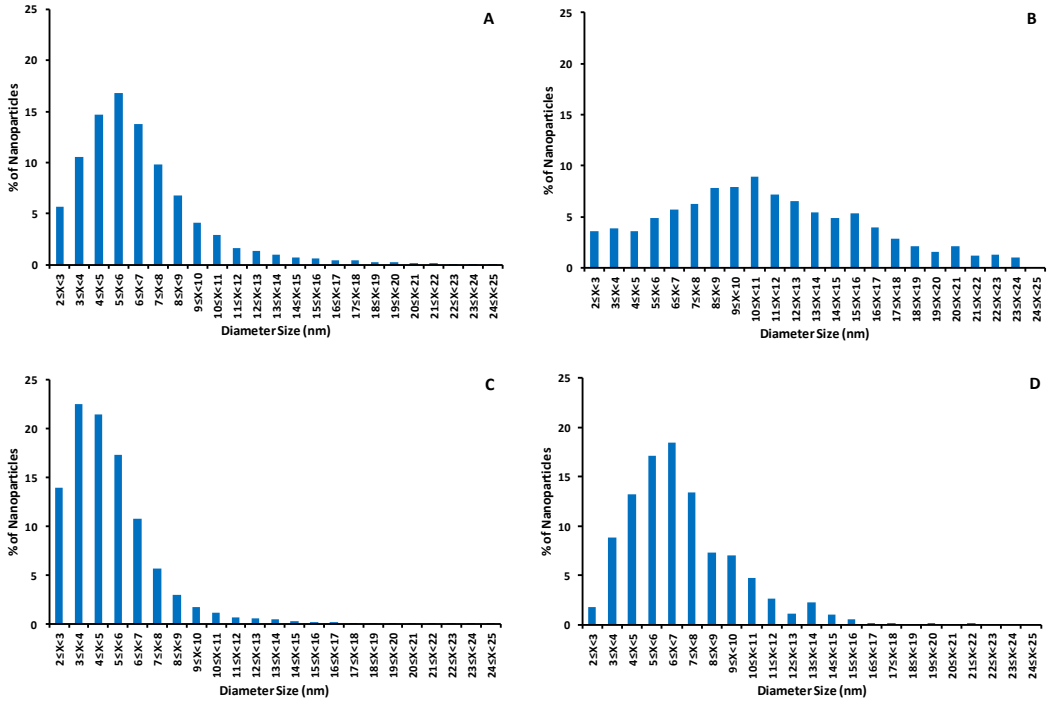

Figure 4.7. Distribution of AgNPs sizes obtained at 30 °C using broths from **A**). *Psychrobacter* sp, **B**). *A. salmonicida*, **C**). *P. veronii*, **D**). *Y. kristensenii*.

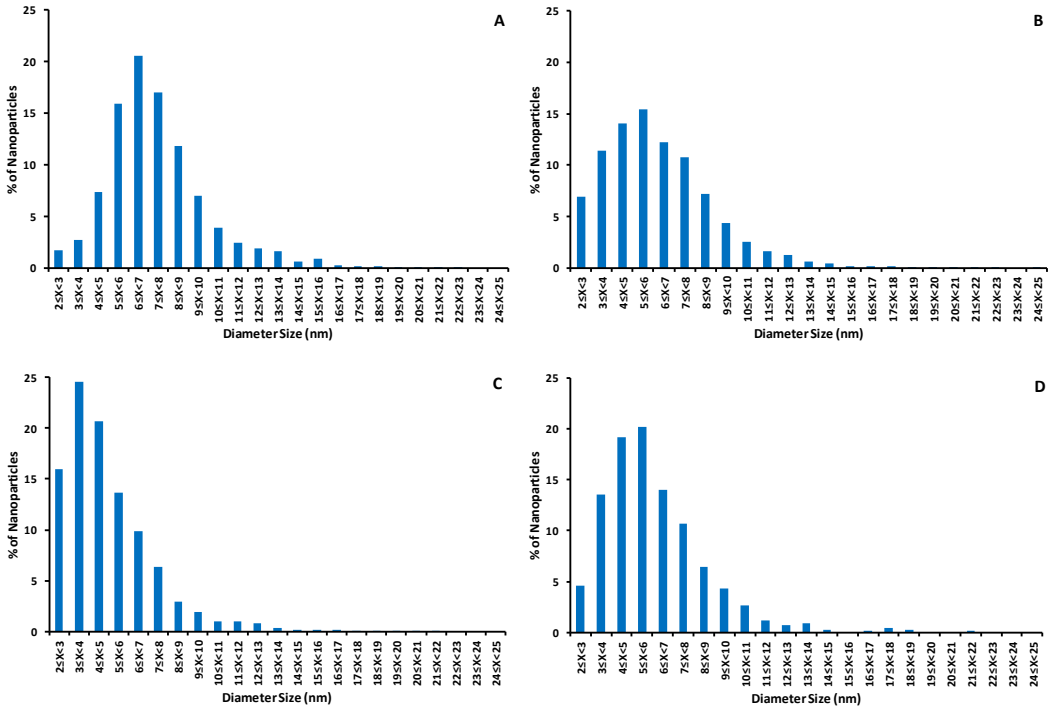

Figure 4.8. Distribution of AgNPs sizes obtained at 4 °C using broths from **A**). *Psychrobacter* sp, **B**). A. *salmonicida*, **C**). *P. veronii*, **D**).*Y. kristensenii*.

The Zeta potentials of the AgNPs were measured using a Zetasizer™ and in all cases negative values were obtained. This value is related with charges surrounding the particles, which provide colloidal stability preventing their aggregation or flocculation. Particles with high values (above 30) are stable for months. The highest potential was obtained from the particles prepared with the broth of *A. salmonicida* at 30 °C, and the lowest from the particles prepared at 4 °C using broths from *P. veronii*.

Table 4.2. Zeta potentials (mV) of the AgNPs prepared with broths from the different bacteria at 4 °C and 30 °C.

T (°C)	*Psychrobacter sp*	*A.salmonicida*	*P.veronii*	*Y.kristensenii*
4	-20.7±2.7	-25.8±2.1	-17.6±1.9	-24.5±2.2
30	-21.1±2.2	-26.8±3.1	-24.2±1.5	-21.7±2.5

To determinate the crystalline nature of the NPs obtained in the different conditions, XRD analysis was performed. XRD is a rapid analytical technique primarily used for phase identification of a crystalline material and can provide information on unit cell dimensions. XRD is based on constructive interference of monochromatic x-ray and a crystalline sample (Fig 4.9 and SI 2).

The results of this analysis showed the presence of crystalline structures in all the AgNPs, with similar 2θ angles for the diffraction peaks around 38.17, 43.92, 64.53, 77.45 and 81.37 degrees. These peaks correspond respectively to the (1 1 1), (2 0 0), (2 2 0), (3 1 1), and (2 2 2) planes of the face-centered cubic structure of metallic silver crystals (JCPDS file no. 04-0783). The relative intensity of the different Bragg reflections indicates a predominant orientation of the crystals with the (1 1 1) planes preferentially parallel to the supporting substrate. This predominant orientation seems to be higher for the AgNPs prepared at 4 °C.

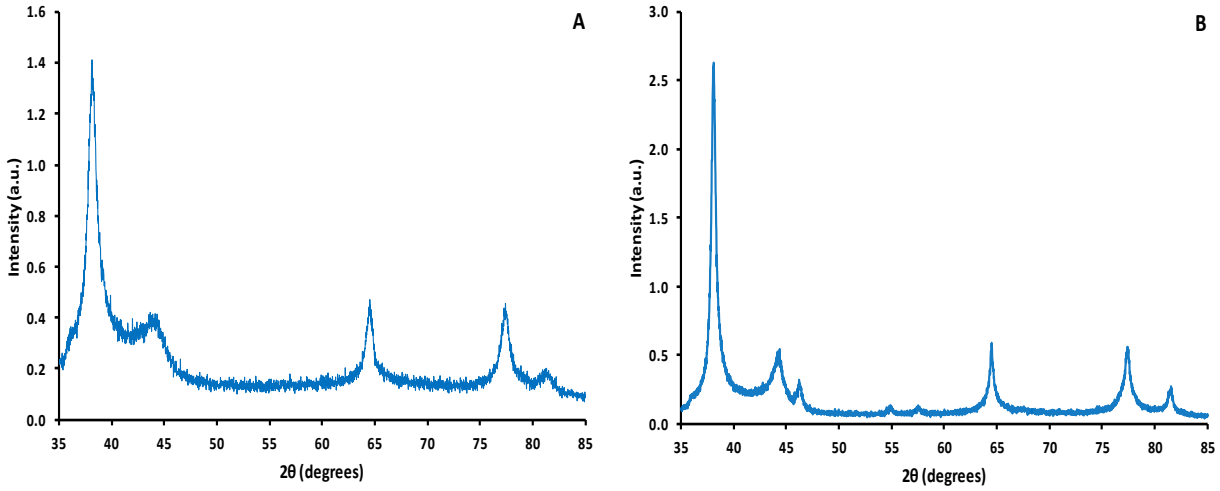

Figure 4.9. X-Ray Difraction pattern of AgNPs synthesis by broths of *Psychrobacter* sp **A**). 30 °C and **B**). 4 °C.

4.1.3. Antibacterial activity of AgNPs

One of the main applications of AgNPs is their use as antimicrobial agents alone or in combination with other antibiotic substances. To determine whether the obtained AgNPs have antimicrobial activity, their corresponding antibacterial tests were performed by the dilution method[15]. Particularly, serial dilutions of the AgNPs were performed using sterile Milli-Q water down to 1/64. Turbidity (or Optical Density) at 550 nm was recorded every hour. In the presence of AgNPs the turbidity increased less than in the control showing that bacteria were growing slower due to the antimicrobial activity of AgNPs. IC_{50} was determined after 7 h.

Two Gram-negative (*E. coli* and *K. pneumoniae*) and one Gram-positive (*S. epidermidis*) from culture collections were evaluated at different concentrations. The results are expressed as the concentration required to achieve 50% of growth inhibition (IC_{50}).

In general, AgNPs were more active against Gram-positive than against Gram-negative bacteria, and those prepared at 4 °C more active than the AgNPs obtained at 30 °C. This is more notorious with aged particles (incubated for 298 days), were the particles incubated at 30 °C were not active, whereas at 4°C were still active, particularly, those obtained from *A. salmonicida* supernatants with an IC_{50} > 10 µg/ml.

Table4.3. IC_{50} (µg of Ag/ml) of AgNPs. *E.c.*: *E. coli*, *K.p.*: *K. pneumoniae*, *S.e.*: *S. epidermidis*; f: fresh prepared (9 days), o: old (298 days) AgNPs.

	T (°C)	*Psychrobacter sp*	*A.salmonicida*	*P.veronii*	*Y.kristensenii*
E.c.	4 (F)	0.9	2.3	1	1.3
	4 (O)	1.5	2.9	1.1	1
	30 (F)	1.4	0.6	1.2	1
K.p.	4 (F)	1	3	1	1.3
	4 (O)	1.6	1.8	1.3	2.9
	30 (F)	1.8	0.7	1.6	1.4
S.e.	4 (F)	0.6	1.8	0.7	1
	4 (O)	0.5	0.8	0.5	1.1
	30 (F)	1.5	0.6	1.3	1.2

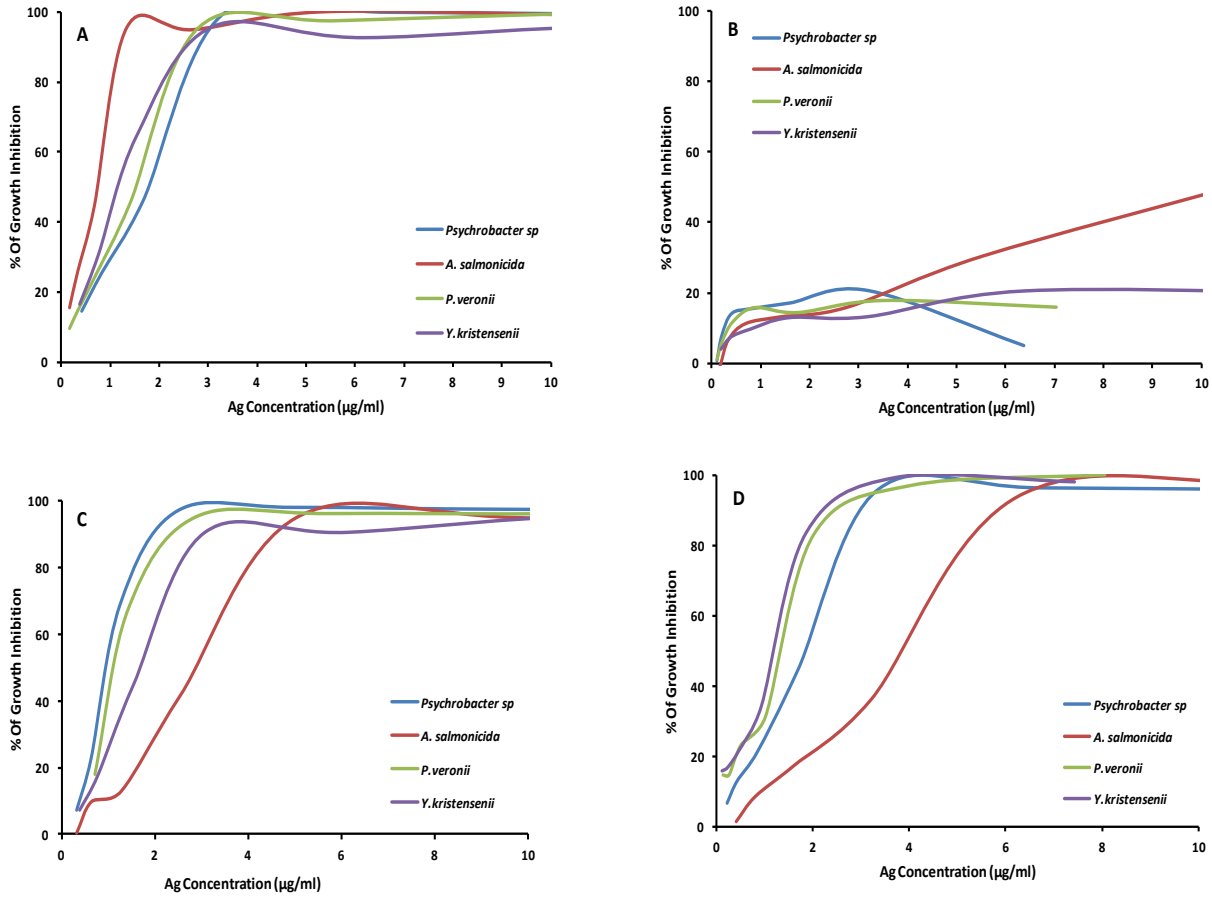

Figure 4.10. Antibacterial activity of AgNPs using *E. coli*. AgNPs used were obtained after 9 days **A**). at 30 °C, **C**). at 4 °C and after 298 days **B**). at 30 °C, **D**). at 4 °C.

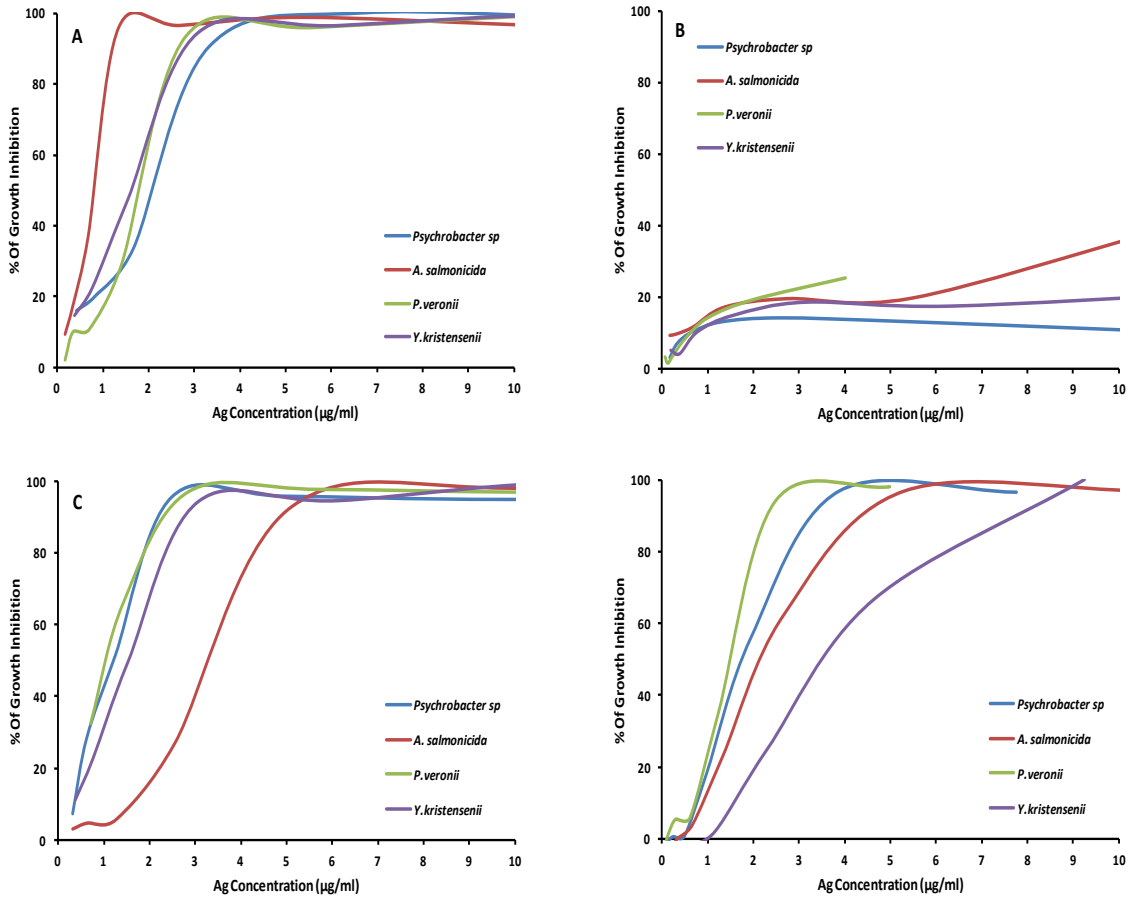

Figure 4.11. Antibacterial activity of AgNPs using *K.pneumoniae*. AgNPs used were obtained after 9 days **A**). at 30 °C, **C**). at 4 °C and after 298 days **B**). at 30 °C, **D**). at 4 °C.

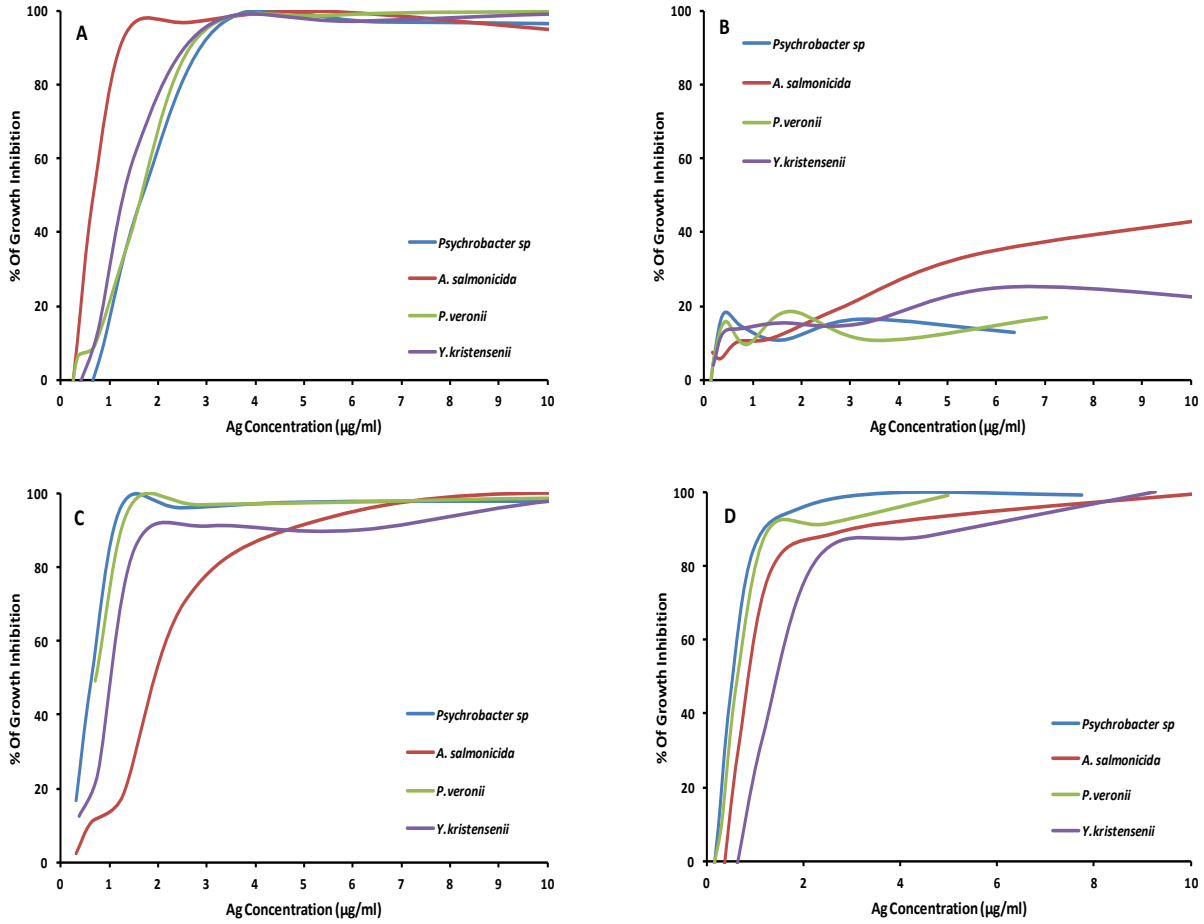

Figure 4.12. Antibacterial activity of AgNPs in *S.epidermidis*. AgNPs used were obtained after 9 days **A**). at 30 °C, **C**). at 4 °C and after 298 days **B**). at 30 °C, **D**). at 4 °C.

4.2. DNA Silver Nanoclusters as novel nanoantibiotics

DNA-AgNCs are novel fluorescent materials which properties can be tuned by the selection of the oligonucleotides sequence employed in their elaboration. In this project we have evaluated their antimicrobial properties.

4.2.1. Preparation and characterization of DNA-AgNCs

To study the antimicrobial properties of fluorescent DNA-AgNCs we selected three sequences (Seq-1, Seq-2 and Seq-3), which were reported before to yield emitters in the blue, yellow and red region[244-246].

The oligonucleotides were prepared by standard solid-phase synthesis and purified by polyacrylamide gel electrophoresis (PAGE). The oligonucleotides were first mixed with six equivalents of $AgNO_3$ and later with six equivalents of $NaBH_4$ to reduce the silver salt to metallic silver. The samples were washed to remove the excess of reagents and then used in the different experiments. The generation of DNA-AgNCs was confirmed by their fluorescence spectra (Fig 4.13).

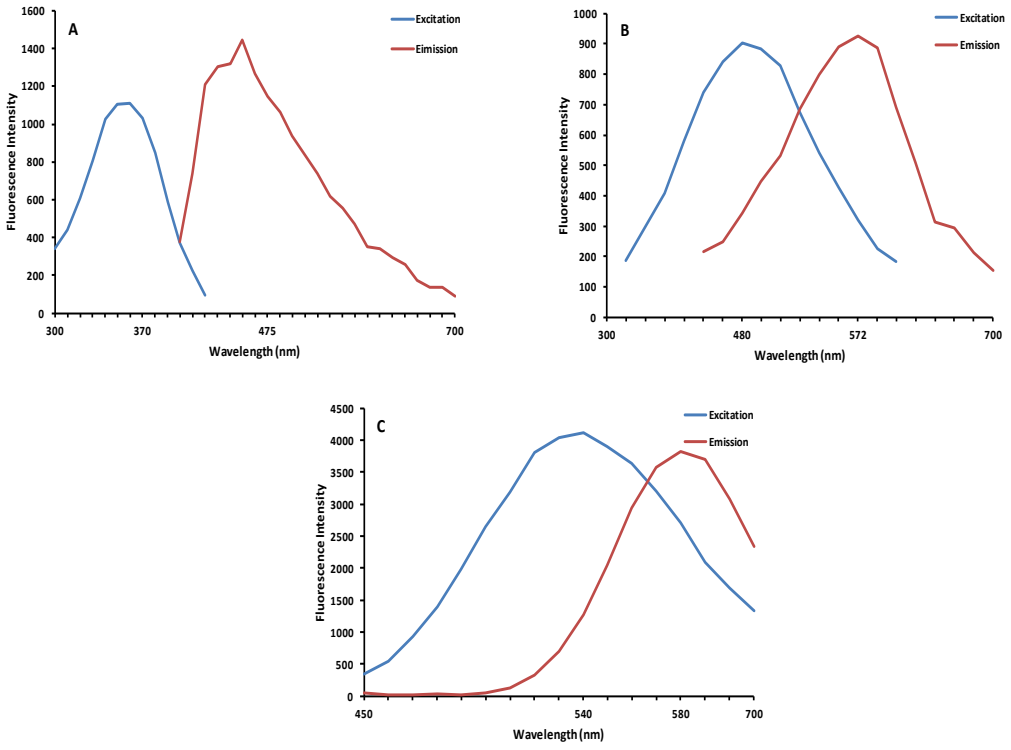

Figure 4.13. Fluorescence excitation and emission spectra of AgNCs stabilized with the ONs **A**). Seq1, **B**). Seq2 and **C**). Seq3.

These DNA-AgNCs were incubated with *E. coli* and *S. epidermidis* and their antibacterial activity was evaluated using the growth curve method[69] , monitoring the optical density at 650 nm. In the control experiment, where no antibacterial agent was added, bacteria growth was observed after 2 hours of incubation. However, the growth was clearly delayed when DNA-AgNCs were present in the solution (Fig 4.14).

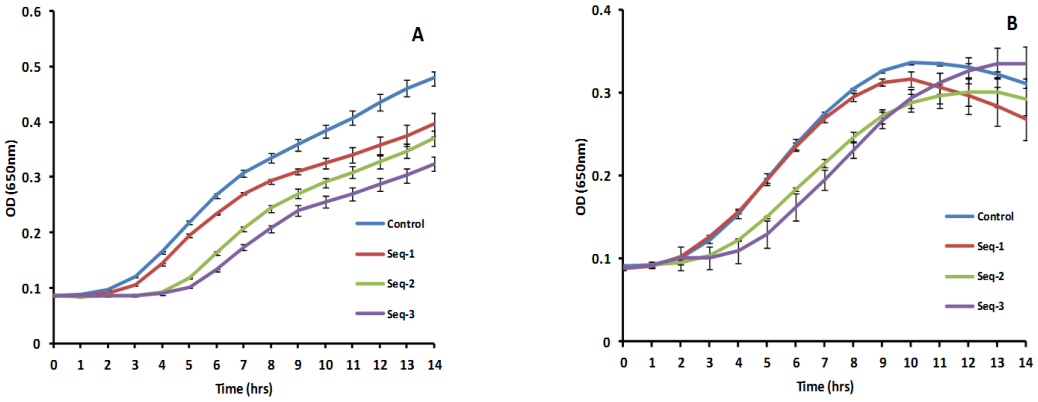

Figure 4.14. Growth curves in the presence of three DNA-AgNCs at 3 µM. **A**). in *E. coli* and **B**). in *S. epidermidis*. The experiments were done in triplicates and the error bars represent the standard deviation.

This behavior was confirmed using a complementary method to evaluate the antimicrobial activity, the Kirby-Bauer disk diffusion susceptibility test[247]. In this test a paper disk containing the reagent is placed on an agar plate where bacteria can grow. The reagent from the disk diffuses and prevents the growth of the bacteria around it, leaving a clear inhibition area (Figure 4.15). As in the previous method the Seq-3 showed the best antimicrobial activity.

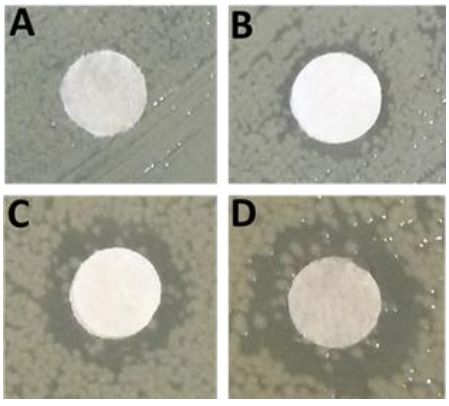

Figure 4.15. Kirby-Bauer disk diffusion susceptibility test. **A**). Control **B**). Seq-1 **C**). Seq-2 **D**). Seq-3. The antibacterial effect is confirmed by the presence of a clear zone surrounding the disks with DNA-AgNCs.

Then, the amount of silver in each sample was quantified, since it could be related with the activity observed. The quantification by TXRF revealed that AgNCs stabilized with Seq-1 have more silver than the other two derivatives (Fig 4.16).

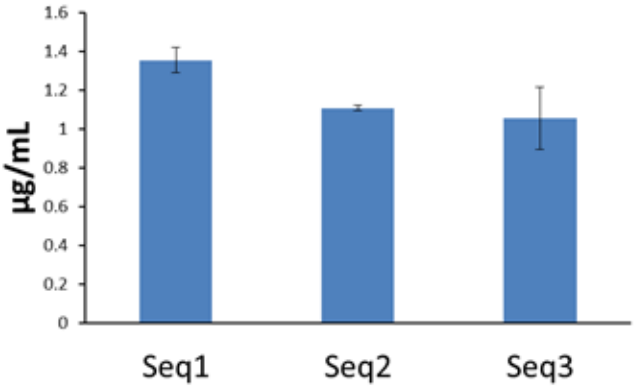

Figure 4.16. Quantification of silver of the DNA-AgNCs by TXRF. The data showed is the average of three independent measurements.

Then, additional sequences were evaluated aiming to find a relationship between the sequences and their antimicrobial activity. The sequences employed yielded emitters in the blue, yellow and red region and are summarized in Table 4.4.

Table 4.4. Sequences employed in the preparation of AgNCs.

Name	Sequence
Seq-1	5´-TTTTCCCCTTTT-3´
Seq-2	5´-CCCTTAATCCCC-3´
Seq-3	5´-CCCCCCCCCCCC-3´
Seq-4	5´-CCCTTTAACCCC-3´
Seq-5	5´-CCCCTTTTCCCC-3´
Seq-6	5´-GGGTTAGGGTCCCCCCACCCTTACCC -3´
Seq-7	5´-GGGTGGGTCCCCCCACCCACCC -3´
Seq-8	5´-CCTCCTTCCTCC -3´
Seq-9	5´-AGGTCGCCGCCC -3´
Trimer (Seq-3)	(5´-CCCCCCCCCCCC-3´)$_3$-Benzene

Then, the antimicrobial activity of the DNA-AgNCs was evaluated as before. All the samples showed some antimicrobial activity, which varies depending on the sequence employed (Fig 4.17). However, there is not a clear correlation between the sequence employed and the activity, observed.

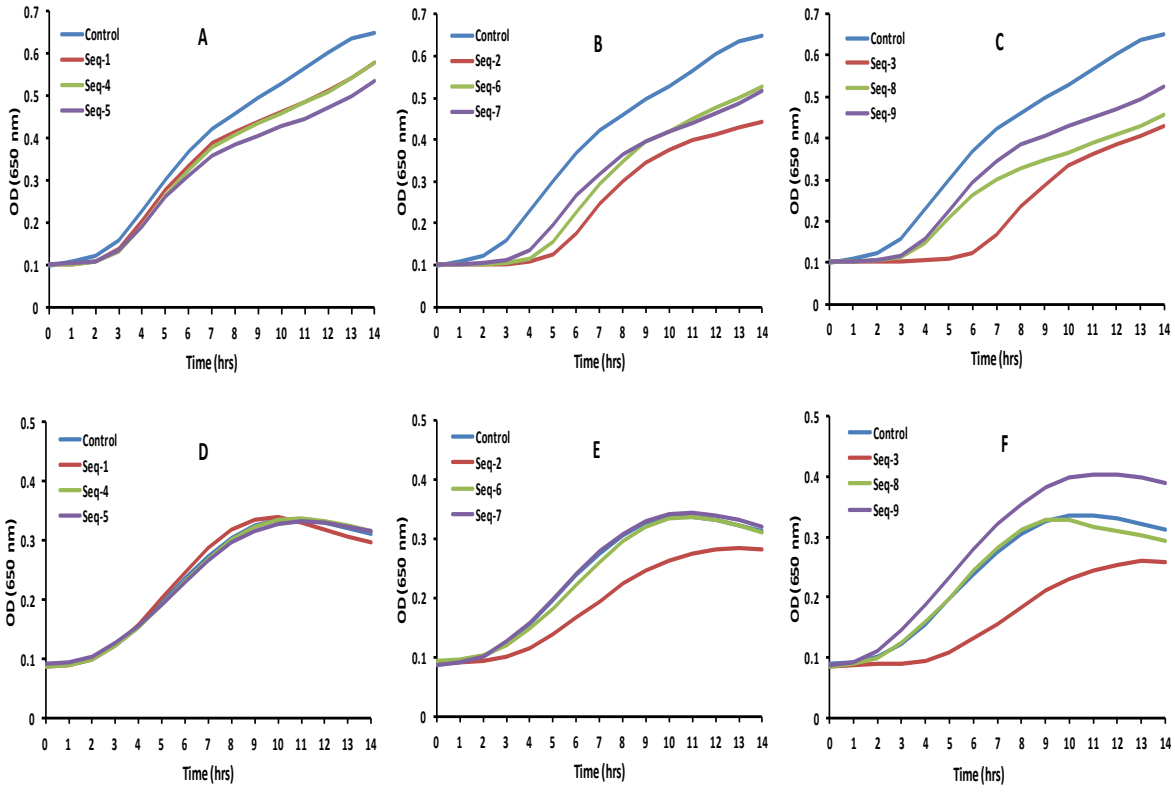

Figure 4.17. *E. coli* and *S. epidermidis* growth curves in the presence of DNA-AgNCs at 3µM.

E.coli: **A**). Blue emitters **B**). Yellow emitters, and **C**). Red emitters. *S. epidermidis*: **D**). Blue emitters, **E**). Yellow emitters and **F**). Red emitters.

Cytosines are known to bind tighter to silver than other nucleobases, and therefore they might modulate the antimicrobial activity. Unfortunately, we could not find a clear correlation between the activity and the number of cytosines (Fig. 4.18). For instance, Seq-3, Seq-6 and Seq-7 have the same amount of cytosines but different antimicrobial activity. On the other hand, Seq-2 has less cytosines than Seq-5, Seq-6, Seq-7, and Seq-8 but has better antimicrobial activity.

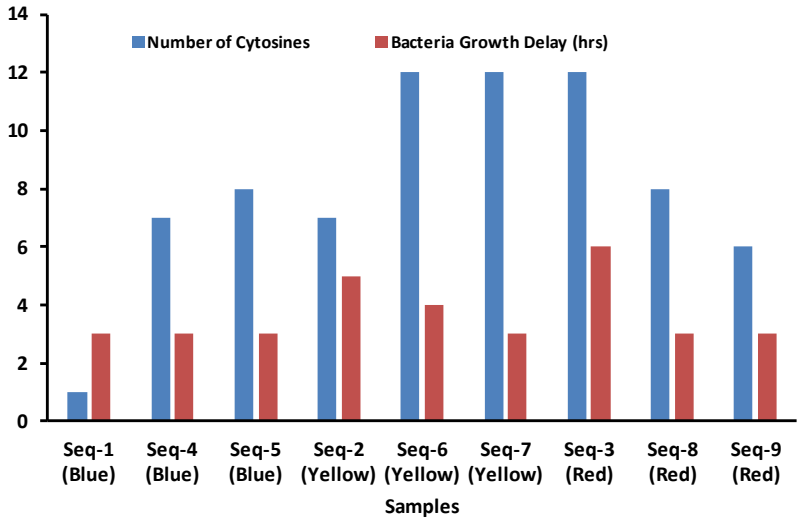

Figure 4.18. Representation of antimicrobial activity and number of cytosines for each samples.

On the other hand, when the three different groups of emitters are compared it seems clear that blue emitters have the lowest activity (Fig 4.17 A and 4.17 D), whereas yellow (Fig 4.17 B and 4.17 E) and red emitters (Fig 4.17 C and 4.17 F) showed similar activity, where the red emitter obtained with Seq-3 showed the best activity.

Since the amount of silver or the sequence cannot explain completely the differences in activity we wondered if the structure of the complexes generated could play a role. For this reason we carried out CD studies to compare their structure using Seq-1, Seq-2 and Seq-3 (Fig 4.19). Thus, we look at the structures before and after the formation of the DNA-AgNCs at different temperatures. In the case of Seq-1 the CD showed the characteristic peaks of an unfolded DNA strand with a positive band at 280 and a negative one around 255 (Fig. 4.19 A). In this case the temperature did not affect significantly the spectra since the strand was already unfolded. After the formation of AgNCs those bands decreased considerably (Fig 4.19 B).

On the other hand, Seq-2 and Seq-3 showed the characteristic peaks of an i-motif with a dominant positive band around 290 nm and negative one close to 260 nm (Fig 4.19 C and 4.19 E) . These i-motif structures where destabilized as the temperature increases to yield the standard arrangement for DNA, with a positive band at 280 and a negative one at 255. In the case of Seq-2, the i-motif was denatured at lower temperatures compared with Seq-3. In this case the structure was unfolded at 55 °C, whereas

Seq-3 required temperatures up to 75 °C to completely unfold the i-motif. In both cases the generation of AgNCs induced great changes in the CD spectra, with negative bands around 215 and 270 and positive one near 240 (Fig 4.19 D and 4.19 f). In the case of Seq-3 the bands were more pronounced and the band at 290 characteristic of i-motif disappeared completely. It is remarkable the high stability of the structures obtained with both sequences, which CD did not change along the different temperatures tested (Fig 4.19).

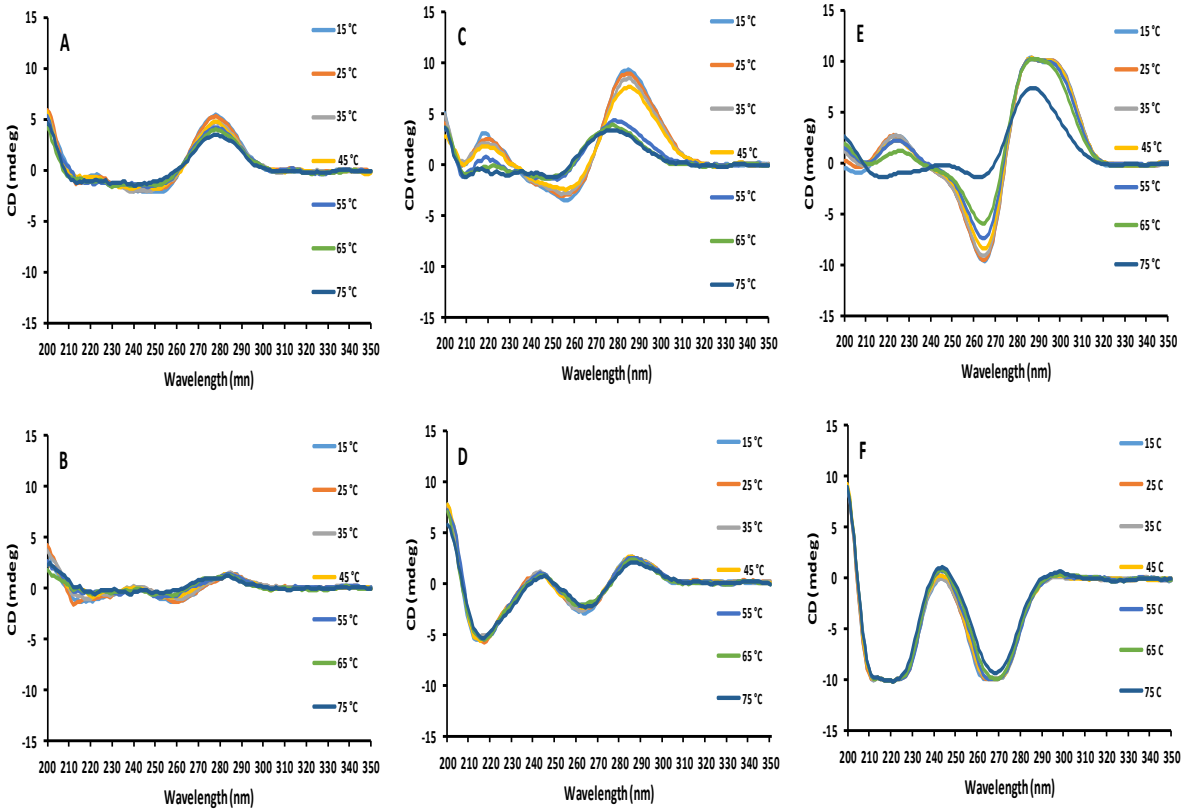

Figure 4.19. CD of the samples Seq-1, Seq-2 and Seq-3 before (**A**, **C** and **E** respectively) and after (**B**, **D** and **F** respectively) the generation of AgNCs.

Besides these considerations, the sample that yielded the higher activity was Seq-3 and for this reason we continued our studies using this derivative. First, we carried out a dose-response study using 5 different concentrations as illustrated in (Fig 4.20).

Inhibition of bacterial growth showed a clear dose-dependent response, where the higher the concentration of the DNA-AgNCs employed, the larger the antimicrobial inhibition activity. Using the highest concentration (5 µM) the DNA-AgNCs were able to suppress the growth of the bacteria for 14 hours.

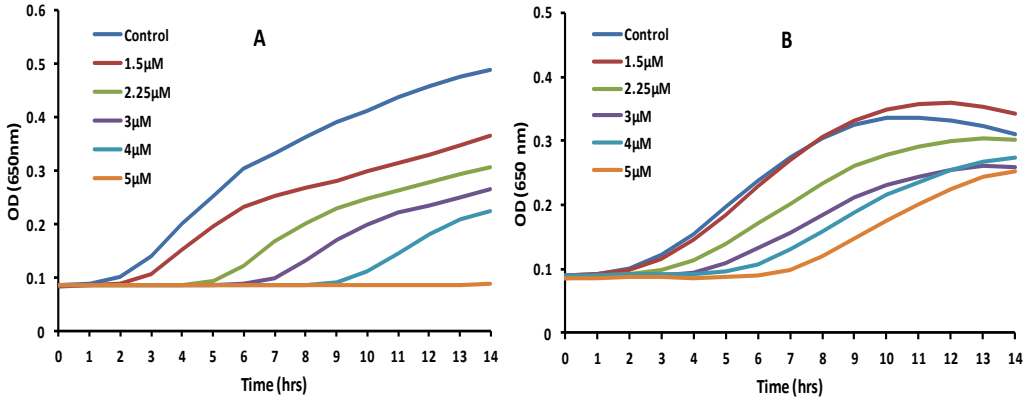

Figure 4.20. A). *E.Coli* and, **B**). *S.epidermidis* growth curves in the presence of AgNCs stabilized with **Seq-3** at different concentrations.

Then, we compared the activity of this derivative with related silver species, such as silver cations and AgNPs, which are known to have antibacterial activity. We employed the $AgNO_3$ used in the preparation of AgNCs as a source of silver cations. AgNPs were prepared by reduction of $AgNO_3$ with $NaBH_4$, following the same procedure as for the preparation of AgNCs, but without the addition of DNA. The same amount of $AgNO_3$ was used in the preparation of the three samples. As shown in (Fig 4.21), AgNCs stabilized with sequence 3 and $AgNO_3$ were found to have better activity than AgNPs.

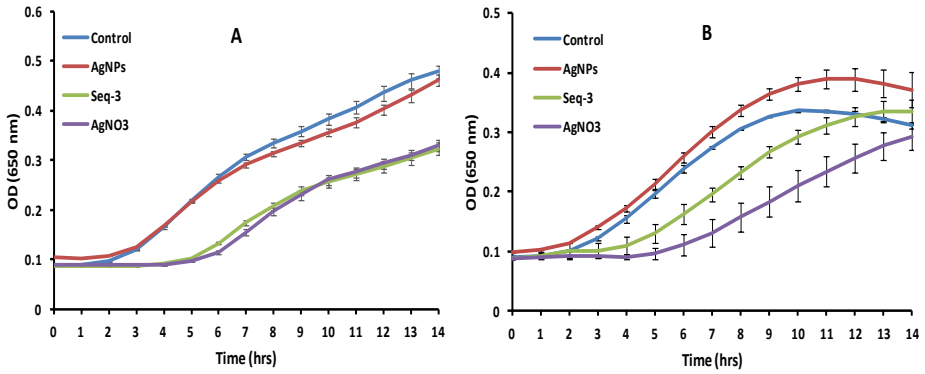

Figure 4.21. Growth curves in the presence of AgNCs stabilized with Seq-3 at 3 µM, AgNPs and $AgNO_3$ in **A)**. *E. coli* and **B)**. *S. epidermidis*. The concentration of silver in all samples was 9.8 µM. The experiments where done in triplicates and the error bars represents standard deviation.

Finally, motivated by the good properties of the AgNCs generated with the Seq-3 as antibacterial agent, a derivative with increased inhibitory activity was designed. Our research groups has recently reported the use of oligonucleotides trimers in the preparation of AgNCs, which have shown increased fluorescence and stability[146]. Thus, we planned to use the same strategy to prepare a trimer that could yield AgNCs with better antimicrobial activity.

For this purpose a click reaction between a benzene derivative bearing three azides and the Seq-3 modified with an alkyne group was carried out.

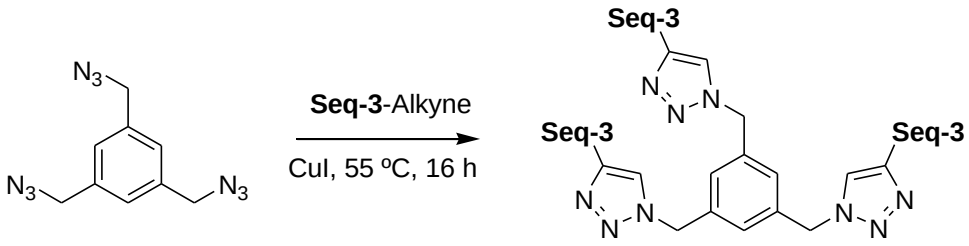

The resulting trimer was purified by gel electrophoresis and used in the preparation of AgNCs. Incubation of this compound with $AgNO_3$ followed by reduction with $NaBH_4$ yielded the corresponding fluorescent AgNCs.

AgNCs stabilized with the trimer system showed excellent inhibition of bacteria growth at low concentration (0.750 µM or 1.5 µM) and even killing all bacteria at 2.25 µM (Fig 4.22).

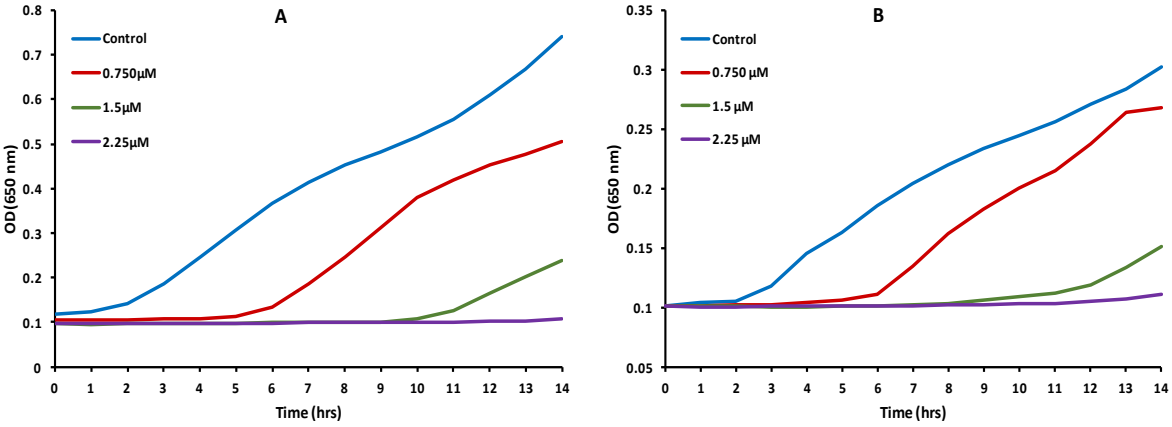

Figure 4.22. Bacteria growth inhibited by the presence of the DNA-AgNCs stabilized by trimers prepared with Seq-3 at different concentrations in **A**). *E. coli* and **B**). *S. epidermidis*.

Regarding the mechanism of action of these derivatives, it is not completely clear and multiple mechanism could be involved. For instance, silver salts can inhibit some key enzymes, reduce the level of antioxidants, disrupt the cell membrane and increase the amount of ROS. The later one is the most general process implicated in the antibacterial properties of silver derivatives. For this reason we checked the production of ROS using the fluorescent probe 2´,7´-dichlorodihydrofluorescin diacetate (DCFH-DA). ROS production was evaluated in *E. coli* and *S. epidermidis* bacteria after the incubation of DNA-AgNCs for 14 hours in the dark. The results showed an increase in ROS production when DNA AgNCs were present (Fig 4.23).

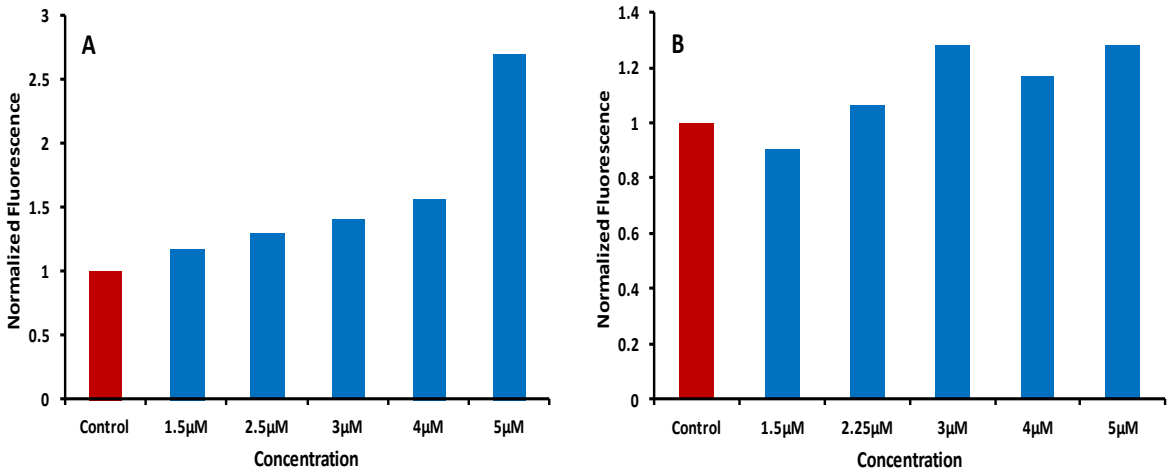

Figure 4.23. Seq-3 DNA-AgNCs enhanced to the ROS production in **A**). *E. coli* and **B**). *S. epidermidis.*

4.3. Photodynamic Therapy using Photosensitizers conjugated to oligonucleotides

4.3.1. Characterization of oligonucleotides modified with Photosensitizers

PDT is a promising method for the control and treatment of infectious diseases that utilizes light-sensitive molecules known as photosensitizer (PS). When these derivatives are excited with the light, the amount of ROS is increased, which can induce the death of the cells. One of the main advantages of PDT compared to traditional approaches is that bacteria are less prone to develop resistance after therapy [190].

In this case we decided to explore the effect of PS conjugated to oligonucleotides and later combine them with AgNCs. We decided to use the sequences Seq-2, Seq-3, Seq-7 and Seq-8,

previously employed in the preparation of AgNCs and the derivative of fluorescein, 5-hexachlorofluorescein (HEX), as a PS.

Only the first three sequences were labeled with HEX, and Seq-8 was used as control to assess the role of the PS. The samples were labeled as PS1, PS2, PS3 and Control respectively in the experiments. The system was evaluated against Gram-positive (*Staphylococcus aureus*) and Gram-negative (*Escherichia coli* and *Pseudomonas aeruginosa*) bacteria.

The absorption spectra of purified oligonucleotides modified with HEX (PS1, PS2 and PS3), showed two representative peaks, one at 260 nm (oligonucleotides) and other at 540 nm (HEX) (Fig 4.24). The control strand (Control) only showed the characteristic peak at 260 nm. oligonucleotides were also analyzed by MALDI-TOF (Table 4.5).

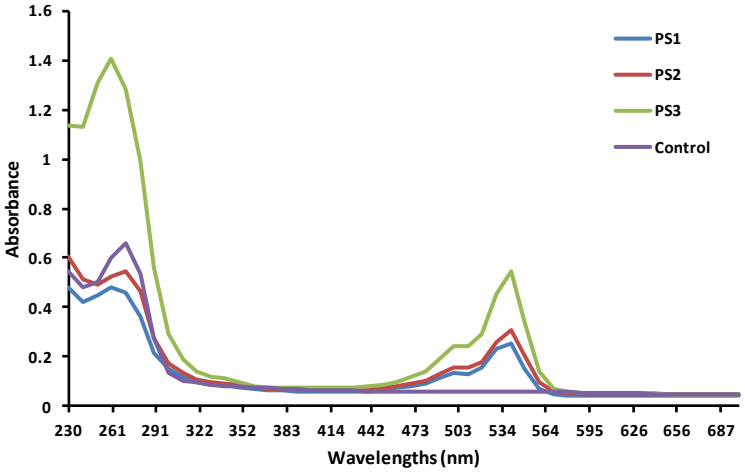

Figure 4.24. UV-Vis absorption spectra of oligonucleotides employed.

Table 4.5. MALDI-TOF of the oligonucleotides.

Name	Sequence	Calculated mass	Found
PS1	5´-HEX- CCCTTAATCCCC-3´	4245.43	4245.10
PS2	5´-HEX- CCCCCCCCCCCC-3´	4152.33	4152.08
PS3	5´-HEX- GGGTGGGTCCCCCCACCCACCC -3´	7362.43	7360.21

The fluorescence intensity of the sequences (PS1, PS2 and PS3) was recorded at the same concentration of the oligonucleotides as well as the fluorescence of the AgNCs obtained with them. The fluorescence intensity due to the HEX, with and without AgNCs, showed the following order: PS3 > PS1 > PS2 (Fig 4.25).

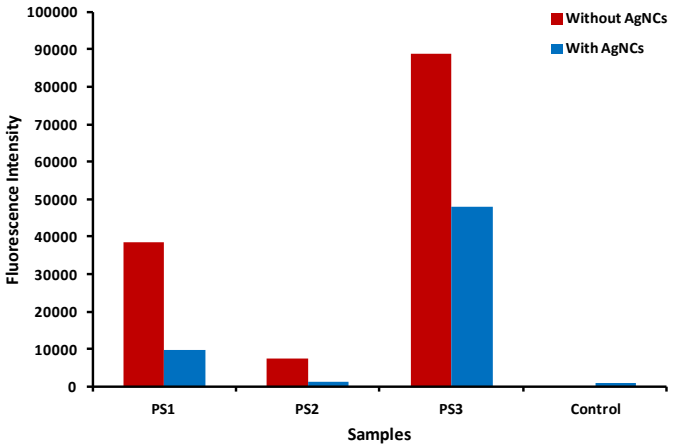

Figure 4.25. Fluorescence intensity of ONs –HEX and ONs-HEX-AgNCs obtained after 16h.

(ex/em: 536 / 557 nm) (Control= Seq-8)

4.3.2. Antibacterial activity

The susceptibility of the *E. coli*, *S. aureus* and *P. aeruginosa* to these systems was determined by the growth curve method (Materials and Methods 3.11.3). A light source, with a maximum at 525 nm, was employed during two hours to induce the production of ROS and then the samples were incubated at 37 °C for 20 h under mild shaking. The OD measured at 650 nm was used to monitor the bacteria growth. In the case of PS1 the bacteria growth was significantly inhibited at 0.750 and 1.5 µM in *S. aureus* and *E. coli*., when the light system was applied (Fig 4.26 A and Fig 4.26 B). Surprisingly, when the concentration employed was increased (3 µM) the antimicrobial activity disappeared (Fig 4.26).

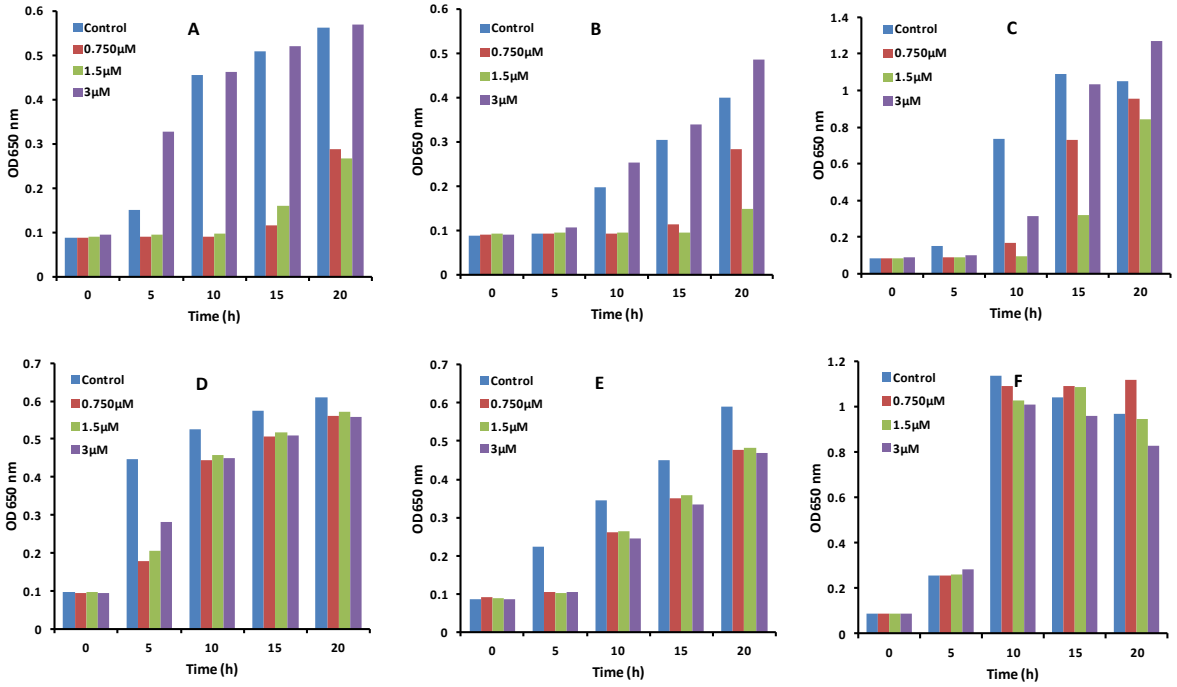

Figure 4.26. Optical density of bacteria cultures incubated with PS1 at different concentrations. **A,D**). *S. aureus*, **B,E**). *E. coli* and **C,F**). *P. aeruginosa.* A decrease in the optical density is associated with antibacterial activity. **A,B,C** with irradiation and **D,E,F**, without irradiation.

In the case of PS2, good antibacterial activity was observed against *S. aureus* at 0.750 µM (Fig 4.27 A) and against *E. coli* at 0.750 µM and 1.5 µM (Fig 4.27 B), after light irradiation. Remarkably, PS2 showed some activity even in the dark against *E. coli* (Fig 4.27 E).

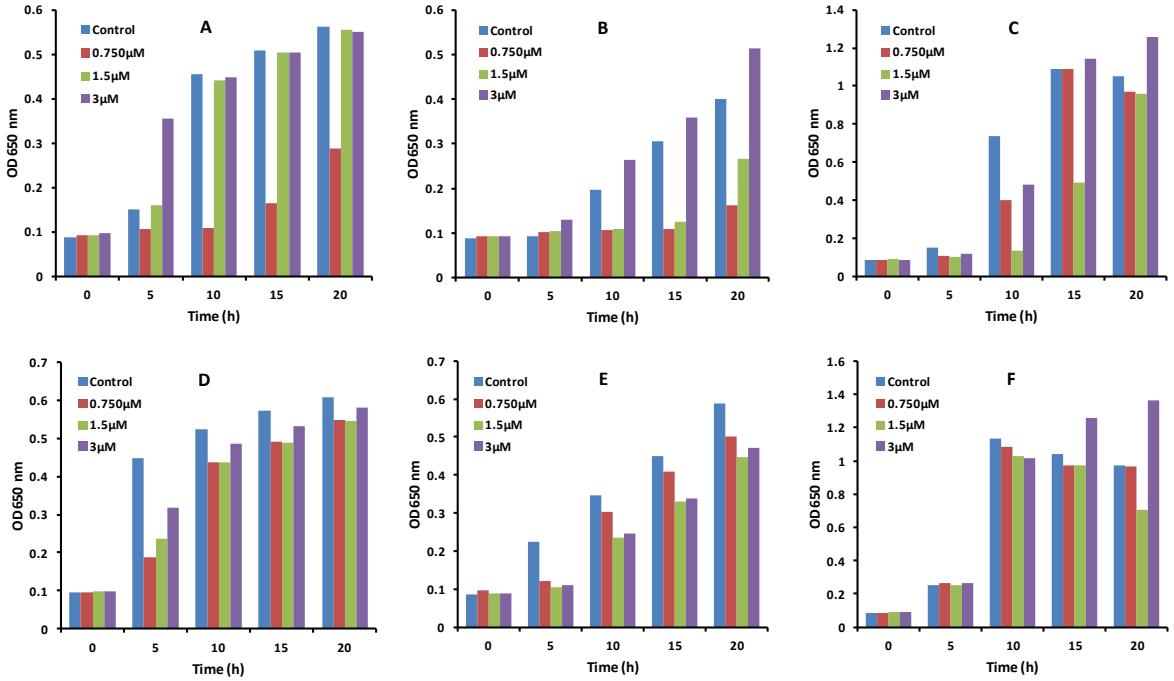

Figure 4.27. Optical density of bacteria cultures incubated with PS2 at different concentrations. **A,D**). *S. aureus*, **B,E**). *E. coli* and **C,F**). *P. aeruginosa.* A decrease in the optical density is associated with antibacterial activity. **A,B,C** with irradiation and **D,E,F**, without irradiation.

PS3 showed significant antibacterial activity against *S. aureus* at low concentration (0.750 µM) (Fig 4.28 A). However, in the other cases the antimicrobial effect was not that clear.

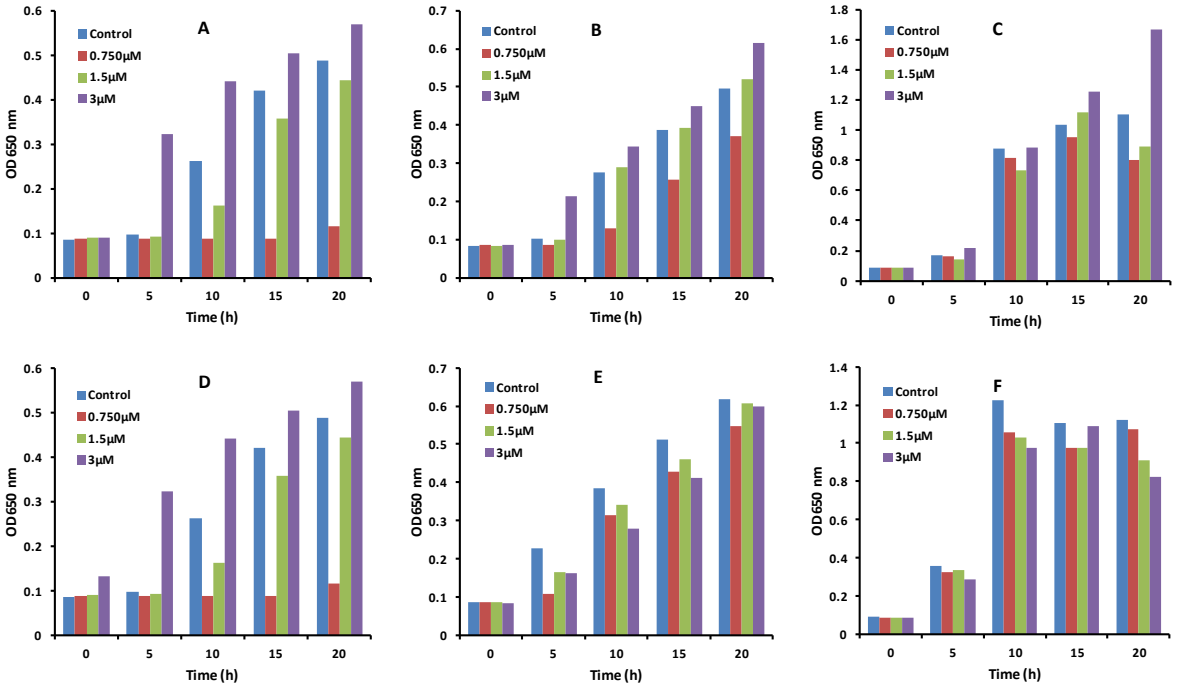

Figure 4.28. Optical density of bacteria cultures incubated with PS3 at different concentrations. **A,D**). *S. aureus*, **B,E**). *E. coli* and **C,F**). *P. aeruginosa.* A decrease in the optical density is associated with antibacterial activity. **A,B,C** with irradiation and **D,E,F**, without irradiation.

The control sequence did not show any antimicrobial activity with or without the light system (Fig 4.29).

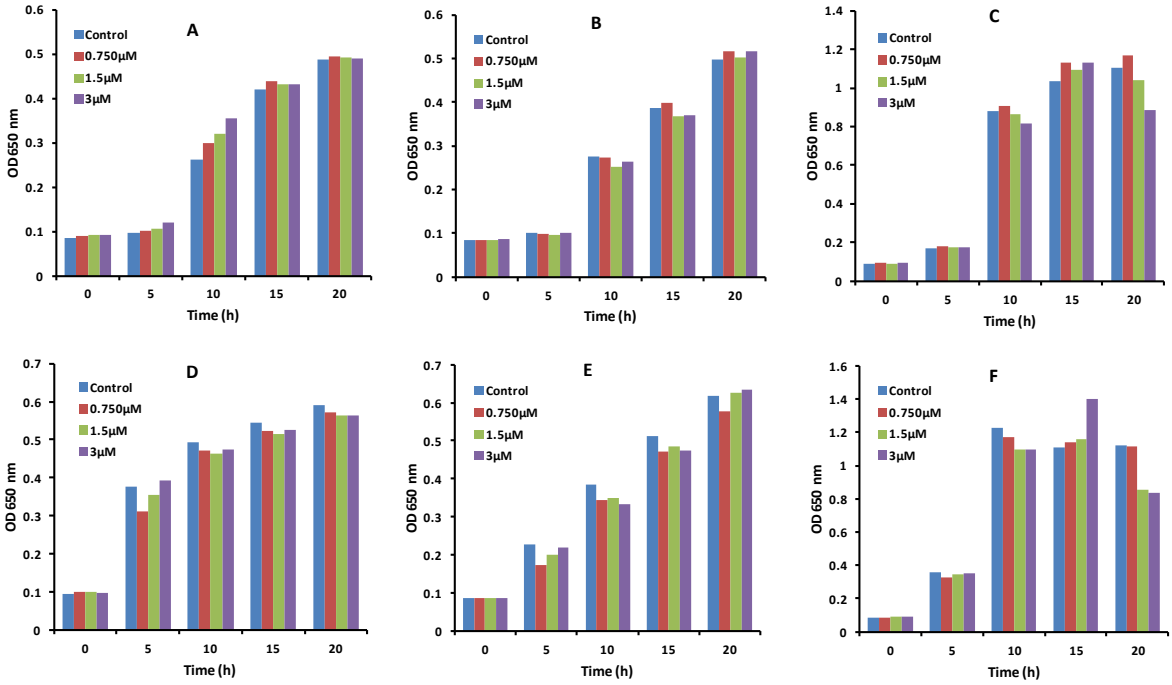

Figure 4.29. Optical density of bacteria cultures incubated with Control at different concentrations. **A,D**). *S. aureus*, **B,E**). *E. coli* and **C,F**). *P. aeruginosa.* A decrease in the optical density is associated with antibacterial activity. **A,B,C** with irradiation and **D,E,F**, without irradiation.

These results point out that the systems are active against Gram-positive and Gram-negative bacteria, however the results depend on the sequences and bacteria employed, as illustrated in Fig 4.30, where the activity of the three systems and bacteria are compared after 20 h at 0.750 µM.

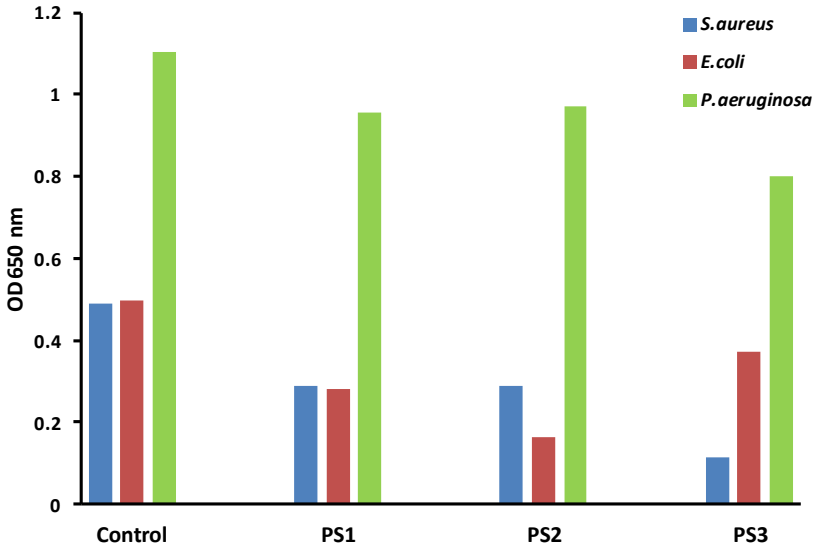

Figure 4.30. Optical density obtained from bacteria treated with the oligonucleotides and light at 0.750 µM after 20 h.

Then, we decided to evaluate the effect on the antimicrobial activity of this system in combination with the formation of AgNCs. When PS1-AgNCs was employed a good antimicrobial activity was observed against *S. aureus* and *E. coli* at 0.750 µM and 1.5 µM, after the light irradiation (Fig 4.31). In this case, some activity was also observed in the dark, due to the presence of AgNCs (Fig 4.31 E).

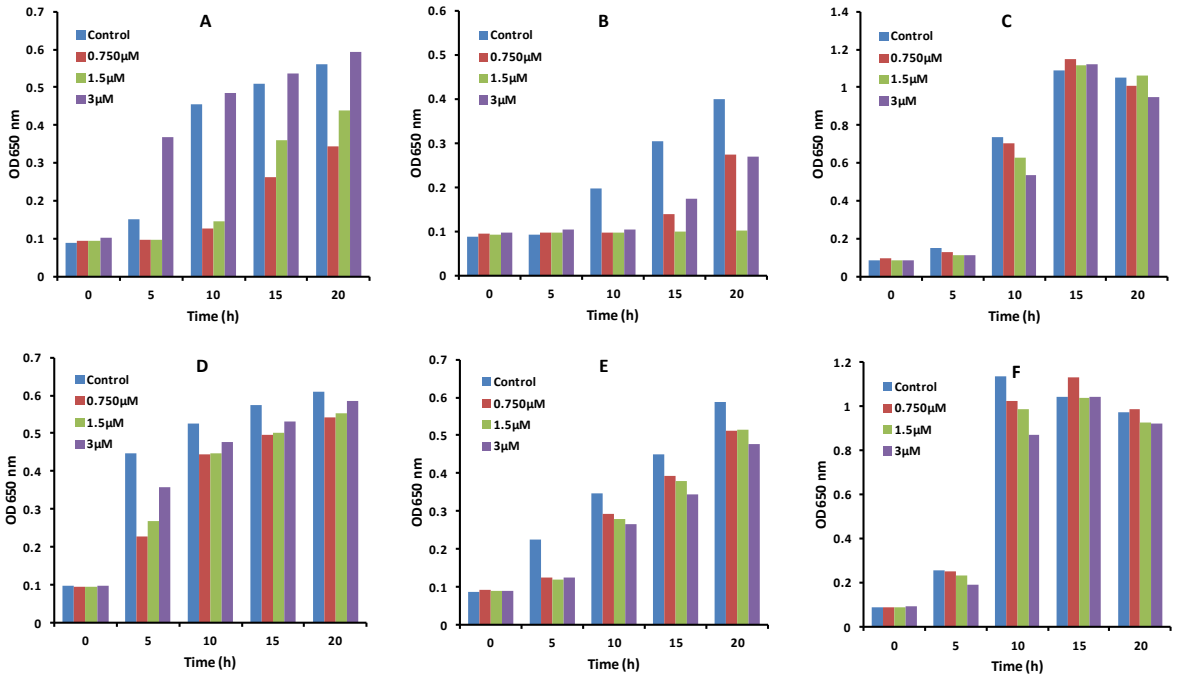

Figure 4.31. Optical density of bacteria cultures incubated with PS1-AgNCs at different concentrations. **A,D**). *S. aureus*, **B,E**). *E. coli* and **C,F**). *P. aeruginosa.* A decrease in the optical density is associated with antibacterial activity. **A,B,C** with irradiation and **D,E,F**, without irradiation.

In the case of PS2-AgNCs good antibacterial activity was observed against *E. coli* at every concentration when the light system was applied (Fig 4.32).

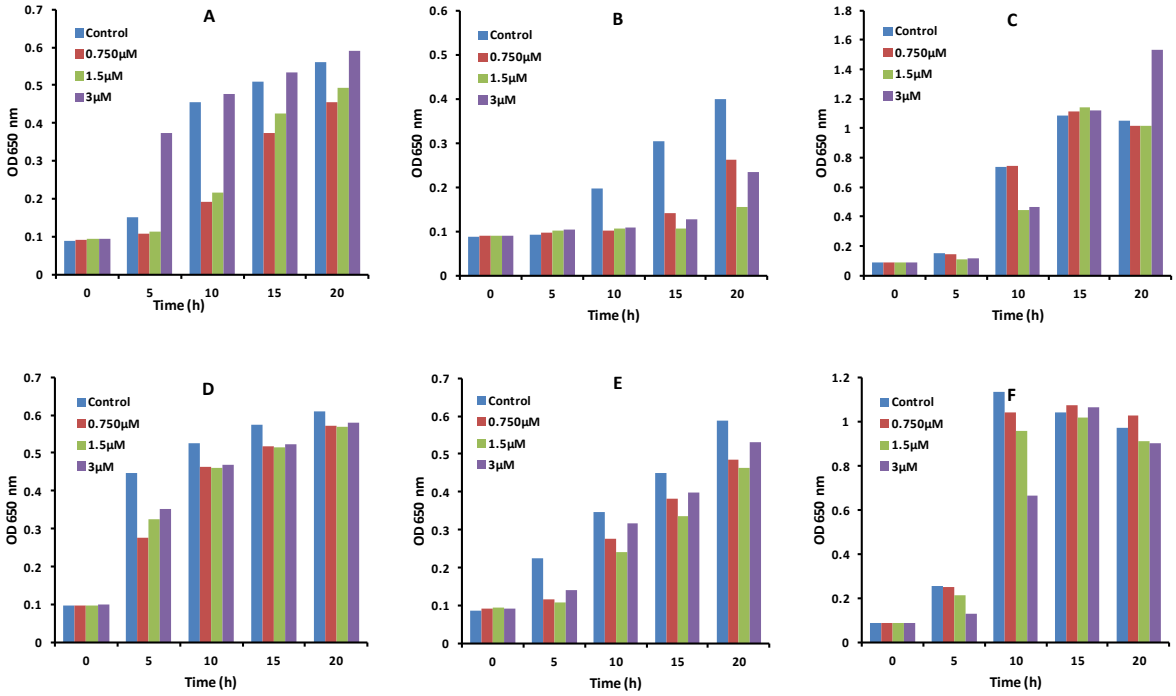

Figure 4.32. Optical density of bacteria cultures incubated with PS2-AgNCs at different concentrations. **A,D**). *S. aureus*, **B,E**). *E. coli* and **C,F**). *P. aeruginosa.* A decrease in the optical density is associated with antibacterial activity. **A,B,C** with irradiation and **D,E,F**, without irradiation.

PS3-AgNCs showed good antibacterial activity against *S. aureus* at 0.750 and 1.5 µM, with irradiation (Fig 4.33 A). In the other cases the antimicrobial effect was not so clear.

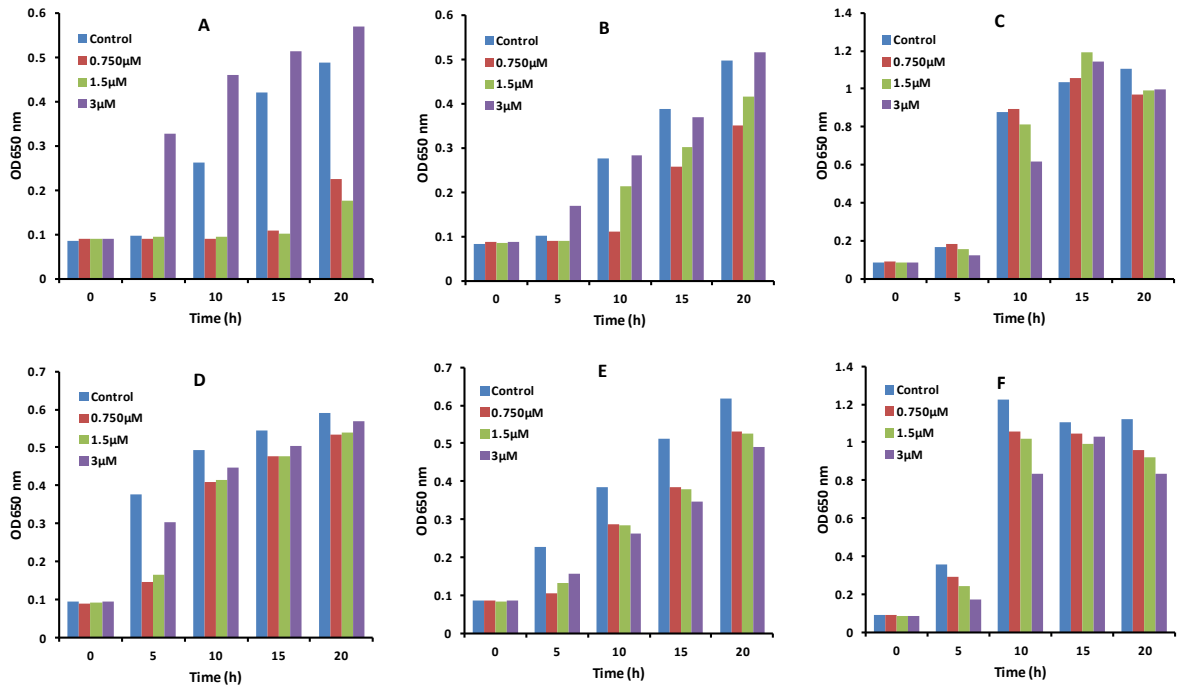

Figure 4.33. Optical density of bacteria cultures incubated with PS2-AgNCs at different concentrations. **A**,**D**). *S. aureus*, **B,E**). *E. coli* and **C,F**). *P. aeruginosa*. A decrease in the optical density is associated with antibacterial activity. **A,B,C** with irradiation and **D,E,F,** without irradiation.

4.3.3. ROS

Finally, we evaluated the production of ROS by PS1 when the light system was used in *S. aureus* (Fig 4.34). The experiments revealed that ROS production is increased at 0.750 µM and 1.5 µM but not at 3 µM. These results are in agreement with the antibacterial activity observed where at 3 µM the system is not active (Fig 4.26 A) Thus, one of the mechanism involved in the antimicrobial activity of PS1, and probably in the other systems, is the production of ROS.

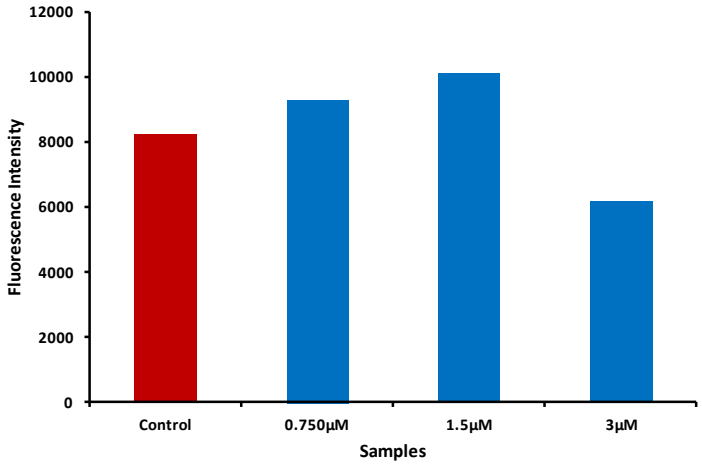

Figure 4.34. PS1 ROS generation in the *S. aureus*.

4.4. p21 regulation with oligonucleotides conjugated to gold nanoparticles

Antisense oligonucleotides have been used for a number of years to modify the expression of specific genes both *in vivo* and *in vitro*[248, 249]. The main limitations in this kind of approaches are the efficient delivery of the oligonucleotides into the target cells, and their stability. To overcome these limitations we are exploring the use of AuNPs as delivery systems of different oligonucleotides (antisense and siRNA) in the regulation of p21.

Particularly we have evaluated two antisenses, one Gapmer and one siRNA. The sequences employed in these experiments are summarized in Table 4.6. They were prepared with a dithiolane group at the 3'-end to ease the conjugation with AuNPs. A nonsense sequence (NS) was employed as control in the experiments.

Table 4.6. Functional oligonucleotides evaluated to control p21 gene expression.

Name	Sequence
Antisense-1	5´-AGA CAA CGG CAC ACU UUG C-TTTTT-3´
Antisense-2	5´-AUA GAA AUC UGU CAG GCU G-TTTTT-3´
Gapmer	5´-GAU AGA AAT CTG TCA GGC UG-3´
siRNA	
Passenger (Sense)	5´-CAG CCU GAC AGA UUU CUA U-TTTTT-3´
Guide (Antisense)	5´-AUA GAA AUC UGU CAG GCU G-TT-3´

First, we evaluated the inhibition activity of AuNPs modified with the oligonucleotides using Western blot. We observed that after stimulation with Con A of $CD4^+$ positive T-cells and incubation with AuNPs modified with antisense 1 and 2 the p21 expression decreased after 2 hours (Fig 4.35 A). This effect was slightly more intense when antisense 2 was employed, for this reason the next experiments were done with this sequence. We also found that the inhibition of p21 was more effective at short times (Fig 4.35 B).

Amaxa kit was used to transfect Antisense 2 in the same concentration following the procedure provided by the manufacturer to compare the inhibition. In this case the effect of antisense 2 was observed after 14 hours (Fig 4.35 C).

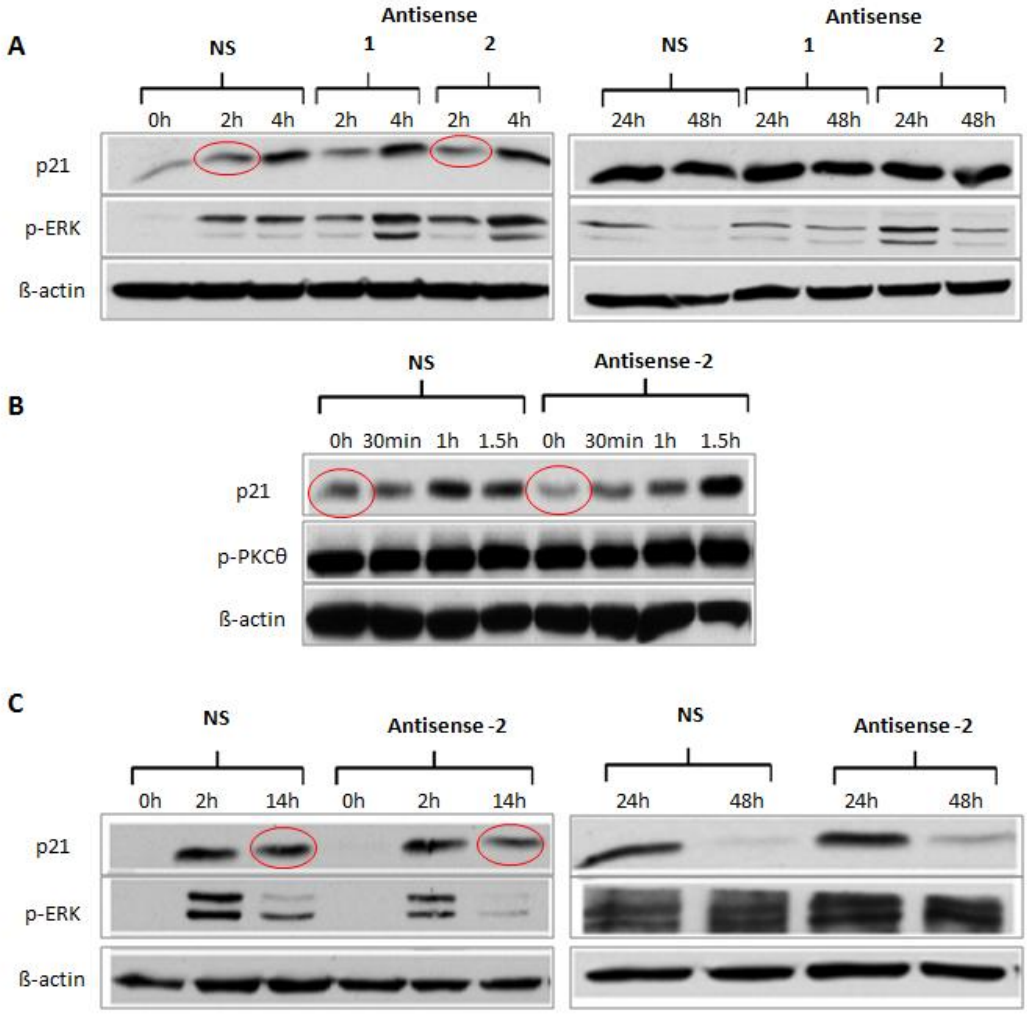

Figure 4.35. Western Blot of different proteins from T Cells treated with antisense and nonsense oligonucleotides internalized by **A**). Modified AuNPs **B**). Modified AuNPs at short times. **C**). Amaxa kit.

Then, the effect of the sequence employed in antisense 2 with a Gapmer desing was evaluated. This design could provide better activity since the interaction with RNAase H is more efficient than in the previous case. Particularly the inhibition was observed up to 1.5 hours (Fig 4.36).

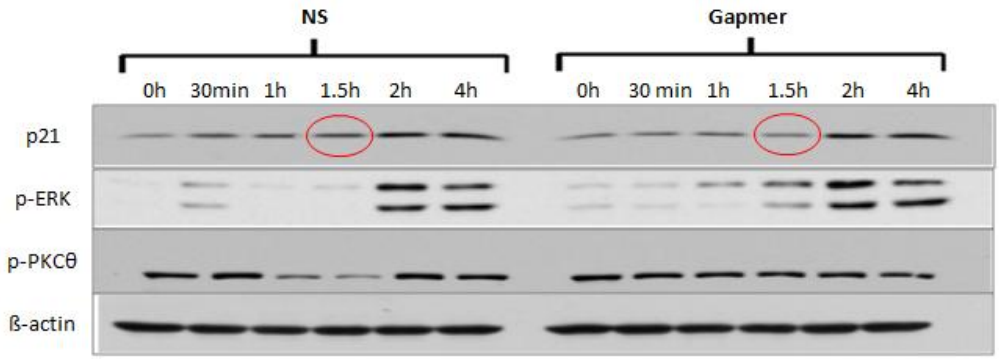

Figure 4.36. T-cells treated with Gapmer-AuNPs at different time points.

Besides the western blot, we used flow cytometry to quantify the transfection efficiency of the oligonucleotides using AuNPs and the Amaxa kit after 24 and 48 hours. The results obtained revealed that the transfection efficiency mediated by AuNPs was 32.7% and 44.6% after 24 and 48 hours, respectively (Fig 4.37 A). Whereas using the Amaxa kit the efficiency was 49.9% and 62.3% after 24 and 48 hours, respectively (Fig 4.37 B).

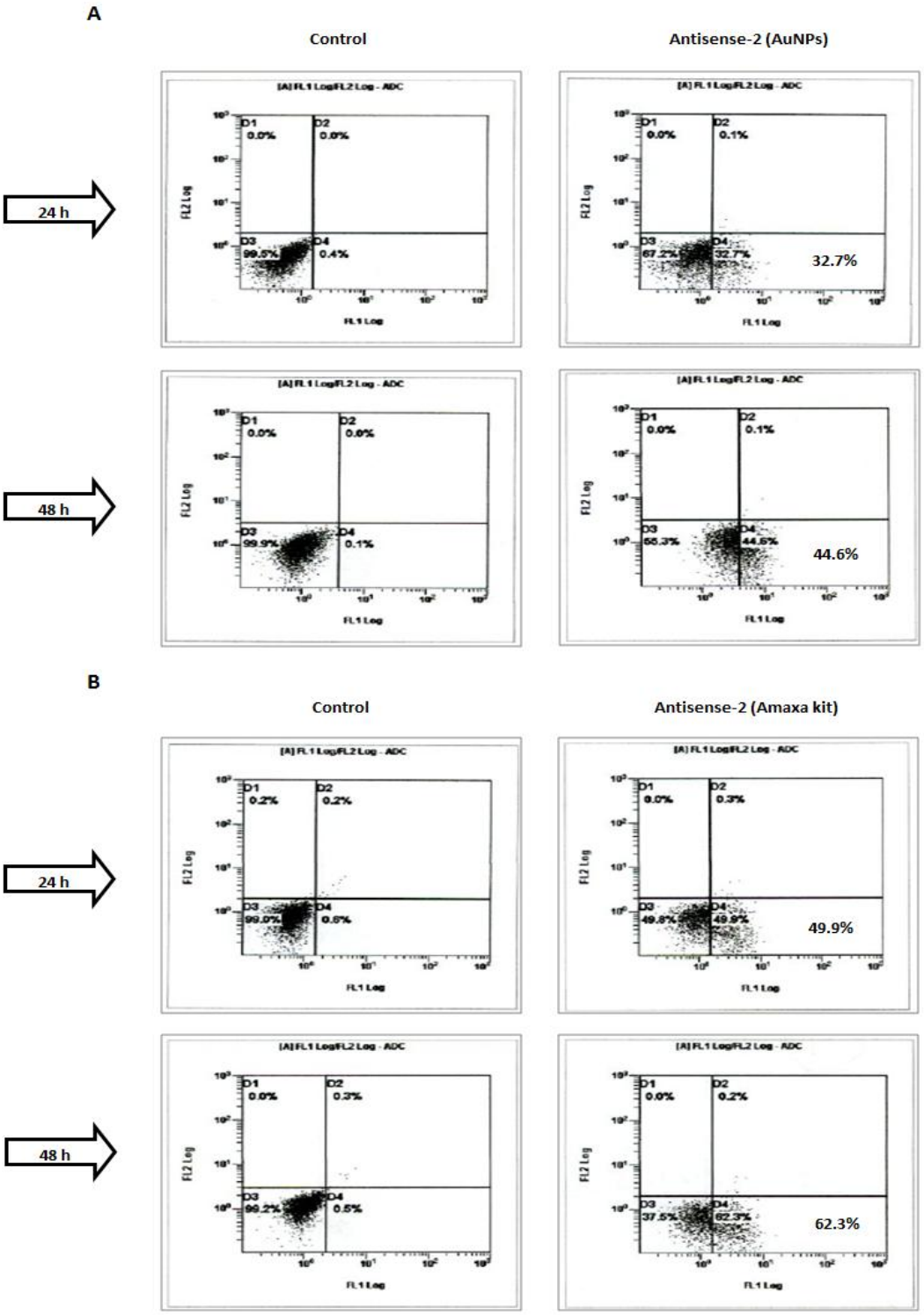

Figure 4.37. T-cells transfection efficiency measured by Flow cytometry using **A**). Antisense2-AuNPs, **B**). Antisense2-Amaxa kit.

Then, we evaluated the effect of AuNPs modified with siRNAs against p21, which were able to reduce the expression of the protein.

AuNPs modified with siRNA (at 120 nM) were incubated with T-cells at different time points. The western blot revealed that expression of p21 is decreased up to one hour (Fig 4.38 A) and the expression is recovered during the following hours (Fig 4.38 B). When higher concentration of AuNPs-siRNAs (150 nM) was employed the expression of p21 was affected even after 4 h (Fig 4.38 C).

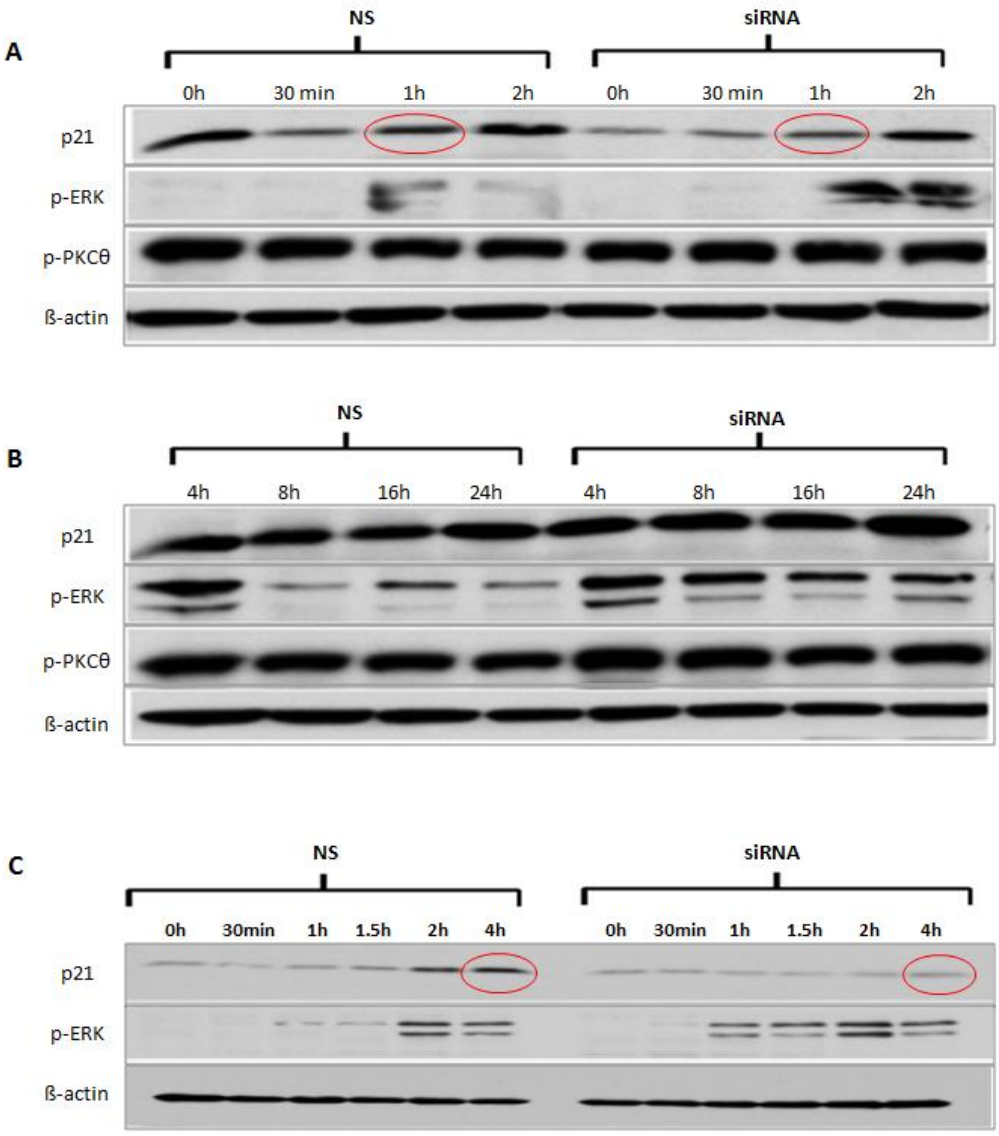

Figure 4.38. Western blot of T-cells treated with AuNPs modified with siRNAs against p21. **A, B**). 120nM and **C**). 150 nM.

5. DISCUSSION

DISCUSSION

5.1. Nanotechnology and Antibiotic Resistance Bacteria

The discovery and implementation of antibiotics in the early twentieth century transformed human health and wellbeing. However, the emergence of pathogenic bacteria resistant to many or all current antibiotics is currently a major public health concern and of particular importance in clinical settings. Nowadays, advanced technologies based in biotechnology and nanotechnology have a great potential to tackle this problem. In this sense, silver-based nanomaterials, such as AgNPs, have shown remarkable antimicrobial properties and are used in multiple applications. The work presented in this thesis was motivated by the excellent properties of AgNPs and has been focused in the development of a green process for the production of AgNPs as well as the development of novel nanoantibiotics based on DNA-AgNCs. In addition, the preliminary results of a collaboration where different oligonucleotides are used to control the gene expression of p21 in T-cell has been included as well. The first part of this thesis was carried out within the Biology Department at Universidad Autónoma de Madrid and the others at IMDEA Nanociencia. Below is included the discussion of the four topics addressed in this thesis.

5.2. Synthesis and antimicrobial activity of silver nanoparticles generated with Antarctic bacteria broths

AgNPs can be produced using different bacteria extracts, however, Antarctic bacteria have not been employed so far, and their broths might be very different compared with other species. In this work, in this case, the effect of light, temperature and salt concentration in the generation of AgNPs has been studied.

The production of AgNPs using bacteria broths was followed by UV–vis spectroscopy, showing a progressive increase in the absorbance at 450 nm due to the formation of AgNPs at 4 ˚C and 30 ˚C, but only when the incubation was carried out under the light (Figure 4.1). In addition, when NaCl was added to the reaction mixture, the yield decreased significantly (Figure 4.2)[68]. Several reports have shown a negative effect due to the presence of Cl^-[250,251], although others demonstrated that AgCl can be employed in the synthesis of AgNPs[238].

In this case the production of AgNPs was reduced in the presence of NaCl (5 g/l, 85.5 mM), particularly, at 4 °C. Thus we can conclude that, the presence of NaCl is deleterious for AgNPs production during the preparation of the broths from psychrophilic bacteria, despite growing in salty areas (Figure 4.2). In this experiments the highest yield was obtained using broths from *Y. kristensenii* at 30 °C, and the lowest using *A. salmonicida* at 4 °C (Table 4.1).

The sizes of the AgNPs obtained by the different bacteria were similar (around 6 nm), with the exception of the AgNPs produced at 30 °C using broths from *A. salmonicida*, which were noticeably larger (11.1 nm).

Size distributions for the different AgNPs obtained are shown as histograms in figure 4.7 and 4. 8. The PDI of the AgNPs obtained was around 0.2 in most cases (Table 4.1).

A PDI of 0.0 corresponds to monodisperse AgNPs, up to 0.1 AgNPs are considered as near (or narrow) monodisperse, from 0.1 to 0.4 AgNPs are moderate polydisperse, and values >0.4 indicate high polydispersity.

The highest (0.25) and lowest (0.1) PDI were obtained when broths from *Psychrobacter sp.* were employed at 30 °C and 4 °C, respectively (Table 4.1). In general the PDI was lower when the reaction was carried out at 4 °C. In the case of *P. veronii* the PDI was almost the same under both conditions.

The zeta potentials of the AgNPs obtained by this method were negative (Table 4.1). In this case, the highest potential was obtained at 30 °C using broths form *A. salmonicida* (-26.8 $\pm$ 3.1) and the lowest at 4 °C using broths from *P. veronii* (-17.6 $\pm$ 1.9).

The zeta potential is usually employed to predict the colloidal stability of NPs, and it correlates well in the case of *P. veronii,* which UV-Vis spectra show a significant drop in the intensity when the particles where aged for 10 months compared with particles obtained after 9 days (Fig. 4.4 C).

The antibacterial activity of AgNPs obtained in this thesis was tested in three bacteria from culture collections, two Gram-negative (*E. coli* and *K. pneumoniae*) and one Gram-positive (*S. epidermidis*). In general, AgNPs were more active against Gram-positive than against Gram-negative bacteria and more active when prepared at 4 °C than those obtained at 30 °C (Table 4.3). However, AgNPs obtained using *A. salmonicida* broths showed lower activity when prepared at 4 °C than when obtained at 30 °C, highlighting the importance of the broth employed. Indeed, the particles obtained from broths of this bacteria showed the highest

antimicrobial activity against *E. coli* and *K. pneumoniae*, and an excellent activity against *S. epidermidis*.

Regarding the mechanism of action of AgNPs the release of silver ions seems to be critical in the activity of AgNPs,[38] although their interaction with the bacteria cell envelopes have to be considered as well[252,253]. In this regard, the decrease in activity of aged AgNPs could be related to the generation of a corona surrounding the particle[254], which can prevent the release of silver ions and/or disrupt the interaction with the bacteria. Thus, the interaction between the AgNPs and bacteria will depend not only on the size, surface or surface/volume ratio of the NPs but also on the composition of the corona.

In this regard, it is worth mentioning that the UV–vis spectra of the AgNPs kept for 10 months (at 4 °C and 30 °C) did not change much in most cases (Fig 4.3 and 4.4), however their antimicrobial activities showed significant variations. Particularly, it decreased against the Gram-negative bacteria tested and increased slightly against *S. epidermidis* when kept at 4 °C (Fig 4.12).

In addition, AgNPs prepared at 4 °C using broths from *A. salmonicida* reported different behavior depending on the bacteria tested. Particularly, the aging process decreased their activity against *E. coli* but increased it against *K. pneumoniae*. However, in the case of AgNPs obtained from *Y. kristensenii* broths at 4 °C, the effect of aging in the activity turned to be the other way around, where the aged ones were more active against *E. coli* and less active against *K. pneumoniae*.

This phenomenon may be due to a combination of the different envelopes present in the species and the different corona surrounding the AgNPs. These results stress out the need for standardizing the bacteria tested in this kind of studies since differences can be observed not only among Gram-negative and Gram-positive bacteria but also depending on the particular species and also on the strain used as highlighted recently[255].

The activity of commercial available AgNPs stabilized with citrate was also evaluated at 8.5 µg/ml affording inhibition of 59.6%, 42.5% and 36.1% for *E. coli*, *S. epidermidis* and *K. pneumoniae*, respectively. Remarkably, the AgNPs prepared herein using broths from different bacteria showed more than 80% of inhibition at the same concentration in every bacteria. These results highlight the importance of the methods employed in the preparation of AgNPs to achieve good antimicrobials.

5.3.DNA silver nanoclusters as novel nanoantibiotics

DNA-AgNCs have recently emerged as new materials with interesting fluorescent properties, since they are more stable to photobleaching than organic dyes an smaller than quantum dots or fluorescent proteins. They contain few atoms of silver (2-10) and have a small size (<2 nm), close to the Fermi distance, that makes them fluorescent materials.

One of the most striking characteristics of DNA-AgNCs is the tunability of their fluorescent properties, which is an indication for the specific arrangement of the silver atoms[256,257]. In this sense, it is possible to modulate their excitation and emission wavelength by the sequence of the oligonucleotides employed in their preparation. Although the fluorescent properties of DNA-AgNCs cannot be predicted, emitters from the blue to the near-infrared have been reported, depending on the oligonucleotides sequence[258,259].

On the other hand the use of silver materials to treat bacterial infections is as old as history, however, DNA-AgNCs have not been evaluated before and their tunability by oligonucleotides could make them an interesting platform for the development of novel nanoantibiotics.

Among the first sequences tested, Seq-1, Seq-2 and Seq-3, the later one showed the best antimicrobial activity. This result could be explained by the differences of silver bound to the oligonucleotides, since cytosines bind silver better than other nucleobases[135] and Seq-3 has higher number of cytosines. However, quantification of silver in the different samples using TRXF revealed that Seq-1 contained more silver than the other derivatives and Seq-2 and Seq-3 contained almost the same amount (Fig 4.16). These results indicate that the activity of DNA-AgNCs is not only due to the presence of silver and other factors might modulate the antibacterial effect (e.g. sequence, structure).

Thus, additional sequences were evaluated to shed some light on the behavior observed (Fig. 4.17). The sequences were grouped by the emission color and although there is not a clear correlation between the sequence and the activity, it seems that blue emitters have the lowest activity, whereas yellow and red emitters have good antimicrobial activity. The amount of cytosines does not play any significant role, since sequences with the same number of cytosines have different activity (Fig 4.18).

Since we could not explain the different activity based on the sequence or the silver content we explored if it might be related with the structure and stability of the DNA-AgNCs. It is known

that the fluorescence properties of the AgNCs are strongly affected by their structure and environment[41] and we wonder if a similar behavior could be found in the case of their antibacterial activity. For this reason, CD studies were carried out to compare the structure and stability before and after the formation of the DNA-AgNCs at different temperatures (Fig 4.19).

The results revealed that Seq-2 and Seq-3 are folded into a secondary structure, such as an i-motif, before the generation of AgNCs. What is more, the new structures generated with these oligonucleotides after the formation of AgNCs are very robust since they do not change when heated at 75 °C. Interestingly, the CD spectra of the three samples evaluated revealed a pattern that match the antibiotic activity observed. It seems that as the derivatives are more structured they are more active (Fig 4.19B, 4.19D and 4.19F). The derivative obtained with Seq-3 presents larger CD signals at 220 nm and 270 nm, whereas the intensity obtained with Seq-2 is smaller and in the case of Seq-1 there is no significant CD signal. The prominent bands in Seq-3 DNA-AgNCs suggest a more structured conformation than for the other two and this difference might be related to the different activities observed. For instance, this nanostructure may interact better with the cell membrane and even improve the uptake of AgNCs[260].

The Seq-3 was used in further studies, such as a dose-dependent experiment and a comparative study against other silver derivatives. DNA-AgNCs stabilized with Seq-3 showed a nice dose-dependent response, which were able to suppress the growth of *E. coli* at 5 μM for at least 14 hours. However, at this concentration the system was only able to delay the growth up to 7 hours in *S. epidermidis* (Fig 4.20).

When the derivative was compared to silver salts or AgNPs, it showed a good activity, which was similar to silver nitrate in *E. coli* and less active than silver nitrate but better than AgNPs in *S. epidermidis*.

The excellent activity obtained with DNA-AgNCs might be due the combination of different mechanisms of action, such as, the intercalation of AgNCs in the DNA and the release of silver cations.

Motivated by the good properties of the AgNCs generated with the Seq-3 as antibacterial agent, we decided to prepare a modified derivative aiming to increase their inhibitory activity. Particularly, we wanted to evaluate the use of trimers, previouly reported by our group, in the stabilization of AgNCs as antimicrobials. This system has been used to obtain AgNCs with increased stability and fluorescence and it might also increase their antimicrobial activity.

Indeed, the AgNCs estabilized with the trimer showed excellent antimicrobial activity in both bacterias (Fig 4.22). The enhancement of the antimicrobial activity was more notorious in the case of *S. epidermidis* since at 0.750 μM the inhibition of the trimer was better (5 hrs) than when the single stranded system was used at 2.25 μM (3 hrs).

Finally, the role of DNA-AgNCs in the production of ROS was investigated using the fluorescent probe DCFH-DA in *E. coli* and *S. epidermidis* (Fig. 4.23). The production of ROS was clearly enhanced in the presence of DNA-AgNCs, pointing out that, at least, this is one of the mechanisms of action of DNA-AgNCs as antimicrobials.

5.4. Modified oligonucleotides in photodynamic therapy for bacteria growth control

PDT is being applied in the last years for the treatment of infectious diseases and superficial tumors[261, 262]. The technique involves the excitation with light of special molecules known as photosensitizers (PS), close to the target cells (e.g. bacteria, cancer cells). This process generates reactive oxygen species, which induce the death of the surrounding cells[263].

In this section we evaluated the use of oligonucleotides modified with the fluorescent dye 6-carboxy-2´,4,4´,5´,7,7´-hexachloro fluorescein (HEX) in PDT against bacteria.

Four different oligonucleotides were employed in this study, particularly, Seq-2, Seq-3 and Seq-7, which were conjugated with HEX, and Seq-8 used as control. In addition, these ONs-HEX were also employed in the preparation of AgNCs. The antibacterial activity of the system was assessed using two Gram-negative (*E. coli* and *P. aeruginosa*) and one Gram-positive (*S. aureus*) bacteria.

The cell wall of Gram-positive bacteria presents a thick and porous cell wall of inter-connected peptidoglycan layers that surround a cytoplasmic membrane[254,264], Gram-negative bacteria have an outer membrane, a thinner peptidoglycan layer and a cytoplasmic membrane[254].

The mechanism of action of PDT requires that the PS penetrates the cell walls [265] of the bacteria and end up in the plasma membrane or in the cytoplasm, however, the membrane barriers of the bacterial cell limit the simple diffusion of PS into the bacterial cytosol[266]. For this reason, Gram-positive bacteria are more sensitive to PDT than Gram-negative bacteria[267].

In our experiments with Seq-2, Seq-3, and Seq-7 containing HEX, and further modified by AgNCs where employed at 0.750, 1.5, and 3 µM. All samples reported good antibacterial activity when irradiated and employed at low concentration (Fig 4.26 and 4.31). However, when the oligonucleotides where employed at high concentration (3µM) the activity dropped significantly. This might be due to a self-quenching processes of HEX, which can be enhanced as the concentration increases[268].

We also observed different sensitivity of our bacterial strains to our system, which might be related to the different bacterial cell wall structure, as mentioned before.

5.5. Regulation of p21 by oligonucleotides conjugated to gold nanoparticles

Oligonucleotides can be used to control the expression of genes using different strategies, such as Antisense[269], Gapmer[270], and siRNA[213,214].

Antisense oligonucleotides are short and single stranded which are complementary to specific mRNA transcripts that promote the degradation of target mRNA by RNase H or by forming a stable DNA-RNA duplex. To elicit RNase H activation, chimera oligonucleotides with a DNA region and modified ribonucleotide regions are generally utilized as the antisense strands. These chimera oligonucleotides, named “Gapmer”, have wing regions consisting of modified ribonucleotides such as 2´-OMe RNA at both sides and a window region in the center consisting of DNA residues[271,272].

siRNAs are double stranded molecules, consisting of a guide strand that is perfectly complementary to a target mRNA and a passenger strand. The RNA duplex is recognized by a RISC complex, which will release the passenger strand and will use the guide one to find the target sequence in the cytoplasm.

However, one limitation of the use of oligonucleotides *in vitro* and *in vivo* is they low stability and poor translocation efficiencies. For this reason multiple approaches addressing this limitation are being developed.

For the delivery of nucleic acids, several lipid-based vectors (e.g., Transfectam[273] and Lipofectamine[274]) are available. However, despite their good transfection efficacy in cell culture, they have several limitations in clinical applications, e.g., toxicity, low storage stability, lack of targeting efficacy, and limited *in vivo* tracking/monitoring.

On the other hand, electroporation systems like the Amaxa kit employed here are expensive and a large amount of cells die during the process.

For these reasons, novel delivery systems such as AuNPs might be a good alternative to overcome the limitations of the current transfection systems. Particularly, AuNPs can be fabricated with low size dispersity[275] modified easily with a variety of molecules[276,277] , have very low toxicity[278,279] , good biodistribution[280,281] and can be excreted[282,283].

In this study, cyclin-dependent kinase inhibitor p21 was targeted by Antisense, Gapmer, and siRNA, using AuNPs as delivery system. Flow cytometry (Fluorescence-Activated Cell Sorting, FACS) was used to assess the transfection efficiency, showing that transfection efficiency mediated by AuNPs was 32.7% after 24 hours, while using the Amaxa kit was 49.9% (Fig.4.37). Importantly, using AuNPs, we observed a decrease in p21 expression as early as 1 hour after secondary stimulation (Fig 4.35 B). This difference could be related to the mechanism of AuNPs and Amaxa kit delivery systems, where the later might release the oligonucleotides slower (Fig 4.35 C).

The inhibition observed with the NPs modified with antisense 1 and 2 was very poor. However, we observed better inhibition in the case of antisense 2 and for this reason we employed this sequence in the preparation of other type of antisense (Gapmer) and a siRNA.

AuNPs modified with gapmer were able to decrease the expression of p21 after 1 h better than the previous antisense employed (Fig 4.36).

In the case of AuNPs functionalized with siRNAs the reduction of the expression was higher than in the previous cases. Particularly when the concentration was 120 nM the decrease in the expression was observed up to 1 h, and when the concentration employed was 150 nM the inhibition was maintained after 4 hrs (Fig 4.38).

Our data showed that the use of AuNPs as delivery systems of oligonucleotides in T-cells is very convenient since the system induces minimal death and leads to a very early reduction of the target protein. These characteristic are very important for systems where manipulation of a target protein should be rapid. This is the case for activation of T-cells, which occurs within the first hours after their stimulation.

6. CONCLUSIONS

CONCLUSIONS

Synthesis and antimicrobial activity of silver nanoparticles generated with Antarctic bacteria broths

1. Four new psychrophilic Antarctic bacteria have been employed in the synthesis of AgNPs.
2. Biosynthesis of AgNPs was successful at low (4 °C) and medium (30 °C) temperatures.
3. The diameter of AgNPs obtained depend on the bacteria and temperature used and ranged 5-11 nm.
4. The AgNPs obtained are excellent antimicrobials against Gram-negative and Gram-positive bacteria, presenting a very low IC_{50} >10 µg/ml.
5. AgNPs at 4 °C are stable and active antibacterials even 10 months under light.

DNA silver nanoclusters as novel nanoantibiotics

6. DNA-stabilized AgNCs show antibacterial activity against Gram-positive and Gram-negative bacteria.
7. Antibacterial activity depends on the sequence of the oligonucleotides employed.
8. Trimers of selected sequences (Seq3), improved antibacterial activity providing an excellent inhibition of bacteria growth at low concentration (750 nM).
9. ROS levels increased in the presence of DNA-AgNCs. Thus, we speculate that the antibacterial activity of DNA-AgNCs could be partially due to oxidative damage.

Photodynamic Therapy using Photosensitizers conjugated to oligonucleotides

10. Oligonucleotides modified with a fluorescence dye (HEX) are able to kill bacteria upon exposure to the proper light. The final activity can be enhanced by the addition of AgNCs.
11. The activity of ONs-HEX seems to be better at low concentrations, were self-quenching and aggregation are reduced.

p21 regulation with oligonucleotides conjugated to gold nanoparticles

12. AuNPs can be used to deliver different bioactive oligonucleotides (antisense and SiRNAs), into cells.

13. This method allows the reduction at very early time points of the target protein without inducing cell death, as is the case in electroporation methods (like the Amaxa kit).

7. CONCLUSIONES

CONCLUSIONES

Síntesis y actividad antimicrobiana de nanopartículas de plata obtenidas a partir de medio de bacterias de la Antártica.

1. Cuatro nuevas bacterias psicrófilas de la Antártica han sido utilizadas en la preparación de AgNPs.

2. La obtención de las AgNPs puede llevarse a cabo a distintas temperaturas (4 °C y 30 °C) .

3. El diámetro de las AgNPs depende de la bacteria y temperatura empleadas, el cual se encuentra entre 5-11 nm.

4. Las nanopartículas obtenidas han mostrado buena actividad (IC_{50} >10 µg/ml) contra bacterias Gram-negativas y positivas.

5. AgNPs preparadas a 4 °C mantienen su actividad tras 10 meses incubadas bajo la luz.

Nanoclústeres de Plata estabilizados por ADN como nuevos nanoantibióticos.

6. DNA-AgNCs se han mostrado activos contra bacterias Gram-positivas y negativas.

7. La actividad antibacteriana depende de la secuencia empleada.

8. La preparación de un trímero con la secuencia Seq-3 mejora su actividad, inhibiendo el crecimiento bacteriano a muy baja concentración (750 nM).

9. La producción de ROS es aumentada en presencia de DNA-AgNCs , lo que sugiere que la actividad puede deberse en parte a daño oxidativo.

Terapia fotodinámica utilizando fotosensibilizadores conjugados a oligonucleótidos.

10. Oligonucleótidos modificados con una molécula fluorescente (HEX) son capaces de eliminar bacterias cuando son excitados con luz. La actividad final puede verse mejorada en algunos casos mediante la formación de los correspondientes AgNCs.

11. La actividad de estos sistemas parece ser mayor a baja concentración donde los efectos de *self-quenching* y agregación son menores.

Regulación de p21 con oligonucleótidos conjugados a nanopartículas de oro.

12. Las AuNPs pueden utilizarse para transportar diferentes oligonucleótidos con actividad biológica a las células.

13. Este método permite la reducción de la expresión de la proteína deseada a tiempos cortos con muy baja toxicidad, comparado con técnicas de electroporación (Amaxa kit).

8. REFERENCES

REFERENCES

1. Farokhzad, O.C. & Langer, R. Nanomedicine: developing smarter therapeutic and diagnostic modalities. *Adv. Drug Deliv*. *Rev*.**58**, 1456–1459 (2006).
2. Liu, Y., Miyoshi, H. & Nakamura, M. Nanomedicine for drug delivery and imaging: a promising avenue for cancer therapy and diagnosis using targeted functional nanoparticles.*Int. J. Cancer*. **120**, 2527–2537 (2007).
3. Koutsopoulos, S. Molecular fabrications of smart nanobiomaterials and applications in personalized medicine. *Advanced Drug Delivery Reviews*. **64**, 1459-1476 (2012).
4. Alon, N. Miroshnikov, Y. Perkas, N. Nissan, I. Gedanken. A. Shefi, O. Substrates coated with silver nanoparticles as a neuronal regenerative material. *International Journal of Nanomedicine.* **9**, 23-31 (2014).
5. Hirano, K. Ishido, T. Yamamoto, Y, S. Murase, N. Ichikawa, M. Yoshikawa, K. Baba, Y. Itoh, T. Plasmonic imaging of brownian motion of single DNA molecules spontaneously binding to Ag nanoparticles. *Nano Lett.* **13**, 1877-82 (2013).
6. Hao, Y. Zhou, B. Wang, F. Li, J. Deng, L. Liu, Y, N. Construction of highly ordered polyaniline nanowires and thei applications in DNA sensing. *Biosensors and Bioelectronics*. **52**, 422-426 (2014).
7. Gharagozloo, M. Majewski, S. Foldvari,M. Therapeutic applications of nanomedicine in autoimmune diseases: From immunosuppression to tolerance induction. *Nanomedicine: Nanotechnology, Biology and Medicine.* **11**, 1003-1018 (2015).
8. Gupta, A, S. Nanomedicine approaches in vascular disease: a review. *Nanomedicine: Nanotechnology, Biology, and Medicine*. **7**, 763-779 (2011).
9. Burgo, L, S, D. Hernández, R, M. Orive, G. Pedraz, J, L. Nanotherapeutic approaches for brain cancer management. *Nanomedicine: Nanotechnology, Biology, and Medicine*. **10**, 905-919 (2014).
10. Jiang, T. Carbone, J, E. Lo, K, W, H. Laurencin, C,T. Electrospinning of polymer nanofibers for tissue regeneration. *Progress in Polymer Science*. **46**, 1-24 (2015).
11. Meir, R. Shamalov, K. Betzer, O. Motiei, M. Fried, M,H. Yehuda,R. Popovtzer, A. Popovtzer, A. Cohen, C, J. Nanomedicine for Cancer Immunotherapy: Tracking CancerSpecificT‐Cellsin Vivowith Gold Nanoparticles and CT Imaging. *ACS NANO*. **9**, 6363-6372 (2015).

12. Wang, Y. Miao, L. Satterlee,A. Huang, L. Delivery of oligonucleotides with lipid nanoparticles. *Advanced Drug Delivery Reviews*. **87**, 68-80 (2015).

13. Toman, P. Lien, C, F. Ahmad, Z. Dietrich, S. Smith, J,R. An, Q. Molnár, E. Pilkington, G, J. Górecki, D, C. Tsibouklis,J. Barbu, E. Nanoparticles of alkylglyceryl-dextran-graft-poly(lactic acid) for drug delivery to the brain: Preparation andin vitro investigation. *Acta Biomaterialia*. **23**, 250-262 (2015).

14. Chen,W. Li, Y. Yang, S. Yue, L. Jiang, Q. Xia, W. Synthesis and antioxidant properties of chitosan and carboxymethyl chitosan-stabilized selenium nanoparticles. *Carbohydrate Polymers*. **132**, 574-581 (2015).

15. Davidovi, S. Miljkovi , M. Lazi, V. Jovi ,D. Joki, B. Dimitrijevi , S. Radeti , M. Impregnation of cotton fabric with silver nanoparticles synthesized by dextran isolated from bacterial species Leuconostoc mesenteroides T3. *Carbohydrate Polymers*. **131**, 331-336 (2015).

16. Li, X. Xue, M. Raabe, O, G. Aaron, H,L. Eisen, E, A. Evans, J, A. Hayes, F, A. Inaga, S. Tagmount, A. Takeuchi, M. Vulpe, C. Zink, J, I. Risbud, S, H. Pinkerton, K, E. Aerosol droplet delivery of mesoporous silica nanoparticles: A strategy for respiratory-based therapeutics. *Nanomedicine: Nanotechnology, Biology, and Medicine*. **11**, 1377-1385 (2015).

17. Kumar, P. Lambadi, P, R. Navani, N, K. Non-enzymatic detection of urea using unmodified gold nanoparticles based aptasensor. *Biosensors and Bioelectronics*. **72**, 340-347 (2015).

18. Xu, Y, F. Gao, M, R. Zheng, Y, R. Jiang, J. Yu, S, H. Nickel/Nickel(II) Oxide Nanoparticles Anchored onto Cobalt(IV) Diselenide Nanobelts for the Electrochemical Production of Hydrogen. *Angew. Chem. Int. Ed*. **52**, 8546- 8550 (2013).

19. Gan, W. Xu, B. Dai, H, L. Activation of Thiols at a Silver Nanoparticle Surface. *Angew. Chem. Int. Ed*. **50**, 6622-6625 (2011).

20. Scharlach, C. Kratz, H. Wiekhorst, F. Warmuth, C. Schnorr, J. Genter, G. Ebert, M. Mueller, S. Schellenberger, E. Synthesis of acid-stabilized iron oxide nanoparticles and comparison for targeting atherosclerotic plaques: Evaluation by MRI, quantitative MPS, and TEM alternative to ambiguous Prussian blue iron staining. *Nanomedicine: Nanotechnology, Biology, and Medicine*. **11**, 1085-1095 (2015).

21. Hayat, A. Haider, W. Raza, Y. Marty, J, L. Colorimetric cholesterol sensor based on peroxidase like activity of zinc oxide nanoparticles incorporated carbon nanotubes. *Talanta*. **143**, 157-161 (2015).

22. Liang, G. Ronald, J. Chen, Y. Ye, D. Pandit, P. Ma, M, L. Rutt, B. Rao, J. Controlled Self-Assembling of Gadolinium Nanoparticles as Smart Molecular Magnetic Resonance Imaging Contrast Agents. *Angew. Chem. Int. Ed*. **50**, 6283-6286 (2011).

23. Ahmad, R. Mohsin, M. Ahmad, T. Sardar, M. Alpha amylase assisted synthesis of TiO2nanoparticles: Structural characterization and application as antibacterial agents. *Journal of Hazardous Materials.* **283**, 171-177 (2015).

24. Alexander, J, W. History of the medical use of silver. *Surg. Infect*. **10**, 289-292 (2009).

25. Klasen, H, J. Historical review of the use of silver in the treatment of burns.I. Early uses. *Burns*. **26**, 117-130 (2000).

26. Silver,S. & Phung, L, T. Bacterial heavy metal resistance: New Surprises. *Annu. Rev. Microbiol.* **50**, 753-789 (1996).

27. Nowack, B. Krug, H, F. Height, M. 120 Years of Nanosilver History: Implications for Policy Makers. *Environ. Sci. Technol.* **45**, 1177-1183 (2011).

28. Khlebtsov, N, G. Dykman, L, A. Optical properties and biomedical applications of plasmonic nanoparticles. *Journal of Quantitative Spectroscopy & Radiative Transfer*. **111**, 1-35 (2010).

29. Amendola, V. Bakr, O, M. Stellacci, F. A Study of the Surface Plasmon Resonance of Silver Nanoparticles by the Discrete Dipole Approximation Method: Effect of Shape, Size, Structure, and Assembly. *Plasmonics*. **5**, 85-97 (2010).

30. Feng, D. Li, L. Zhao, J. Zhang, Y. Simultaneous electrochemical detection of multiple biomarkers using gold nanoparticles decorated multiwall carbon nanotubes as signal enhancers. *Anal. Biochem*. **482**, 48-54 (2015).

31. Petoukhoff, C, E. & O'Carroll, D, M. Absorption-induced scattering and surface plasmon out-coupling from absorber-coated plasmonic metasurfaces. *Nature Communications*. **6**, 7899 (2015).

32. Guerrini, L. Krpetic, Z. Lierop, D, V. Alvarez-Puebla, R,A. Graham, D. Direct Surface-Enhanced Raman Scattering Analysis of DNA Duplexes. *Angew. Chem. Int. Ed*. **54**, 1144-1148 (2015).

33. Gao, Y. Li, X. Li, Y. Li, T. Zhao, Y. Wu, A. A simple visual and highly selective colorimetric detection of Hg^{2+} based on gold nanoparticles modified by 8-hydroxyquinolines and oxalates. *Chem. Commun*.**50**, 6447–6450 (2014).

34. Wu, S. Chen, Y. Sung, Y. Colorimetric detection of Fe3+ ions using pyrophosphate functionalized gold nanoparticles. *Analyst.* **136**, 1887–1891 (2011).

35. Wu, Z. Zhao, H. Xue, Y. Cao, Q. Yang, J. He, Y. Li, X.Yuan, Z. Colorimetric detection of melamine during the formation of gold nanoparticles. *Biosens. Bioelectron*.**26**, 2574–2578 (2011).

36. Xia, F. Zuo, X. Yang, R. Xiao, Y. Kang, D. Vallee-Belisle, A. Gong, X. Yuen, J, D. Hsu, B, B, Y. Heeger, A , J.Plaxco, K, W. Colorimetric detection of DNA, small molecules, proteins, and ions using unmodified gold nanoparticles and conjugated polyelectrolytes. *PNAS.* **107**,10837–10841 (2010).

37. Stevanovi, M, M. Skapin, S, D. Bracko, I. Milenkovic, M. Petkovi, J. Filipi, M. Uskokovic,D,P. Poly(lactide-co-glycolide)/silver nanoparticles: Synthesis, characterization, antimicrobial activity, cytotoxicity assessment and ROS-inducing potential. *Polymer*. **53**, 2818- 2828 (2012).

38. Ouay, B, L. Stellacci, F. Antibacterial activity of silver nanoparticles: A surface science insight. *Nano Today*. **10**, 339-354 (2015).

39. Patel, V. Berthold, D. Puranik, P. Gantar, M. Screening of cyanobacteria and microalgae for their ability to synthesize silver nanoparticles with antibacterial activity. *Biotechnology Reports*. **5**, 112-119 (2015).

40. Lee, S, J. Heo, D, N. Moon, J, H. Ko, W, K. Lee, J, B. Bae, M,S. Park, S, W. Kim, J, E. Lee, D, H. Kim, E, C. Lee, C, H. Kwon, I, K. Electrospun chitosan nanofibers with controlled levels of silver nanoparticles. Preparation, characterization and antibacterial activity. *Carbohydrate Polymers* . **111**, 530-537 (2014).

41. Glišic, S. Cakic, M. Nikolic, G. Danilovic, B. Synthesis, characterization and antimicrobial activity of carboxymethyl dextrane stabilized silver nanoparticles. *Journal of Molecular Structure.* **1084**, 345-351 (2015).

42. Jiang, B. Tian, C. Song, G. Pan, Q. Wang, Z. Shi, L. Qiao, Y. Fu, H. A green route to synthesize novel Ag/C antibacterial agent. *Materials Research Bulletin*. **47**, 458-463 (2012).

43. Rhim, J, W. Wang, L, F. Hong, S, I. Preparation and characterization of agar/silver nanoparticles compositefilms with antimicrobial activity. *Food Hydrocolloids*. **33**, 327-335 (2013).

44. Zhang, Q. Li, N. Goeblt, J. Lu, Z. Yin, Y. A systematic study of the synthesis of silver nanoplates: is Citrate a 'magic' reagent?. *J Am. Chem. Soc.* **133**, 18931–18939 (2011).

45. Sotiriou, G, A. & Pratsinis, S, E. Antibacterial activity of nanosilver ions and particles. *Environ. Sci. Technol*. **44**, 5649–5654 (2010).

46. Rolda´n, M, V. Pellegri, N. Sanctis, O. Electrochemical method for Ag-PEG nanoparticles synthesis. *J. Nanopart*. **2013**, 524150–524156 (2013).

47. Sotiriou, G, A. Teleki, A. Camenzind, A. Krumeich, F. Meyer, A. Panke, S. Pratsinis, E. Nanosilver on nanostructured silica: antibacterial activity and Ag surface area. *Chem. Eng. J.* **170**, 547–554 (2011).

48. Tran, Q, H. Nguyen, V, Q. Le, A,T.Silver nanoparticles: synthesis, properties, toxicology, applications and perspectives. *Adv. Nat. Sci.: Nanosci. Nanotechnol.***4**, 033001 (20pp) (2013).

49. Tien, D. Tseng, k, h. Liao, C, Y. Huang, J,C. Tsung, T, T. Discovery of ionic silver in silver nanoparticle suspension fabricated by arc discharge method. *J. Alloys Compd*. **463**, 408–411 (2008).

50. Kosmala, A. Wright, R.Zhang, Q. Kirby, P. Synthesis of silver nano particles and fabrication of aqueous Ag inks for inkjet printing. *Mater. Chem. Phys*. **129**, 1075–1080 (2011).

51. Asanithi, P. Chaiyakun, S. Limsuwan, P. Growth of silver nanoparticles by DC magnetron sputtering. *J. Nanomater.* **2012**, 963609–963616 (2012).

52. Gopinathan, P. Ashok, A, M. Selvakumar, R. Bacterial flagella as biotemplate for the synthesis of silver nanoparticle impregnated bionanomaterial. *Applied Surface Science*. **276**, 717-722 (2013).

53. Li, G. He, D. Qian, Y. Guan, B. Gao, S. Cui, Y. Yokoyama, K. Wang, L. Fungus-mediated green synthesis of silver nanoparticles using Aspergillus terreus. *Int. J. Mol. Sci.* **13**, 466–476 (2012).

54. Mourato, A. Gadanho, M. Lino, A, R. Tenreiro, R. Biosynthesis of crystalline silver and gold nanoparticles by extremophilic yeasts. *Bioinorg. Chem. Appl*. **2011**, 546074–546081 (2011).

55. Ramesh, P, S. Kokila, T. Geetha, D. Plant mediated green synthesis and antibacterial activity of silver nanoparticles using *Emblica officinalis* fruit extract. *Spectrochimica Acta Part A: Molecular and Biomolecular Spectroscopy*. **142**, 339-343 (2015).

56. Ge, L. Li, Q. Wang, M. Ouyang, J. Li, X. Xing, M, M. Nanosilver particles in medical applications: synthesis, performance, and toxicity. *Int. J. Nanomed.* **9**, 2399–2407 (2014).

57. Roy, N. Gaur, A. Jain, A. Bhattacharya, S. Rani, V. Green synthesis of silver nanoparticles: An approach to overcome toxicity. *ENVIRONMENTAL TOXICOLOGY AND PHARMACOLOGY*. **36**, 807-812 (2013).

58. Narayanan, K, B. Sakthivel, N. Biological synthesis of metal nanoparticles by microbes. *Advances in Colloid and Interface Science.* **156**, 1-13 (2010).

59. Quester, K. Avalos-Borja, M. Castro-Longoria, E. Biosynthesis and microscopic study of metallic nanoparticles. *Micron*. **54-55**, 1-27 (2013).

60. Schröfel, A. Kratošová, G. Šafarík, I. Šafarˇíková, M. Raška, I. Shor, L, M. Applications of biosynthesized metallic nanoparticles – A review. *Acta Biomaterialia*. **10**, 4023-4042 (2014).

61. Klaus, T. Joerger, R. Olsson, E. Granqvist, C, G. Silver-based crystalline nanoparticles, microbially fabricated. *PNAS*. **96**, 13611-13614 (1999).

62. Ghorbani, H, R. Safekord, A, A. Attar, H. Sorkhabadi, S, M, R. Biological and Non-biological Methods for Silver Nanoparticles Synthesis. *Chem. Biochem. Eng*. **25**, 317-326 (2011).

63. Kalimuthu,K. Babu, R,S. Venkataraman, D. Bilal, M. Gurunathan, S. Biosynthesis of silver nanocrystals by Bacillus licheniformis. *Colloids and Surfaces B: Biointerfaces*. **65**, 150-153 (2008).

64. Reidy, B. Haase,A. Luch,A. Dawson, K, A. Lynch, I. Mechanisms of Silver Nanoparticle Release, Transformation and Toxicity: A Critical Review of Current Knowledge and Recommendations for Future Studies and Applications. *Materials*. **6**, 2295-2350 (2013).

65. Kivistö, A, T. & Karp, M, T. Halophilic anaerobic fermentative bacteria. *Journal of Biotechnology.* **152**, 114-124 (2011).

66. Juibari,M. M. Abbasalizadeh, S. Salehi Jouzani, GH. Noruzi, M. Intensified biosynthesis of silver nanoparticles using a native extremophilic Ureibacillus thermosphaericus strain. *Materials Letters*. **65**, 1014-1017 (2011).

67. Dziewit, L. Grzesiak, J. Ciok, A. Nieckarz, M. Zdanowski, M, K. Sequence determination and analysis of three plasmids of *Pseudomonas* sp. GLE121, a psychrophile isolated from surface ice of Ecology Glacier (Antarctica). *Plasmid*. **70**, 254-262 (2013).

68. Javani, S. Marín, I. Amils, R. Abad, J, P. Four psychrophilic bacteria from Antarctica extracellularly biosynthesize at low temperature highly stable silver nanoparticles with outstanding antimicrobial activity . *Colloids and Surfaces A: Physicochem. Eng. Aspects.* **483**, 60-60 (2015).

69. Shivaji, S. Madhu, S. Singh, S. Extracellular synthesis of antibacterial silver nanoparticles using psychrophilic bacteria. *Process Biochemistry*. **46**, 1800-1807 (2011).

70. Ramanathan, R. Mullane, A, P, O. Parikh, R, Y. Smooker, P ,M. Bacterial Kinetics-Controlled Shape-Directed Biosynthesis of Silver Nanoplates Using *Morganella psychrotolerans*. *Langmuir.* **27**, 714-719 (2011).

71. Andersson, D,I. & Hughes, D. Antibiotic resistance and its cost: is it possible to reverse resistance?. *Nature Reviews | Microbiology*. **8**, 260-271 (2010).

72. Piddock, L, J, V. Multidrug-resistance efflux pumps — not just for resistance. *Nature Reviews | Microbiology*. **4**, 629- 636 (2006).

73. Pasberg-Gauhl, C. A need for new generation antibiotics against MRSA resistant bacteria. *Drug Discovery Today: Technologies | Drug resistance*. **11**, 109- 116 (2014).

74. Lupoli, T, J. Lebar, M, D. Markovski, M. Bernhardt, T. Kahne, D. Walker, S. Lipoprotein Activators Stimulate Escherichia coli Penicillin-Binding Proteins by Different Mechanisms. *J. Am. Chem. Soc*. **136**, 52-55 (2014).

75. Chifiriuc, C, M. Grumezescu, A, M. Saviuc, C. Croitoru, C. Mihaiescu, D, E. Lazar, V. Improved antibacterial activity of cephalosporins loaded in magnetic chitosan microspheres. *International Journal of Pharmaceutics*. **436**, 201-205 (2012).

76. Phelan, R, M.& Townsend, C, A. Mechanistic Insights into the Bifunctional Non-Heme Iron Oxygenase Carbapenem Synthase by Active Site Saturation Mutagenesis. *J. Am. Chem. Soc.* **135**, 7496-7502 (2013)

77. Martins, A, C. Pezoti, O. Cazetta, A, L. Bedin, K, C. Yamazaki, D, A, S. Bandoch, G, F, G. Asefa, T. Visentainer, J, V. Almeida, V, C. Removal of tetracycline by NaOH-activated carbon produced from macadamia nut shells: Kinetic and equilibrium studies. *Chemical Engineering Journal*. **260**, 291-299 (2015).

78. Bujnowski, K. Synoradzki, L. Zevaco, T, A. Dinjus, E. Augustynowicz-Kope, E. Napiorkowska, A. Rifamycin antibioticsd new compounds and synthetic methods. Part 4: Study of the reaction of 3-formylrifamycin SV with secondary amines and ketones. *Tetrahedron*. **71**, 158- 169 (2015).

79. Xiong, W. Sun, Y. Ding, X. Zhang, Y. Zhong, X. Liang, W. Zeng, Z. Responses of plasmid-mediated quinolone resistance genes and bacterial taxa to (fluoro) quinolones-containing manure in arable soil. *Chemosphere*. **119**, 473-478 (2015).

80. Taieb, A. Ortonne, J, P. Ruzicka, T. Roszkiewicz, J. Berth-Jones, J. Peirone, M, H. Jacovella, J. Superiority of ivermectin 1% cream over metronidazole 075% cream in treating inflammatory lesions of rosacea: a randomized, investigator-blinded trial. *British Journal of Dermatology*. **172**, 1103-1110 (2015).

81. Silhavy, T, J. Kahne, D. Walker, S. The Bacterial Cell Envelope. *Cold Spring Harb Perspect Biol*. **2**:a000414 (2010).

82. Bradley, J, S. Which antibiotic for resistant Gram positives, and why?. *Journal of infection*. **68**, S63-S75 (2014).

83. http://theamazingmedicine.blogspot.com.es/2013/07/microbiology-iv-domain bacteria.html. (Accessed 20, September, 2015).

84. https://www.koofers.com/flashcards/mcb-chapter-3-cell-structu/review. (Accessed 20, September, 2015).

85. http://hawashpharma.blogspot.com.es/2011/07/difference-between-gram-positive-and.html. (Accessed 20, September, 2015).

86. Bi, S. Ranzoni, A. Huang, J, X. Hansford, K. Cooper, M, A. Affinities and in-plane stress forces between glycopeptide antibiotics and biomimetic bacterial membranes. *Sensing and Bio-Sensing Research*. **3**, 24-30 (2015).

87. Silver, L, L. Does the cell wall of bacteria remain a viable source of targets for novel antibiotics?. *biochemical pharmacology*. **71**, 996-1005 (2006).

88. Sharma, P. Tomar, K. Goswami, P. Sangwan, V. Singh, R. Antibiotic resistance among commercially available probiotics. *Food Research International*. **57**, 176-195 (2014).

89. Madhavan, H, N. & Muralis, S. Mechanisms of Development of Antibiotic Resistance in Bacteria Among Clinical Specimens. *J Clin Biomed Sci*, **1**, 42-48 (2011).

90. Douglas Morier, Antibiotic resistance, ENCYCLOPAEDIA BRITANNICA, Accessed, 20 , August, 2015.

91. Lara, H, H. Garza-Trevino, E, N. Ixtepan-Turrent, L.Singh, D, K. Silver nanoparticles are broad-spectrum bactericidal and virucidal compounds. *J. Nanobiotechnol*. **9**, 30 (2011) .

92. Rai, M, K. Deshmukh, S,D. Ingle, A, P. Gade, A, K. Silver nanoparticles: the powerful nanoweapon against multidrug-resistant bacteria. *J. Appl. Microbiol.* **112**, 841-852 (2012).

93. Randall, C, P. Arya, G. Nicole, J. David, B. Alex, O, J. Silver resistancein Gram-negative bacteria: a dissection of endogenous and exogenous mechanisms. *Journal of Antimicrobial Chemotherapy.* **70**, 1037-1046 (2015).

94. Kristel, M. Natalie, L. Jacques, M. Simon, S. Rob, V, H. Antimicrobial silver: uses, toxicity and potential for resistance. *BioMetals*. **26**, 609-621 (2013).

95. Liu,Y. He, L. Mustapha, A. Li, H. Hu, Z,Q. Lin, M. Antibacterial activities of zinc oxide nanoparticles against Escherichia coli O 157:H7. *J. Appl. Microbiol.* **107**, 1193-1201 (2009).

96. Chamundeeswari, M. Sobhana,S,S. Jacob, J, P. Kumar, M, G. Devi, M, P. Sastry, T, P. Mandal, A, B. Preparation, characterization and evaluation of a biopolymeric gold nanocomposite with antimicrobial activity. *Biotechnol. Appl. Biochem.* **55**, 29-35 (2010).

97. Huang, W,C. Tsai, P, J. Chen, Y, C. Multifunctional Fe3O4@Au nanoeggs as photothermal agents for selective killing of nosocomial and antibiotic-resistant bacteria. *Small*. **5**, 51-56 (2009).

98. Sharma, V, K. Yngard, R, A. Liu, Y. Silver nanoparticles: green synthesis and their antimicrobial activities. *Adv. Colloid Interface Sci.* **145**, 83-96 (2008).

99. Morones, J.R., Elechiguerra, J. L., Camacho, A. and Ramirez, J.T. The bactericidal effect of silver nanoparticles. *Nanotechnology.* **16**, 2346–2353 (2005).

100. Sondi, I. and Salopek-Sondi, B. Silver nanoparticles as antimicrobial agent: a case study on *E. coli* as a model for gram-negative bacteria. *J Colloid Interface Sci*. **275**, 77–82 (2007).

101. Kim, J.S., Kuk, E., Yu, K.N., Kim, J.H., Park, S.J., Lee, H.J., Jeong, D.H. and Cho, M.H. Antimicrobial effects of silver nanoparticles. *Nanomed Nanotechnol Biol Med*.**3**,95–101 (2007).

102. Hwang, E.T., Lee, J.H., Chae, Y.J., Kim, Y.S., Kim,B.C.,Sang, B. and Gu, M.B. Analysis of the toxic mode of action of silver nanoparticles using stress-specific bioluminescent bacteria. *Small*.**4**, 746–750 (2008).

103. Ouda, S, M. Some Nanoparticles Effects on Proteus sp. and Klebsiella Sp. Isolated from Water. *American Journal of Infectious Diseases and Microbiology.* **2**, 4-10 (2014).

104. Shrivastava, S., Bera, T., Roy, A., Singh, G., Ramachandrarao, P.and Dash, D. Characterization of enhanced antibacterial effects of novel silver nanoparticles. *Nanotechnol*.**18**,103–112 (2008).

105. Mittler, R. Vanderauwera, S. Suzuki, N. Miller, G. Tognetti, V, B. Vandepoele, K. Gollery, M. Shulaev, V. Breusegem, F, V. ROS signaling: the new wave?. *Trends in Plant Science*. **16**, 300-309 (2011).

106. Schmitt, F, J. Renger, G. Friedrich, T. Kreslavski, V, D. Zharmukhamedov, S, K. Los, D, A. Kuznetsov, V, V. Allakhverdiev, S, I. Reactive oxygen species: Re-evaluation of generation, monitoring and role in stress-signaling in phototrophic organisms. *Biochimica et Biophysica Acta*. **1837**, 835-848 (2014).

107. Azizova, O, A. Panasenko, O. Volnov, T. Vladimirov, Y, A. Free radical lipid oxidation affects cholesterol transfer between lipoproteins and erythrocytes. *Free Radic. Biol. Med.* **7**, 251–257 (1989).

108. Lyras, L. Perry, R,H. Perry, E, K. Ince, P,G. Jenner, A. Jenner, P. Halliwell, B. Oxidative damage to proteins, lipids, and DNA in cortical brain regions from patients with dementia with Lewy bodies. *J. Neurochem*. **71**, 302–312 (1998).

109. Cadet, J. Douki, T. Ravanat, J, L. Oxidatively generated base damage to cellular DNA. *Free Radic. Biol. Med*., **49**, 9–21 (2010).

110. González, F, B. & Demple, B. Metabolic sources of hydrogen peroxide in aerobically growing Escherichia coli. *J Biol Chem*. **270**, 13681-13687 (1995).

111. Albesa, I. Becerra, M, C. Battan, P, C. Paez, P, L. Oxidative stress involved in the antibacterial action of different antibiotics. *Biochemical and Biophysical Research Communications.* **317**, 605-609 (2004).

112. Xu, H. Qu, F. Xu, H. Lai, W. Wang, Y,A. Aguilar, Z, P. Wei, H. Role of reactive oxygen species in the antibacterial mechanism of silver nanoparticles on Escherichia coli O157:H7. *Biometals.* 25, 45-53 (2012).

113. Yuan, X. Setyawati, M, I. Tan, A, S. Ong, C, N. Leong, D, T. Xie, J. Highly luminescent silver nanoclusters with tunable emissions: cyclic reduction–decomposition synthesis and antimicrobial properties. *NPG Asia Materials.* **5**, e39 (2013).

114. Gomes, A. Fernandes, E. Lima, J, L, F, C. Fluorescence probes used for detection of reactive oxygen species. *J. Biochem. Biophys. Methods*. **65**, 45-80 (2005).

115. Lokina, S. Stephen, A. Kaviyarasan, V. Arulvasu, C. Narayanan, V. Cytotoxicity and antimicrobial activities of green synthesized silver nanoparticles. *European Journal of Medicinal Chemistry*. **76**, 256-263 (2014).

116. Ramar, M. Manikandan, B. Marimuthu, P, N. Raman, T. Mahalingam, A. Subramanian, P. Karthick, S. Munusamy, A. Synthesis of silver nanoparticles using Solanum trilobatumfruits extract and its antibacterial, cytotoxic activity against human breast cancer cell line MCF 7.

Spectrochimica Acta Part A: Molecular and Biomolecular Spectroscopy. **140**, 223-228 (2015).

117. Fadeel, B. & Garcia-Bennett, A, E. Better safe than sorry: Understanding the toxicological properties of inorganic nanoparticles manufactured for biomedical applications. *Advanced Drug Delivery Reviews*. **62**, 362-374 (2010).

118. Dar, M, A. Ingle, A. Rai, M. Enhanced antimicrobial activity of silver nanoparticles synthesized by Cryphonectriasp. evaluated singly and in combination with antibiotics. *Nanomedicine: Nanotechnology, Biology, and Medicine*. **9**, 105-110 (2013).

119. Fayaz, A, M. Balaji, K. Girilal, M. Yadav, R. Kalaichelvan, P, T. Venketesan, R. Biogenic synthesis of silver nanoparticles and their synergistic effect with antibiotics: a study against gram-positive and gram-negative bacteria. *Nanomedicine: Nanotechnology, Biology, and Medicine.* **6**, 103-109 (2010).

120. Raimondi, F. Scherer, G, G. Kötz, R. Wokaun, A. Nanoparticles in energy technology: examples from electrochemistry and catalysis. *Angew. Chem. Int.Ed Engl*. **44**, 2190-2209 (2005).

121. Franci, G. Falanga, A. Galdiero, S. Palomba, L. Rai, M. Morelli, G. Galdiero, M. Silver Nanoparticles as Potential Antibacterial Agents. *Molecules*. 20, 8856-8874 (2015).

122. Pal, S. Tak, Y, K. Song, J, M. Dose the antibacterial activity of silver nanoparticles depend on the shape of the nanoparticle? A study of the gram-negative bacterium Escherichia coli. *Appl. Environ. Microbiol.* **27**, 1712-1720 (2007).

123. Agnihotri, S. Mukherji, S. Mukherji, S. Size-controlled silver nanoparticles synthesized over the range 5–100 nm using the same protocol and their antibacterial efficacy. *RSC Adv.* **4**, 3974-3983 (2014).

124. Syu, Y, Hung, J. Chen, J. Chuang, H. Impacts of size and shape of silver nanoparticles on Arabidopsisplant growth and gene expression. *Plant Physiology and Biochemistry*. **83**, 57-64 (2014).

125. Roy, E. Patra, S. Saha, S. Madhuri, R. Sharma, P, K. Shape-specific silver nanoparticles prepared by microwave assisted green synthesis using pomegranate juice for bacterial inactivation and removal. *RSC Advances*. DOI: 10.1039/C5RA18575K (2015).

126. Wilcoxon, J, P. & Abrams, B, L. Synthesis, structure and properties of metal nanoclusters. *Chem. Soc. Rev.* **35**, 1162- 1194 (2006).

127. Buceta, D. Piñeiro, Y. Vázquez-Vázquez, C. Rivas, J. López-Quintela, M, A. Metallic Clusters: Theoretical Background, Properties and Synthesis in Microemulsions. *Catalysts*. **4**, 356-374 (2014).

128. Zheng, J. Nicovich, P, R. Dickson, R, M. Highly Fluorescent Noble Metal Quantum Dots. *Annu Rev Phys Chem.* **58**, 409-431 (2007).

129. Petty,J,T. Zheng,J. Hud,N,V. Dickson,R,M. DNA-templated Ag nanocluster formation. *J. Am. Chem. Soc*. **126**, 5207–5212 (2004).

130. Kuperman, M, V. Chernii, S, V. Yu. Losytskyy, M. V. Kryvorotenko, D. Derevyanko, N, O. Slominskii, Y, L. Kovalska, V, B. Yarmoluk, S, M. Trimethine cyanine dyes as fluorescent probes for amyloid fibrils: The effect ofN,N´-substituents. *Anal. Biochem*. **484**, 9-17 (2015).

131. Charneca, A. Karmali, A. Vieira, M. Non-enzymatic assay for glucose by using immobilized whole-cells of *E. coli* containing glucose binding protein fused to fluorescent proteins. *Sensors and Actuators B.* **221**, 236-241 (2015).

132. Hosseini, M. Ganjali, M, R. Rafiei-Sarmazdeh, Z. Faridbod, F. Goldooz, H. Badiei, A. Nourozi, P. A novel Lu^{3+} fluorescent nano-chemosensor using new functionalized mesoporous structures. *Analytica Chimica Acta.* **771**, 95-101 (2013).

133. Wang, X. Gao, W. Xu, S. Xu, W. Luminescent fibers:In situ synthesis of silver nanoclusters on silk via ultraviolet light-induced reduction and their antibacterial activity. *Chemical Engineering Journal*. **210**, 585-589 (2012).

134. Zhang, X. Wu, F, G. Liu, P. Wang, H, Y. Gu, N. Chen, Z. Synthesis of ultrastable and multifunctional gold nanoclusters with enhanced fluorescence and potential anticancer drug delivery application. *Journal of Colloid and Interface Science.* **455**, 6-15 (2015).

135. Lu, F. Zhou, S. Zhu, J, J. Photochemical synthesis of fluorescent Ag nanoclusters and enhanced fluorescence by ionic liquid. *International journal of hydrogen energy*. **38**, 13055-13061 (2013).

136. Coutino-Gonzalez, E. Roeffaers, M, B, J. Dieu, B. Cremer, G, D. Leyre, S. Hanselaer, P. Fyen, W. Sels, B. Hofkens, J. Determination and Optimization of the Luminescence External Quantum Efficiency of Silver-Clusters Zeolite Composites. . *Phys. Chem. C*. **117**, 6998-7004 (2013).

137. Lesniak, W. Bielinska, A, U. Sun, K. Janczak, K, W. Shi, X. Baker, J, R. Balogh, L, P. Silver/Dendrimer Nanocomposites as Biomarkers: Fabrication, Characterization, in Vitro Toxicity, and Intracellular Detection. *Nano Lett.* **5**, 2123, 2130 (2005).

138. Shang, L. & Dong, S. Facile preparation of water-soluble fluorescent silver nanoclusters using a polyelectrolyte template. *Chem. Commun*. **9**, 1088-1090 (2008).

139. Shen, Z. Duan, H. Frey, H. Water-Soluble Fluorescent Ag Nanoclusters Obtained from Multiarm Star Poly(acrylic acid) as "Molecular Hydrogel" Templates. *Adv. Mater*. **19**, 349-352 (2007).

140. Zhang, J. Xu, S. Kumacheva, E. Photogeneration of Fluorescent Silver Nanoclusters in Polymer Microgels. *Adv. Mater.* **17**, 2336-2340 (2005).

141. Pal, S. Varghese, R. Deng, Z. Zhao, Z. Kumar, A. Yan, H. Liu, Y. Site-Specific Synthesis and In Situ Immobilization of Fluorescent Silver Nanoclusters on DNA Nanoscaffolds by Use of the Tollens Reaction. *Angew. Chem. Int. Ed*. **50**, 4176-4179 (2011).

142. Yu, J. Patel, S, A. Dickson, R, M. In Vitro and Intracellular Production of Peptide-Encapsulated Fluorescent Silver Nanoclusters. *Angew. Chem. Int. Ed.* **46**, 2028-2030 (2007).

143. Rao, Y, U, B. & Pradeep, T. Luminescent $Ag_7$and Ag_8Clusters by Interfacial Synthesis. *Angew. Chem. Int. Ed.* **49**, 3925-3929 (2010).

144. Adhikari, B. & Banerjee, A. Facile Synthesis of Water-Soluble Fluorescent Silver Nanoclusters and Hg^{II} Sensing. *Chem. Mater*. **22**, 4364- 4371 (2010).

145. Cathcart, N. Mistry, P. Makra, C. Pietrobon, B. Coombs, N. Jelokhani-Niaraki, M. Kitaev, V. Chiral Thiol-Stabilized Silver Nanoclusters with Well-Resolved Optical Transitions Synthesized by a Facile Etching Procedure in Aqueous Solutions. *Langmuir*. **25**, 5840-5846 (2009).

146. Latorre, A. Lorca, R. Zamora, F. Somoza, A. Enhanced fluorescence of silver nanoclusters stabilized with branched oligonucleotides. *Chem. Commun*. **49**, 4950-4952 (2013).

147. Li, J. Zhu, J, J. Xu, K. Fluorescent metal nanoclusters: From synthesis to applications. *Trends in Analytical Chemistry.* **58**, 90-98 (2014).

148. Chen, P, C. Chiang, C, K. Chang, H, T. Synthesis of fluorescent BSA–Au NCs for the detection of Hg2+ ions. *J Nanopart Res*. **15**, 1336 (2013).

149. Zhou, Z. Du, Y. Dong, S. DNA–Ag nanoclusters as fluorescence probe for turn-on aptamer sensor of small molecules. *Biosensors and Bioelectronics*. **28**, 33-37 (2011).

150. Liu, H. Wang, Y. Zhang, L. Shao, Y. Zheng, B. Fluorescent silver nanoclusters as probes for selective recognition of DNA CGG trinucleotide repeat. *Materials Letters*. **139**, 265-267 (2015).

151. Cao, H. Chen, Z. Zheng, H. Huang, Y. Copper nanoclusters as a highly sensitive and selective fluorescence sensor for ferric ions in serum and living cells by imaging. *Biosensors and Bioelectronics*. **62**, 189-195 (2014).

152. Peng, J. Shao, Y. Liu, L. Zhang, L. Liu, H. Wang, Y. Ag nanoclusters as probes for turn-on fluorescence recognition of TpG dinucleotide with a high selectivity. *Analytica Chimica Acta*. **850**, 78-84 (2014).

153. Liu, J. DNA-stabilized, fluorescent, metal nanoclusters for biosensor development. *Trends in Analytical Chemistry.* **58**, 99-111 (2014).

154. Tian, X. Kong, X, J. Zhu, Z, M. Chen, T, T. Chu, X. A new label-free and turn-on strategy for endonuclease detection using a DNA–silver nanocluster probe. *Talanta*. **131**, 116-120 (2015).

155. Park, J. Lee, J. Ban, C. Kim, W, J. An approach toward SNP detection by modulating the fluorescence of DNA-templated silver nanoclusters. *Biosensors and Bioelectronics*. **43**, 419-424 (2013).

156. Li, N. Zhao, P. Astruc, D. Anisotropic Gold Nanoparticles: Synthesis, Properties, Applications, and Toxicity. *Angew. Chem. Int. Ed.* **53**, 1756-1789 (2014).

157. Trouiller, A, J. Hebi, S. el Bahhaj, F. Napporn, T, W. Chemistry for on cotheranostic gold nanoparticles. *European Journal of Medicinal Chemistry*. **99**, 92-112 (2015).

158. Thakor, A, S. Jokerst, J. Zavaleta, C. Massoud, T, F. Gambhir, S,S. Gold Nanoparticles: A Revival in Precious Metal Administration to Patients. *Nano Lett.* **11**, 4029-4036 (2011).

159. Kimling, J.Maier, M. Okenve, B. Kotaidis, V.Ballot, H. Plech, A.Turkevich Method for Gold Nanoparticle Synthesis Revisited. *J. Phys. Chem. B*. **110**, 15700-15707 (2006).

160. Perala, S,R,K. & Kumar, S. On the Mechanism of Metal Nanoparticle Synthesis in the Brust–Schiffrin Method. *Langmuir*. **29**, 9863-9873 (2013).

161. Rajput, J. Kumar, A, R. Zinjarde, S. A simple microemulsion based method for the synthesis of gold nanoparticles. *Materials Letters*. **63**, 2672-2675 (2009).

162. Mihaly, M. Fleancu, M, C. Olteanu, N, L. Bojin, D. Meghea, A. Enachescu, M. Synthesis of gold nanoparticles by microemulsion assisted photoreduction method. *C. R. Chimie*. **15**, 1012-1021 (2012).

163. Murphy, C., J. Sau, T, K. Gole, A, M. Orendorff, C, J. Gao, J. Gou, L. Hunyadi, S, E. Li, T. Anisotropic Metal Nanoparticles: Synthesis, Assembly, and Optical Applications.J. *Phys.Chem. B*.,**109**, 13857–13870 (2005).

164. Kneipp, J. Kneipp, H. McLaughlin, M. Brown, D. Kneipp, K. In Vivo Molecular Probing of Cellular Compartments with Gold Nanoparticles and Nanoaggregates. *Nano Lett*. **6**, 2225-2231 (2006).

165. Perfe´zou, M. Turner, A. Merkoc¸I, A. Cancer detection using nanoparticle-based sensors. *Chem. Soc. Rev.* **41**, 2606-2622 (2012).

166. Kitching, M. Ramani, M. Marsili, E. Fungal biosynthesis of gold nanoparticles: mechanism and scale up. *Microbial Biotechnology*. **8**, 904-917 (2015).

167. Sanghi, R. Verma, P. Puri, S. Enzymatic Formation of Gold Nanoparticles Using *Phanerochaete Chrysosporium*. *Advances in Chemical Engineering and Science*. **1**, 154-162 (2011).

168. Abalaka, M, E. Daniyan, S, Y. Adeyemo, S, O. Damisa, D. The Antibacterial Efficacy of Gold Nanoparticles Derived from Gomphrena celosioidesand Prunus amygdalus (Almond) Leaves on Selected Bacterial Pathogens. *International Scholarly and Scientific Research & Innovation*. **8**, 336-339 (2014).

169. Dreaden, E, C. Alkilany, A, M. Huang, X. Murphy, C, J. El-Sayed, M, A. The golden age: gold nanoparticles for biomedicine. *Chem. Soc. Rev*. **41**, 2740-2779 (2012).

170. Radwan, S, H. & Azzazy, H, M. Gold nanoparticles for molecular diagnostics. *Expert.Rev.Mol.Diagn.* **9**, 511-524 (2009).

171. Xie, X. Xu, W. Liu, X. Improving Colorimetric Assays through Protein Enzyme-Assisted Gold Nanoparticle Amplification. *ACCOUNTS OF CHEMICAL RESEARCH*. **45**, 1511-1520 (2012).

172. Larguinho, M. Baptista, P, V. Gold and silver nanoparticles for clinical diagnostics—From genomics to proteomics. *JOURNAL OF PROTEOMICS*. **75**, 2811-2823 (2012).

173. Hedayati, M, K. Faupel, F. Elbahri, M. Review of Plasmonic Nanocomposite Metamaterial Absorber. *Materials.* **7**, 1221- 1248 (2014).

174. Giljohann, D, A. Seferos, D, S. Daniel, W, L. Massich, M, D. Patel, P, C. Mirkin, C, A. Gold Nanoparticles for Biology and Medicine. *Angew. Chem. Int. Ed.* **49**, 3280-3294 (2010).

175. Kim, D. & Jon, S. Gold nanoparticles in image-guided cancer therapy. *Inorganica Chimica Acta*. **393**, 154-164 (2012).

176. Gandra, N. Portz, C. Nergiz, S,Z. Fales, A. Vo-Dinh, T. Singamaneni, S. Inherently Stealthy and Highly Tumor-Selective Gold Nanoraspberries for Photothermal Cancer Therapy. *Scientific Reports*. **5**, 10311 (2014).

177. Sun, T. Zhang, Y, S. Pang, B. Hyun, D, C. Yang, M. Xia, Y. Engineered Nanoparticles for Drug Delivery in Cancer Therapy. *Angew. Chem. Int. Ed*. **53**, 12320-12364 (2014).

178. Ding, Y. Jiang, Z. Saha, K. Kim, S, C. Kim, S, T. Landis, R, F. Rotello, V, M. Gold Nanoparticles for Nucleic Acid Delivery. *Molecular Therapy*. **22**, 1075-1083 (2014).

179. Pissuwan, D. Niidome, T. Cortie, M, B. The forthcoming applications of gold nanoparticles in drug and gene delivery systems. *Journal of Controlled Release*. **149**, 65-71 (2011).

180. Mitton, D. Ackroyd, R. FRCS. A brief overview of photodynamic therapy in Europe. *Photodiagnosis and Photodynamic Therapy.* **5**, 103-111 (2008).

181. Ackroyd, R. Kelty, C. Brown, N. Reed, M. The History of Photodetection and Photodynamic Therapy. *Photochemistry and Photobiology*. **74**, 656-669 (2001).

182. Li, K. Zhang, Y, Y. Jiang, G, Y. Hou, Y, J. Zhang, B, W. Zhou, Q, X. Wang, X, S. A bivalent cationic dye enabling selective photoinactivation against Gram-negative bacteria*. Chem. Commun*. **51**, 7923-7926 (2015).

183. Heukers, R. Henegouwen, B. Oliveira, S. Nanobody–photosensitizer conjugates for targeted photodynamic therapy. *Nanomedicine: Nanotechnology, Biology, and Medicine*. **10**, 1441-1451 (2014).

184. Yuan, H. Chong, H. Wang, B. Zhu, C. Liu, L. Yang, Q. Lv, F. Wang, S. Chemical Molecule-Induced Light-Activated System for Anticancer and Antifungal Activities. *J. Am. Chem. Soc*. **134**, 13184-13187 (2012).

185. Liu, K. Liu, Y. Yao, Y. Yuan, H. Wang, S. Wang, Z. Zhang, X. Supramolecular Photosensitizers with Enhanced Antibacterial Efficiency. *Angew. Chem. Int. Ed.* **52**, 8285-8289 (2013).

186. Carvalho, C, M, B. Alves, E. Costa, L. Tome, J, P, C. Faustino, M, A, F. Neves, M, G, P, M ,S. Tome´, A, C. Cavaleiro, J, A, S. Almeida, A. Cunha, A. Lin, Z. Rocha, J. Functional Cationic Nanomagnet-Porphyrin Hybrids for the Photoinactivation of Microorganisms. *ACS NANO*. **4**, 7133-7140 (2010).

187. Bruno, G,J. A Review of Therapeutic Aptamer Conjugates with Emphasis on New Approaches. *Pharmaceuticals*. **6**, 340-357 (2013).

188. Yuan, Q. Wu, Y. Wang, J. Lu, D. Zhao, Z. Liu, T. Zhang, X. Tan, W. Targeted Bioimaging and Photodynamic Therapy Nanoplatform Using an Aptamer-Guided G-Quadruplex DNA Carrier and Near-Infrared Light. *Angew. Chem. Int. Ed.* **52**, 13965-13969 (2013).

189. Garcez, A,S. Núñez, S, C. Azambuja,N. Fregnani,E,R. Rodriguez, H, M, H. Hamblin, M,R. Suzuki, H. Ribeiro, M, S. Effects of Photodynamic Therapy on Gram-Positive and Gram-

Negative Bacterial Biofilms by Bioluminescence Imaging and Scanning Electron Microscopic Analysis. *Photomedicine and Laser Surgery.* **31**, 519-525 (2013).

190. Tavares, A. Carvalho, C, M, B. Faustino, M, A. Neves, M,G,P,M,S. Tomé, J, P, C. Tomé, A, C. Cavaleiro, J, A, S. Cunha, A. Gomes, N,C,M. Alves, E. Almeida, A. Antimicrobial Photodynamic Therapy: Study of Bacterial Recovery Viability and Potential Development of Resistance after Treatment. *Mar. Drugs*. **8**, 91-105 (2010).

191. James, N, S. Chen, Y. Joshi, P. Ohulchanskyy, T, Y. Ethirajan, M. Henary, M. Strekowsk, L. Pandey, R, K. Evaluation of Polymethine Dyes as Potential Probes for Near Infrared Fluorescence Imaging of Tumors: Part – 1. *Theranostics.* **3**, 692-702 (2013).

192. Rossoni, R, D. Junqueira, J, C. Santos, E, L, S. Costa, A, C, B. Jorge, A, O, C. Comparison of the efficacy of Rose Bengal and erythrosine in photodynamic therapy against Enterobacteriaceae. *Lasers Med Sci*. DOI 10.1007/s10103-010-0765-1 (2010).

193. Gillings, M, R. & Westoby, M. DNA technology and evolution of the Central Dogma. *Trends in Ecology & Evolution.* **29**, 1-2 (2014).

194. Mikhed, Y. Görlach, A. Knaus, U, G. Daiber, A. Redox regulation of genome stability by effects on gene expression, epigenetic pathways and DNA damage/repair. *Redox Biology*. **5**, 275-289 (2015).

195. Burnside, K. & Rajagopal, L. Regulation of prokaryotic gene expression by eukaryotic-like enzymes. *Current Opinion in Microbiology*. **15**, 125-131 (2012).

196. Deng, Y. Wang, C, C. Choy, K, W. Du, Q. Chen, J. Wang, Q. Li, L. Chung, T, K, H. Tang, T. Therapeutic potentials of gene silencing by RNA interference: Principles, challenges, and new strategies. *Gene*. **538**, 217-227 (2014).

197. Gleave, M, E. & Monia, B, P. ANTISENSE THERAPY FOR CANCER. *NATURE REVIEWS | CANCER*. **5**, 468-479 (2005).

198. Gangar, A. Fegan, A. Kumarapperuma, S, C. Huynh, P. Benyumov, A. Wagner, C, R. Targeted Delivery of Antisense Oligonucleotides by Chemically SelfAssembled Nanostructures. *Mol. Pharmaceutics.* **10**, 3514-3518 (2013).

199. Winkler, J. Saadat, K. Gavilan, M, D. Urban, E. Noe, C, R. Oligonucleotideepolyamine conjugates: Influence of length and position of 2´-attached polyamines on duplex stability and antisense effect. *European Journal of Medicinal Chemistry*. **44**, 670-677 (2009).

200. Morse, T, O, W. & Gunsch, C, K. A computational analysis of antisense off-targets in prokaryotic organisms. *Genomics*. **105**, 123-130 (2015).

201. Felber, A, E. Puxan, N, B. Deleavey, G, F. Castagner, B. Damha, M, J. Leroux, J, C. The interactions of amphiphilic antisense oligonucleotides with serum proteins and their effects onin vitro silencing activity. *Biomaterials*. **33**, 5955-5965 (2012).

202. Lee, J, J, A. & Yokota, T. Antisense Therapy in Neurology. *J. Pers. Med*. **3**, 144-176 (2013).

203. Evers, M, M. Toonen, L, J, A. Roon-Mom, W, M, C, V. Antisense oligonucleotides in therapy for neurodegenerative disorders. *Advanced Drug Delivery Reviews.* **87**, 90-103 (2015).

204. Geary, R, S. Norris, D. Yu, R. Bennett, C, F. Pharmacokinetics, biodistribution and cell uptake of antisense oligonucleotides. *Advanced Drug Delivery Reviews*. **87**, 46-51 (2015).

205. Sharma, V, K. Sharma, R, K. Singh, S, K. Antisense oligonucleotides: modifications and clinical trials. *Med. Chem. Commun*. **5**, 1454-1471 (2014).

206. Geary, R, S. Henry, S, P. Grillone , L, R. Fomivirsen: clinical pharmacology and potential drug interactions. *Clin Pharmacokinet*. **41**, 255-60 (2002).

207. Crooke, S, T. & Geary, R, S. Clinical pharmacological properties of mipomersen (Kynamro), a second generation antisense inhibitor of apolipoprotein B. *Br J Clin Pharmacol*. **76**, 269-276 (2013).

208. Vinores, S, A. Pegaptanib in the treatment of wet, age-related macular degeneration. *International Journal of Nanomedicine*. **1**, 263-268 (2006).

209. Roberts, C, T. Andaloussi, S, E, L. Morris, K, V. McClorey, G. Wood, M, J ,A. Small RNA-Mediated Epigenetic Myostatin Silencing. *Molecular Therapy–Nucleic Acids*. **1**, e23, (2012).

210. Davidson, B, L. & McCray Jr, P, B. Current prospects for RNA interference-based therapies. *Nature Reviews | Genetics.* **12**, 329-340 (2011).

211. Kaucsar, T. Racz, Z. Hamar, P. Post-transcriptional gene-expression regulation by micro RNA (miRNA) network in renal disease. *Advanced Drug Delivery Reviews*. **62**, 1390-1401 (2010).

212. Siomi, M, C. Sato, K. Pezic, D. Aravin, A, A. PIWI-interacting small RNAs: the vanguard of genome defence. *Nature Reviews | Molecular Cell Biology*. **12**, 246-258 (2011).

213. Kota, S, K. & Balasubramanian, S. Cancer therapy via modulation of micro RNA levels: a promising future. *Drug Discovery Today*. **15**, 733-740 (2010).

214. Grosswendt, S. Filipchyk, A. Manzano, M. Klironomos, F. Schilling, M. Herzog, M. Gottwein, E. Rajewsky, N. Unambiguous Identification of miRNA:Target Site Interactions by Different Types of Ligation Reactions. *Molecular Cell*. **54**, 1042-1054 (2014).

215. Cheng, G. Circulating miRNAs: Roles in cancer diagnosis, prognosis and therapy. *Advanced Drug Delivery Reviews.* **81**, 75-93 (2015).

216. Kapsogeorgou, E, K. Gourzi, V, C. Manoussakis, M, N. Moutsopoulos, H, M. Tzioufas, A, G. Cellular microRNAs (miRNAs) and Sjögren's syndrome: Candidate regulators of autoimmune response and autoantigen expression. *Journal of Autoimmunity*. **37**, 129-135 (2011).

217. Fuentes, E. Palomo, I. Alarcón, M. Platelet miRNAs and cardiovascular diseases. *Life Sciences*. **133**, 29-44 (2015).

218. Kim, W. Lee, Y. McKenna, N, D. Yi, M. Simunovic, F. Wang, Y. Kong, B. Rooney, R, J. Seo, H. Stephens, R, M. miR-126 contributes to Parkinson's disease by dysregulating the insulin-like growth factor/phosphoinositide 3-kinase signaling. *Neurobiology of Aging*. **35**, 1712-1721 (2014).

219. Soria, G. & Gottifredi, V. PCNA-coupled p21 degradation after DNA damage: The exception that confirms the rule?. *DNA Repair*. **9**, 358-364 (2010).

220. Jung, Y, S. Qian, Y. Chen, X. Examination of the expanding pathways for the regulation of p21 expression and activity. *Cellular Signalling*. **22**, 1003-1012 (2010).

221. Xiong, Y. Hannon,G, J. Zhang, H. Casso, D. Kobayashi, R. Beach,D. p21 is a unicersal inhibitor of cyclin kinases. *Nature*. **366**, 701-704 (1993).

222. Zhang, D. Mattila, M, P. Shahsavani, M. Falk, A. Teixeira, A, I. Herland, A. A 3D Alzheimer's disease culture model and the induction of P21-activated kinase mediated sensing in iPSC derived neurons. *Biomaterials.* **35**, 1420-1428 (2014).

223. Yeo, D. Huynh, N. Beutler, J, A. Christophi, C. Shulkes, A. Baldwin, G, S. Nikfarjam, M. He, H. Glaucarubinone and gemcitabine synergistically reduce pancreatic cancer growth via down-regulation of P21-activated kinases. *Cancer Letters*. **346**, 264-272 (2014).

224. Ivanovska, I. Ball, A, S. Diaz, R, L. Magnus, J, F. Kibukawa, M. Schelter, J, M. Kobayashi, S, V. Lim, L. Burchard, J. Jackson, A, L. Linsley, P, S. Cleary, M, A. MicroRNAs in the miR-106b Family Regulate p21/CDKN1A and Promote Cell Cycle Progression. *Molecular and Cellular Biology*. **28**, 2167-2174 (2008).

225. Kai, A, K, L. Cheung, Y, K. Yeung, P, k, K. Wong, J, T, Y. Development of single-cell PCR methods for the *Raphidophyceae*. *Harmful Algae*. **5**, 649-657 (2006).

226. Weisburg, W, G. Barns, S, M. Pelletier, D, A. Lane, D,J. 16S ribosomal DNA amplification for phylogenetic study. J.Bacteriol. **173**, 697-703 (1991).

227. Chen ,X. Zhong, Z. Xu, Z. Chen,L. Wang, Y. 2′ ,7′ -Dichlorodihydrofluorescein as a fluorescent probe for reactive oxygen species measurement: Forty years of application and controversy. *Free Radical Research*. **44**, 587-604 (2010).

228. Bozal, N. Montes, M, J. Tudela, E. Guinea, J. Characterization of several Psychrobacter strains isolated from Antarctic environments and description of Psychrobacter luti sp. nov. and Psychrobacter fozii sp. nov. *International Journal of Systematic and Evolutionary Microbiology.* **53**, 1093-110 (2003).

229. Tewari, R. Dudeja, M. Nandy, S. Das, A, K. Isolation of *Aeromonas salmonicida* from Human Blood Sample: A Case Report. *Journal of Clinical and Diagnostic Research.* **8**, 139-140 (2014).

230. West, T, P. Pyrimidine biosynthesis in *Pseudomonas veronii* and its regulation by pyrimidines. *Microbiological Research.* **167**, 306-310 (2012).

231. Browne, R, M, R. Cianciosi, S. Bordun,A, M. Wauters, G. Pathogenicity of *Yersinia kristensenii* for Mice. *Infection and Immunity*. **59**, 162-167 (1991).

232. Arunkumar, S. Tamilselvan, S. Ashokkumar, T. Geetha, R. Govindaraju, K. Ganesh Kumar, V. Singaravelu, G. Vijai Anand, K. One-pot room temperature novel synthesis of water-soluble CdS nanotriangles via green route. *Materials Letters*. **134**, 225-228 (2014).

233. Chen, H. Wang, J. Huang, D. Chen, X. Zhu, J. Sun, D. Huang, J. Li, Q. Plant-mediated synthesis of size-controllable Ni nanoparticles with alfalfa extract. *Materials Letters*. **122**, 166-169 (2014).

234. Raut R.W, Mendhulkar, V,D. Kashid, S.B. Photosensitized synthesis of silver nanoparticles using Withania somnifera leaf powder and silver nitrate. *J. Photochem. Photobiol. B*. **132**, 45-55 (2014).

235. Saifuddin N, Wong CW, Nur Yasumira AA. Rapid biosynthesis of silver nanoparticles using culture supernatant of bacteria with microwave irradiation. *J Chem*. **6**, 61–70 (2009).

236. Li, X. Fate of Inorganic Nanoparticles in Surface Water Environments, Ph. D. Thesis, University of Ohio, 2011.

237. Gebauer, J, S. Treuel, L. Influence of individual ionic components on the agglomeration kinetics of silver nanoparticles. *J. Colloid Interface Sci*. **354**, 546-554 (2011).

238. Mokhtari, N. Daneshpajouh, S. Seyedbagheri, S. Atashdehghan, R. Abdi, K. Sarkar, S. Minaian, S. Shahverdi, H, R. Shahverdi, A, R. Biological synthesis of very small silver nanoparticles by culture supernatant of *Klebsiella pneumonia*: The effects of visible-light irradiation and the liquid mixing process. *Materials Research Bulletin.***44**, 1415-1421 (2009).

239. Wei, X. Luo, M. Li, W. Yang, L. Liang, X. Xu, L. Kong, P. Liu, H. Synthesis of silver nanoparticles by solar irradiation of cell-free *Bacillus amyloliquefaciens* extracts and AgNO3. *Bioresource Technology.* **103**, 273-278 (2012).

240. Tolaymat, T, M. El Badawy, A, M. Genaidy, A. Scheckel, K, G. Luxton, T, P. Suidan, M. An evidence-based environmental perspective of manufactured silver nanoparticle in syntheses and applications: a systematic review and critical appraisal of peer-reviewed scientific papers. *Sci. Total Environ.* **408**, 999-1006 (2010).

241. Merkus, H, G. Particle Size Measurements: Fundamentals, Practice, Quality, Particle technology series, Springer, 2009 (Chapter 12) p. 308.

242. http://www.materials-talks.com/blog/2014/10/23/polydispersity-what-does-it-mean-for-dls and-chromatography/#sthash. ZdQw8Z1f.dpuf) (last date revised 20–6–2015).

243. Paredes, D. Ortiz, C. Torres, R. Synthesis, characterization, and evaluation of antibacterial effect of Ag nanoparticles against *Escherichia coli*O157:h7 and methicillin resistant *Staphylococcus aureus* (MRSA). *International Journal of Nanomedicine*. **9**, 1717-1729 (2014).

244. Sengupta, B. Ritchie, C, M. Buckman, J, G. Johnsen, K, R. Goodwin, P, M. Petty, J, T. Base-Directed Formation of Fluorescent Silver Clusters. *J. Phys. Chem. C*. **112**, 18776-18782 (2008).

245. Richards, C, I. Choi, S. Hsiang, G, C. Antoku, Y. Vosch, T. Bongiorno, A. Tzeng, Y, L. Dickson, R,M. Oligonucleotide-Stabilized Ag Nanocluster Fluorophores. *J. AM. CHEM. SOC*. **130**, 5038-5039 (2008).

246. Lan, G, Y. Chen, W, Y. Chang, H, T. One-pot synthesis of fluorescent oligonucleotide Ag nanoclusters for specific and sensitive detection of DNA. *Biosensors and Bioelectronics*.**26**, 2431-2435 (2011).

247. Saravanan, M. & Nanda, A. Extracellular synthesis of silver bionanoparticles from *Aspergillus clavatus* and its antimicrobial activity against MRSA and MRSE. *Colloids and Surfaces B: Biointerfaces.* **77**, 214-218 (2010).

248. Roh, Y, H. Lee, J, B. Shopsowitz, K, E. Dreaden, E, C. Morton, S, W. Poon, Z. Hong, J. Yamin, I. Bonner, D, K. Hammond, P, T. Layer-by-Layer Assembled Antisense DNA Microsponge Particles for Efficient Delivery of CancerTherapeutics. *ACS nano*. **8**, 9767-9780 (2014).

249. Devulapally, R. Sekar, N, M. Sekar, T, V. Foygel, K. Massoud, T, F. Willmann, J, K. Paulmurugan, R. Polymer Nanoparticles Mediated Codelivery of AntimiR-10b and AntimiR-21 for Achieving Triple Negative Breast Cancer Therapy. *ACS nano*. **9**, 2290-2302 (2015).

250. El Badawy, A, M. Luxton, T, P. Silva, R, G. Scheckel, K, G. Suidan, M, T. Tolaymat, T, M. Impact of Environmental Conditions (pH, Ionic Strength, and Electrolyte Type) on the Surface Charge and Aggregation of Silver Nanoparticles Suspensions. *Environ. Sci. Technol*. **44**, 1260- 1266 (2010).

251. Sathiyanarayanan,G. Kiran, G, S. Selvin, J. Synthesis of silver nanoparticles by polysaccharide bioflocculant produced from marine *Bacillus subtilis* MSBN17. *Colloids and Surfaces B: Biointerfaces.* **102**, 13-20 (2013).

252. Kahraman, M. Zamaleeva, A, I. Fakhrullin, R, F. Culha, M. Layer-by-layer coating of bacteria with noble metal nanoparticles for surface-enhanced Raman scattering. *Anal Bioanal Chem.* **395**, 2559-2567 (2009).

253. Chatterjee, D,K. Fong, L, S. Zhang, Y. Nanoparticles in photodynamic therapy: An emerging paradigm. *Advanced Drug Delivery Reviews*. **60**, 1627-1637 (2008).

254. Bourre L, Giuntini F, Eggleston IM, Mosse CA, Macrobert AJ, Wilson M. Effective photoinactivation of Gram-positive and Gram-negative bacterial strains using an HIV-1 Tat peptide-porphyrin conjugate. *Photochem Photobiol Sci*. **9**, 1613–20 (2010).

255. Lu, W. Yao, K. Wang, J. Yuan, J. Ionic liquids–water interfacial preparation of triangular Ag nanoplates and their shape-dependent antibacterial activity. *J.Colloid Interf. Sci.* **437**, 35-41 (2015).

256. Schultz, D. Gardner, K. Oemrawsingh, S, S, R. Markeševic, N. Olsson, K. Debord, M. Bouwmeester, D. Gwinn, E. Evidence for Rod-Shaped DNA-Stabilized Silver Nanocluster Emitters. *Adv. Mater*. **25**, 2797-2803 (2013).

257. Teng, Y. Yang, X. Han, L. Wang, E. The Relationship between DNA Sequences and OligonucleotideTemplated Silver Nanoclusters and Their Fluorescence Properties. *Chem. Eur. J*.**20**, 1111-1115 (2014).

258. Yuan, Z. Chen, Y, C. Li, H, W. Chang, H, T. Fluorescent silver nanoclusters stabilized by DNA scaffolds. *Chem. Commun*. **50**, 9800-9815 (2014).

259. Latorre, A. Somoza, A. DNA-Mediated Silver Nanoclusters: Synthesis, Properties and Applications. *Chem Bio Chem*. **13**, 951-985 (2012).

260. Setyawati, M, I. Kutty, R, V. Tay, C, Y. Yuan, X. Xie, J. Leong, D, T. Novel theranostic DNA nanoscaffolds for the simultaneous detection and killing of *Escherichia coli* and *Staphylococcus aureus. ACS Appl.Mater. Interfaces.* **6**, 21822 (2014).

261. Derycke, A, S, L. & de Witte, P, A, M. Liposomes for photodynamic therapy. *Advanced Drug Delivery Reviews*. **56**, 17-30 (2004).

262. Huang, Z. Xu, H. Meyers, A,D. Musani, A, I. Wang, L. Tagg, R. Barqawi, A, B. Chen, Y, K. Photodynamic therapy for treatment of solid tumors – potential and technical challenges. *Technol Cancer Res Treat*. **7**, 309-320 (2008).

263. Rolim, J, P, M, L. de-Melo, M, A, S. Guedes, S, F. Albuquerque-Filho, F, B. de Souza, J, R. Nogueira, N, A, P. Zanin, I, C, J. Rodrigues, L, K, A. The antimicrobial activity of photodynamic therapy against Streptococcus mutans using different photosensitizers. *Journal of Photochemistry and Photobiology B: Biology*. **106**, 40-46 (2012).

264. Lambert, P, A. Cellular impermeability and uptake of biocides and antibiotics in gram-positive bacteria and mycobacteria. *Symp Ser Soc Appl Microbiol*. 46S–54S (2002).

265. George, S. Hamblin, M, R. Kishen, A. Uptake pathways of anionic and cationic photosensitizers into bacteria. *Photochem. Photobiol. Sci.* **8**, 788-795 (2009).

266. Bertoloni G, Rossi F, Valduga G, Jori G, Ali H, van Lier JE. Photosensitizing activity of waterand lipid-soluble phthalocyanines on prokaryotic and eukaryotic microbial cells. Microbios. **71**, 33–46 (1992).

267. Sperandio, F, F. Huang, Y, Y. Hamblin, M, R. Antimicrobial Photodynamic Therapy to Kill Gram-negative Bacteria. *Recent Pat Antiinfect Drug Discov*. **8**, 108-120 (2014).

268. Zhegalova, N, G. He, S. Zhou, H. Kim, D, M. Berezin, M, Y. Minimization of self-quenching fluorescence on dyes conjugated to biomolecules with multiple labeling sites via asymmetrically charged NIR fluorophores. *Contrast Media Mol. Imaging*. **9**, 355-362 (2014).

269. Hori, S, I. Yamamoto, T. Obika, S. XRN2 is required for the degradation of target RNAs by RNase H1-dependent antisense oligonucleotides. *Biochemical and Biophysical Research Communications*. **464**, 506-511 (2015).

270. Souleimanian, N. Deleavey, G, F. Soifer, H. Wang, S. Tiemann, K. Damha, M, J. Stein, C, A. Antisense 2′-Deoxy, 2′-Fluoroarabino Nucleic Acid (2′F-ANA) Oligonucleotides: In Vitro Gymnotic Silencers of Gene Expression Whose Potency Is Enhanced by Fatty Acids. *Molecular Therapy–Nucleic Acids*. **1**, e43 (2012).

271. Liu, J. Zhou, Z. Li, K. Han, M. Yang, J. Wang, S. In vitro and in vivo protection against enterovirus 71 by an antisense phosphorothioate oligonucleotide. *Arch Virol*. DOI 10.1007/s00705-014-2054-y.

272. Sato, M, T. Tokuhiro,S. Kawaida, R. Koizumi, M. Design of ENA gapmer as fine-tuning antisense oligonucleotides with sequence-specific inhibitory activity on mouse PAD14 mRNA expression. *Nucleic Acids Symposium Series*, **50**, 319-320 (2006).

273. Kichler, A. Zauner, W. Ogris, M. Wagner, E. Influence of the DNA complexation medium on the transfection efficiency of lipospermine/DNA particles. *Gene Ther*. **5**, 855–860 (1998).

274. Dalby, B. Cates, S. Harris, A. Ohki, E,C. Tilkins, M,L. Price, P,J. Advanced transfection with Lipofectamine 2000 reagent: primary neurons, siRNA, and high throughput applications. *Methods*. **33**, 95–103 (2004).

275. Daniel, MC. & Astruc, D. Gold nanoparticles: assembly, supramolecular chemistry, quantum-size-related properties, and applications toward biology, catalysis, and nanotechnology. *Chem Rev*. **104**, 293–346 (2004).

276. Bowman, M, C. Ballard, T, E. Ackerson, C, J. Feldheim, D, L. Margolis, D, M. Melander, C. Inhibition of HIV fusion with multivalent gold nanoparticles. *J Am Chem Soc*. **130**, 6896–6897 (2008).

277. Ryan, J, A. Overton, K, W. Speight, M, E. Oldenburg, C, N.Loo, L. Robarge, W. Cellular uptake of gold nanoparticles passivated with BSA-SV40 large T antigen conjugates. *Anal Chem*. **79**,9150–9159 (2007).

278. Kim, S, T. Saha, K. Kim, C. Rotello, V, M. The role of surface functionality in determining nanoparticle cytotoxicity. *Acc Chem Res*. **46**, 681–691 (2013).

279. Chompoosor, A. Saha, K. Ghosh, P, S. Macarthy, D, J.Miranda, O,R. Zhu, Z, J. The role of surface functionality on acute cytotoxicity, ROS generation and DNA damage by cationic gold nanoparticles. *Small*. **6**, 2246–2249 (2010).

280. De Jong, W,H. Hagens, W, I. Krystek, P. Burger, M, C. Sips, A, J. Geertsma, R, E. Particle size-dependent organ distribution of gold nanoparticles after intravenous administration. *Biomaterials*. **29**, 1912–1919 (2008).

281. Sonavane, G. Tomoda, K. Makino, K. Biodistribution of colloidal gold nanoparticles after intravenous administration: effect of particle size. *Colloids Surf B Biointerfaces*. **66**, 274–280 (2008).

282. Wang, B. He, X. Zhang, Z. Zhao, Y. Feng, W. Metabolism of nanomaterials in vivo: blood circulation and organ clearance. *Acc Chem Res*. **46**,761–769 (2013).

283. Zhu, M. Perrett, S. Nie, G. Understanding the particokinetics of engineered nanomaterials for safe and effective therapeutic applications. *Small*. **9**, 1619–1634 (2013).

9. ACKNOWLEDGEMENTS

ACKNOWLEDGEMENTS

I have had the pleasure of working with a number of extraordinary individuals who have helped to guide me through the meandering path I have pursued.

I would like to thank **Prof. Ricardo Amils**, **Prof. Irma Marin**, and thanks a lot to my academic director **Prof. Jose Pascual Abad** for the great opportunity and freedom they has given me to develop my scientific prowess.

I owe a lot to my scientific director **Dr. Alvaro Somoza**. He was more than willing to accept a scientific orphan, nurture my talent and give me unconditional freedom to work in an area of my choice. His excellent display of patience, motivation, knowledge, guidance and exuberance has played a pivotal role in my accomplishments.

I extend my sincere thanks to my scientific co-director **Dr. Aitziber L. Cortajarena** and also **Dr. Cristina Flors** and **Dr. Isabel Rodriguez** which their support and contribution towards my graduate studies.

Dr. Alfonso Latorre. I am at loss of words to describe the support he has provided me during my stay at the **Nanobiotechnology** Lab. I can only say I am very, very grateful.

Also I would like to thank the past and present members of my research group, **Dr. Antonio Aries**, **Dr. Pierre Couleaud**, **Ana Latorre**, **Romina Lorca**, **Christian Duarte Varela**, **Ana Morate Carlotta Vizioli, Ana Morro Chavez, Benedito Eduardo Correia** and **Dr. Nicolas Raho** for the competitive environment they helped create, challenging me to be a better scientist.

I sincerely thank **Dr. Dimitrios Balomenos** (CNB-CSIC, Madrid, Spain), and **Dr. Daniela Palacios** (IRCCS Fondazione Santa Lucia, Rome, Italy) for the exciting joint projects.

I would like to thank **Rahman**, **Maryam**, and **mohammad Vahid**, they excellent display of concern, support and affection has always motivated me and rendered me spellbound.

Finally and most importantly, I would like to thank my family members for their constant support and motivation throughout my academic journey.

10. SUPPLEMENTARY INFORMATION

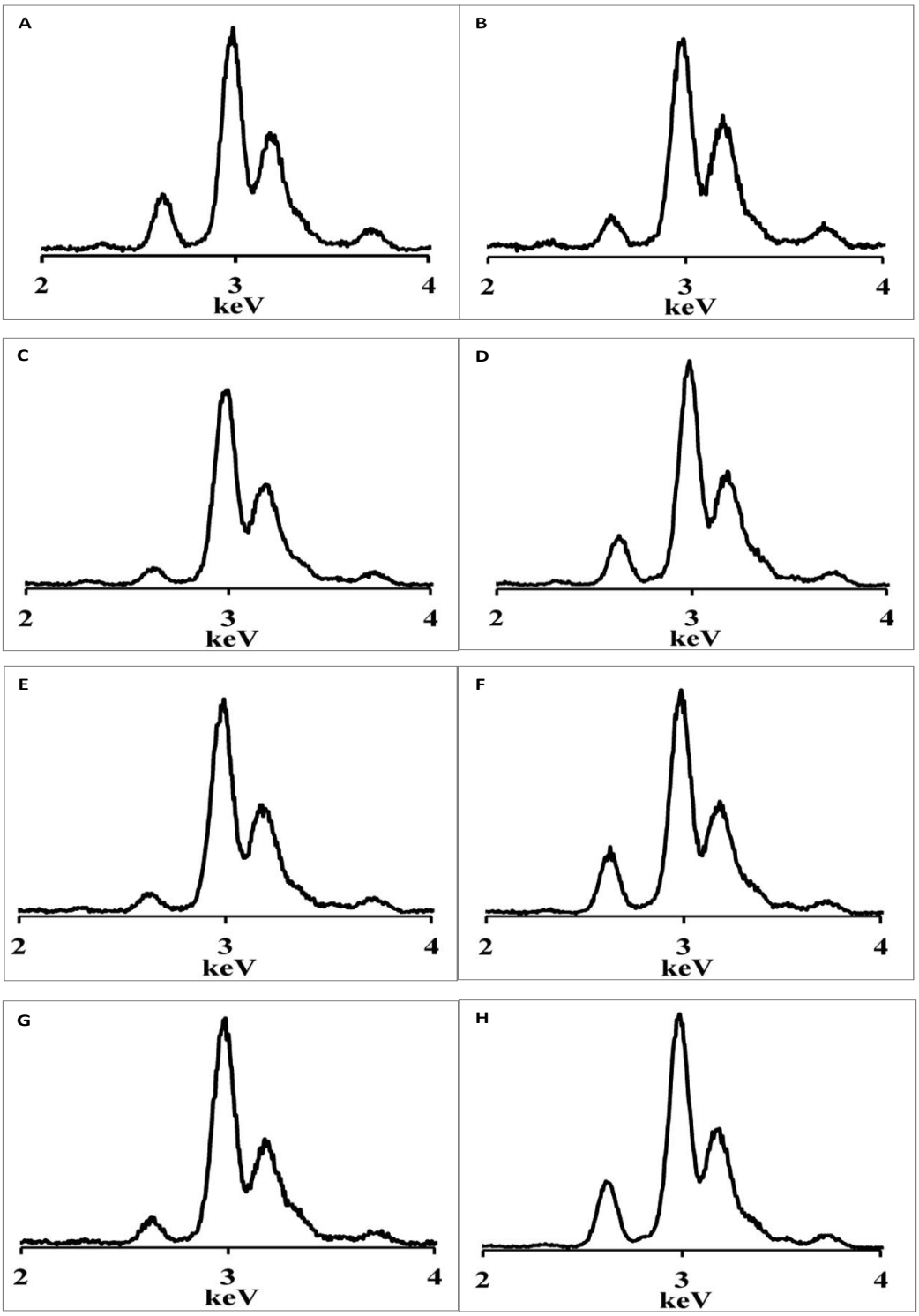

SI.1. Simplified TXRF of the different AgNPs used in this study. Cell-free supernatants used in the preparations were, from **A,B**). *Psychrobacter sp* (30 °C and 4 °C), **C,D**). *A.salmonicida* (30 °C and 4 °C), **E,F**). *P.veronii* (30 °C and 4 °C), **G,H**). *Y.kristensenii* (30 °C and 4 °C), Both peaks at 3 and 3.3 keV come from silver, while small peaks at 2.7 and 3.7 keV correspond to chloride and calcium respectively.

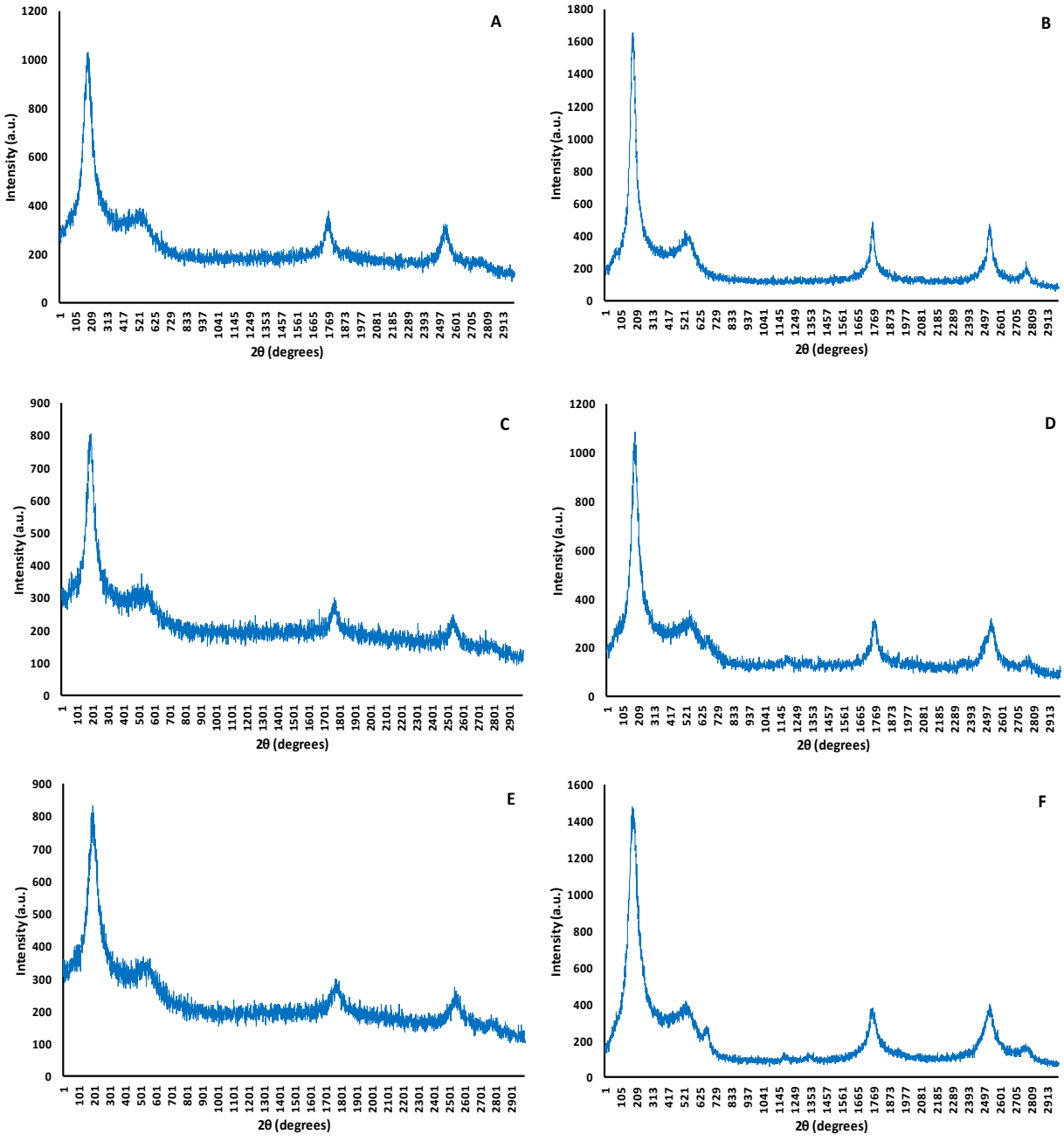

SI.2. X-Ray Diffraction pattern of AgNPs synthesis by broths of **A,B**). *A.salmonicida* (30 °C and 4 °C), **C,D**). *P.veronii* (30 °C and 4 °C), **E,F**). *Y.kristensenii* (30 °C and 4 °C).